Phasor Measurement Unit Test and Applications for Small Signal Stability Assessment and Improvement of Power System

Ghiga, Radu

Publication date:
2017

Document Version
Publisher's PDF, also known as Version of record

Technical University of Denmark

Radu Ghiga

Phasor Measurement Unit Test and Applications for Small Signal Stability Assessment and Improvement of Power Systems

PhD Thesis, March 2017

DTU Electrical Engineering
Department of Electrical Engineering

Radu Ghiga

Phasor Measurement Unit Test and Applications for Small Signal Stability Assessment and Improvement of Power Systems

PhD Thesis, March 2017

Phasor Measurement Unit Test and Applications for Small Signal Stability Assessment and Improvement

Author(s):
Radu Ghiga

Supervisor(s):
Associate Professor, Arne Hejde Nielsen
Associate Professor, Qiuwei Wu

Department of Electrical Engineering
Centre for Electric Power and Energy (CEE)
Technical University of Denmark
Elektrovej 325
DK-2800 Kgs. Lyngby
Denmark

www.elektro.dtu.dk/cee
Tel: (+45) 45 25 35 00
Fax: (+45) 45 88 61 11
E-mail: cee@elektro.dtu.dk

Release date: March 31st, 2017

Class: 1 (Public)

Edition: 1. edition

Comments: This report is a part of the requirements to achieve ph.d. degree at Technical University of Denmark.

PREFACE

This PhD thesis and the work described in it were prepared at the Center for Electric Power and Energy, Department of Electrical Engineering, at the Technical University of Denmark in the period from January 2014 to March 2017. The thesis is part of the requirements to achieve the Ph.D. Degree in Electrical Engineering.

The research was funded by the STRONg^{2}rid project through Nordic Energy Research (NORDEN).

Radu Ghiga
Kgs. Lyngby, 2017-03-31

ACKNOWLEDGEMENT

First of all, I would like to thank my supervisors Arne Hejde Nielsen and Qiuwei Wu for their guidance and consistent support throughout the project.

In particular I would like to thank Kenneth Martin for his help with testing the Phasor Measurement Units, his suggestions for developing the analysis software, and for his valuable advice.

Furthermore, I would like to thank Prof. C.Y. Chung from the University of Saskatchewan, Canada for his help and supervision during my external stay. It proved to be a great and rewarding experience. The colleagues and friends at the University of Saskatchewan I would like to thank for their support during my external stay.

Many thanks to the colleagues and friends at DTU CEE for good collaboration and interesting discussions during my PhD study.

Finally, I would like to thank my family for the support they have given me.

ABSTRACT

The power system is constantly changing and as new technologies are being developed, it is pushing forward towards a decrease in fossil-fuel need. As the conventional generation is being replaced by renewable energy sources (RES) such as wind and solar power, it is expected for the power system to be less predictable. Therefore, the methods used for stability and security assessment will most likely use information from the wide-area measurements systems (WAMS).

The work presented in this thesis deals on one hand with the development of test methods and validation of phasor measurement units (PMUs) which are considered to be one of the key technologies in WAMS, and on the other hand with the possibility of using PMU measurements together with large wind power plants (WPPs) to help improve the damping of inter area oscillations.

To validate the PMUs, a laboratory test setup is assembled. The hardware components are capable of generating, with the required accuracy, the test signals injected in the PMUs. The signals are created according to the requirements defined in the current IEEE C37.118.1-2011 standard, to test the steady-state and dynamic compliance of the PMUs. The performance of the PMUs is evaluated according to the IEEE C37.118.1a-2014 amendment to the standard which defines the allowed error limits for the units. It was found that the devices under test did not meet all the specifications of the IEEE C37.118.1a-2014, especially for the dynamic tests. Furthermore, the PMUs were tested under three scenarios that were not covered by the current standard. It was found that two of the scenarios affected the measurement accuracy of the units, while the third did not have a significant impact on the PMU performance.

A full scale converter based wind turbine (WT) model suitable for small-signal stability analysis was developed during the project. The model can be used in both dynamic simulations of the nonlinear system, and it can be linearized together with the entire power system model in order to study the eigenvalues of the system. In this thesis, the WT model was used as an aggregated WPP with the active and reactive power outputs controlled by a Wind Plant Controller (WPC). The WPP was used to help improve the damping of inter-area oscillations. The WPP was equipped with a power oscillation damping (POD) controller which modulated the active power output of the WPP. Two types of POD were considered in the investigation: a conventional power system stabiliser (PSS) type and a phasor POD. Remote PMU measurements were used as input

signals for the PODs, and measurement latency was included for comparison. It was found that the PODs had similar performance when there was no latency in the input signals. The phasor POD showed a clear advantage when latency was considered. The reason was that the phasor POD can easily and adaptively compensate for delays in the input signals, while the conventional PSS type uses the lead-lag block to achieve a fixed phase compensation which is chosen during the design stage.

RESUMÉ

Elsystemet gennemgår en konstant udvikling og i takt med udviklingen af nye technologier mindskes behovet for fossile brandstoffer. Denne udvikling medfører en udfasning af traditionelle generatorer, som gradvist bliver erstattet af vedvarende energikilder såsom vind- og solenergi. Som resultat af denne udskiftning forventes det at elsystemet bliver mindre pålideligt, for at modvirke dette er det sandsynligt at metoderne brugt til at vurderer elsystmets stabilitet og sikkerhed vil benytte sig af målinger fra et wide-area målesystem (WAMS).

Arbejder præsenteret i denne afhandling er todelt og omhandler på den ene side, udviklingen af testmetoder og validering af phasor måleenheder (PMU), som anses for at være en af de vigtigste teknologier i WAMS. På den anden side, muligheden for at anvende PMU-målinger sammen med store vindfarme for at hjælpe med at forbedre dæmpning af inter-område svingninger.

PMU målingerne er valideret gennem en laboratorieopstilling, hvor hardwarekomponenterne er i stand til at generere testsignaler med den påkrævede nøjagtighed. Signalerne er skabt i henhold til kravene i den aktuelle IEEE C37.118.1-2011 standard, både til test i steady-state og dynamiske situationer. PMU enhedens ydeevne bedømmes efter IEEE C37.118.1a 2014 ændringen af standarden, som definerer de tilladte fejlgrænser for enhederne. Det blev konstateret, at enhederne under testen ikke opfyldte alle specifikationerne i IEEE C37.118.1a-2014, især i de dynamiske situationer. Derudover blev PMU enheden testet i tre scenarier, der ikke er dækket af den nuværende standard. Det blev konstateret, at to af scenarierne, påvirkede målenøjagtighed af enhederne, mens den tredje ikke havde en betydelig effekt på PMU ydeevne.

En fuld skala, konverter baseret, vindmølle model velegnet til analyse af små-signal stabilitet udviklet i løbet af projektet. Modellen kan bruges i dynamiske simuleringer af det ikke-lineære system og kan lineariseres sammen med hele modellen af elsystemet for at studere egenværdierne af systemet. I denne afhandling blev vindmølle modellen, anvendt som en aggregeret vindfarm, hvor den samlede aktive og reaktive effekt styres af en vindfarms koordinator. Vindfarmer blev brugt til at hjælpe med at forbedre dæmpning af inter-område svingninger. Vindfarmer er udstyret med en effekt svingnings dæmper (POD), som regulerer den aktive effekt af vindfarmen. To typer af POD blev undersøgt; en konventionel PSS type og en phasor POD. Fjerntliggende PMU

målinger blev anvendt som indgangssignaler til PODen, hvor måling forsinkelser var inkluderet til sammenligning. Det konstateredes, at de to typer POD havde lignende ydeevne, når der ikke var nogen ventetid i indgangssignalerne. Phasor POD viste en klar fordel, når der blev taget højde for signal forsinkelser. Grunden var, at phasor POD nemt og adaptivt kan kompensere for forsinkelserne i indgangssignaler, mens den konventionelle PSS type anvender en lead-lag blok for at opnå en fast fasekompensering som vælges under designfasen.

TABLE OF CONTENT

LIST OF PUBLICATIONS

The publications which have been prepared as part of the PhD project are the following:

A. R. Ghiga, Q. Wu, K. Martin, W. El-Khatib, L. Chen and A. H. Nielsen, “Steady-State PMU Compliance Test under C37.118.1a – 2014,” in *Proc. IEE PES Innovative Smart Grid Technologies Conference Europe (ISGT Europe)*, Ljubljana, 2016, pp. 1-6.

B. R. Ghiga, Q. Wu, K. Martin, W. Ziad, L. Cheng and A. H. Nielsen, "Dynamic PMU Compliance Test under C37.118.1a™-2014," in *Proc. IEEE PES General Meeting*, Denver, CO, 2015, pp. 1-5.

C. R. Ghiga, K. Martin, Q. Wu, and A.H. Nielsen, “Phasor Measurement Unit Test under Interference Conditions,” submitted at *Transactions on Power System Delivery.*

D. R. Ghiga, Q. Wu, A. H. Nielsen, “Phasor Model of Full Scale Converter Wind Turbines for Small-Signal Stability Analysis,” submitted at *IET Renewable Power Generation Conference.*

E. R. Ghiga, Q. Wu, and A. H. Nielsen, ”Inter-area Power System Oscillation Damping Controller for Full-Scale Converter Wind Turbines using PMU Measurements,” *Unsubmitted manuscript.*

1 INTRODUCTION

1.1 Background

1.1.1 Problem and motivation

The constant worldwide increase in energy consumption is an undeniable reality of the present day. Technological advancements, economic development as well as societal changes contribute to this sustained growth of energy use that reaches new peak every year. For instance, from 2004 to 2013 the electricity consumption increased by approximately 20% worldwide[1]. These figures plus the rapid implementation of new technologies show that the energy consumption will continue to increase in the years to come. In fact it is estimated that the worldwide energy demand will grow by 48% over the period from 2012 to 2040 [1].

Nonetheless, this continuous increasing energy dependency of our present and future world makes breakdowns of the electricity supply a major, more important and more costly risky than ever before. For example, the blackout in the northeast of the United States of America and in Ontario, Canada had a large economic impact. This blackout is estimated to have caused losses between $4 billion and $10 billion U.S. dollars, lasted up to 4 days, and affected approximately 50 million people [2]. The task force appointed to investigate the blackout concluded that one of the main causes was the lack of situational awareness due to inadequate reliability tools. It was therefore recommended to evaluate the real-time operating tools, which are vital for a reliable and secure operation of the power system [2]. In Europe, a blackout affected southern Sweden and eastern Denmark in 2003. Approximately 1.6 million people were affected in Sweden and 2.4 million in eastern Denmark. In the same year, the entire Italian power system collapsed after a sequence of events. The power in northern Italy was restored after 3 hours and in the rest of the country it was restored during the same day. The blackout affected 60 million people [2].

[1] http://data.worldbank.org

Furthermore, this complex situation of energy consumption in the 21st century is a central actor in the fight against global warming that has led the major economies of the world to address ambitious targets of renewable energy sources (RES) development and use [3]. Some of these countries have made remarkable advancements (e.g. renewable electricity output has increased from 2004 to 2012 as follows: in Denmark from 23% to 48%, in Germany from 9% to 23%, in UK from 3.6% to 11% etc)[1], and it can be expected for more states to reach similar figures. However, this unprecedented growth in renewables brings significant challenges in what regards the secure and reliable operation of the electric grid. One challenge is matching the power generation based on RES with consumption at all times due to the forecasting uncertainties. Consequently, research is carried out the area of demand response, energy storage, and other intelligent systems. Another challenge, provided the generation and consumption will match all the time, is the frequent change in the operating point of the power system which is expected due to the changes in generation and consumption patterns.

Most of the tools and methods currently used to determine and monitor the state of the power system are based on off-line studies performed in advance by the power system operators. While this approach is feasible for power systems based on conventional generation, when dealing with a power system that is constantly changing its operating point to match the generation and consumption patterns, these assessment methods might not be sufficient. For the future power system, on-line stability assessment methods should be available in order to ensure the stability and secure operation of the power system [4]. Moreover, the authors propose using measurements from phasor measurement units (PMUs) in order to monitor the power system.

Methods that are using synchronized wide area measurements to accomplish on-line stability assessment have been presented in a number of publications. A new approach for real-time aperiodic small-signal rotor angle stability assessment of power system was developed in [5]. An existing off-line method for voltage stability is adapted to real-time operation in [6] and [7]. It can be noticed that these methods rely on PMU measurements, and in fact, the PMU [8]-[10] is considered one of the key technologies for the development of real-time wide-area measurements systems (WAMS) for real-time monitoring and control applications [11], [12]. Consequently, it is of high importance to ensure the PMUs produce measurements with sufficient accuracy which can be used by different monitoring and control applications, and it is equally important to be able to test these PMUs and validate their performance against the newest available standards.

Besides the challenge of matching the RES generation and consumption at all times, in the interconnected power system electromechanical power system oscillations will occur. Electromechanical oscillations are typical in power systems with conventional

generation [13]. If such oscillations are excited by an event in the power system (e.g. load switching), the rotors of the synchronous generators in one part of the system will swing against the rotors of synchronous generators in another part of the system, which in turn will cause the active power flow between the two areas to oscillate. If there is sufficient damping in the system, the oscillations will die out and a steady-state operating point will be reached. Conversely, if there is insufficient damping for a particular oscillation, it will increase and eventually the equipment that assures the power system safety will trip. This can cause a cascading effect of equipment tripping and finally can lead to a system blackout.

Power system oscillations are covered in terms of nature of their origin, different means of mitigation, possible impact of RES and non-synchronous generation, and their potential as root cause to system blackout in [14] – [16].

The described rotor oscillations are part of rotor angle stability studies, and are usually divided in two categories depending on the disturbance that excites them as: large disturbances (transient stability), and small disturbances (small-signal stability). In this thesis only the small-signal stability will be treated. Small-signal stability is defined as [17]:

> "the ability of the power system to maintain synchronism under small disturbances".

Generally, a disturbance is considered small when the dynamic response of the power system, following the disturbance can be accurately represented by a linear model. A small-signal unstable power system will fail to maintain synchronism between the generators, once the oscillations are excited, and this can manifest in two ways: an aperiodic drift of the rotor angles, or an increase in the amplitude of the rotor angles oscillations. It is not the disturbance type that determines whether an oscillation is stable or not. The stability of the power system is a property that depends on the state of the system, that is, operating point, controller tuning, generators in service, transmission lines, etc. Furthermore, in a real power system there are always small disturbance due to variability in production (e.g. power systems with high RES generation), load variation, etc, thus small-signal instability cannot be tolerated in the actual power system.

Power system oscillations are typically divided into three groups depending on the participation of the synchronous generators in the oscillation [17]:

- Inter-area oscillations where a group of machines in one part of the system is oscillating against another group or groups of machines in

another part of the system. These oscillations have a frequency typically in the range of 0.1 to 0.3 Hz.

- Intra-area oscillations where a group of machines in one part of the system oscillate against another group located in the same part of the system. The frequency of these oscillations is typically 0.4 to 0.7 Hz.

- Local-area oscillations which involve generators located close to each other. This includes detrimental interaction between the controls of the generators. The frequency range of these oscillations is 0.7 to 2 Hz.

Low frequency inter-area oscillations are typical in large longitudinal power systems, and it is not necessary for the power system to be connected by weak inter-ties, as it has been shown analytically in [18].

1.1.2 Focus of the presented work

The focus of this PhD project was divided into several goals. First, the aim was to develop testing methods to verify the PMU compliance under the latest requirements. This involved setting up a laboratory test setup capable of generating the required test signals (three phase voltages and currents) which were injected into the PMUs. The hardware was complemented by software, developed during the period of the PhD project, which was used for creating the required test signals and for analysing and evaluating the measurements reported by the PMUs. The overall test system was used to test several commercial PMUs for compliance under the newest requirements.

Next, the PhD project aimed to investigate the performance of the commercially available PMUs under scenarios that are likely to be encountered in the actual power system and were not covered by the current standard. The results could indicate a possible need to update the standard with additional requirements or it can show that the current standard covers all the important aspects.

The third aspect of the PhD involved developing wind turbines (WTs) and wind power plants (WPPs) models suitable for small-signal stability studies. The aim was to model a Type 4 full-scale converter based WT which can be upscaled to a large WPP and can be used for small signal stability studies. It is desirable to develop a model that can be linearized by the available tools (e.g. Matlab/Simulink) and that can also be used in time domain simulations with the dynamic non-linear power system.

The final aim of the PhD project was to develop a controller that can be used with the WPP to help improve the damping of inter-area power system oscillations. The

controller should take advantage of the availability of wide-area measurements and use the measurement reported by PMUs as input signals.

1.2 State-of-the-art

1.2.1 Phasor Measurement Units, IEEE Standards and Testing

Synchronized phasor measurements were introduced in the mid-80s, and since then the subject of wide-area measurements in power systems has been receiving a topic of high interest within the field of power system research [19]. The first PMU prototype was developed at Virginia Tech in 1988, and based on this prototype a company started building a commercial PMU. The commercial PMU had a number of innovations implemented such as an internal GPS receiver, 16-bit analog-to-digital converter for each analog input. At the time, a large number of these units were installed around the world [19].

The developments at the time in the field of power system data acquisition as well as the emphasis on the future system development showed the need of a standard way of integrating measurement systems in the substations. Therefore, the first PMU standard, the IEEE 1344 was completed in 1995 [20]. Its scope was to address synchronization of data sampling, data-to-phasor conversions, and the timing formats of the input and phasor data output from the PMUs. It did not define any requirements regarding accuracy, response time, software, hardware or any kind of process for computing the phasors.

A complete revision of the IEEE 1344 was released in 2005 in the form of a new standard, the IEEE C37.118-2005 [21]. This standard dealt with issues concerning the use of PMUs in electric power systems. It defined methods for testing the PMUs and evaluating the measurements. It also defined the requirements under steady-state conditions that the PMUs must meet in order to be compliant. Furthermore, the standard covered the accuracy that the equipment used for PMU calibration should have in order for the results to be trustworthy. The IEEE C37.118 included also the protocol for real-time data communication. However, this standard did not include all factors that a PMU can detect in the power system dynamics.

For the next release, the synchrophasor standard IEEE C37.118-2005 [21] was separated into two parts. The first part is the IEEE C37.118.1-2011, which dealt with the measurement of synchrophasors and the requirements related to the performance of the PMUs [22]. The second part, the IEEE C37.118.2-2011 dealt with the real-time communication of the measured data [23]. The standard was separated into two parts because the technology advanced to a point where the measurement requirements and

communication requirements needed more specialized treatment, and the separation facilitates the collaboration with the International Electrotechnical Commission (IEC) standards [24].

The IEEE C37.118.1-2011 identifies two types of requirements for the PMUs: requirements under steady-state and under dynamic conditions. This ensures that the compliant PMUs are able to measure dynamics of the power systems, such as oscillations, or frequency ramps, within the required range of accuracy. Furthermore, the standard defines two performance classes for the PMUs. The measurement or M-class, where the accuracy of the measurements is more important than the processing speed. And the protection or P-class, in which fast reaction and measurements are more important than a high accuracy. Hence, each class has different accuracy requirements. The amendment IEEE C37.118.1a-2014 to this standard was released in 2014, and it was relaxing some of the accuracy requirements [25].

Validation of the PMUs is a topic of high interest since the measurements need to be accurate in order to be used in power system monitoring and control applications. Therefore, a number of publications have tested and compared the performances of different PMUs. Also, different test setups used for the calibration of the PMUs have been proposed. A comparison between four commercial PMUs from different vendors is shown in [26]. At the time of this publication, the IEEE 1344 standard was still active meaning there were no accuracy requirements defined. Three tests were set up to compare the units: balanced three phase voltages, balanced three phase currents, both at nominal frequency, and unbalanced (single phase) voltage at off-nominal frequencies. The voltages and currents were generated by a three phase variable source. The publication concluded that the measurements produced by the PMUs could be used if the power system would be in a steady-state with slowly varying dynamic conditions and a fundamental frequency. However, once the measured signals were no longer at their nominal value, the PMUs would produce inaccurate measurements which could not be used together. The study also acknowledged the need for the following PMU standards accuracy requirements.

In [27] four different PMUs are tested under the 2005 standard [21]. The test setup consists of a relay test set which is synchronized to the GPS and can generate the test signals that are injected in the PMUs. The resulting PMU output is then compared with the reference value. This publication represents an important step towards standardized testing of the PMUs by proposing a way of creating the test signals and providing details about the hardware which is accurate enough for calibrating PMUs. The authors point out a negative aspect of their study: they found that in some cases the PMUs were more precise than the test set and that corrections might be necessary in order to assure the validity of the results.

A more complex PMU test system was implemented at the National Institute of Standards and Technology (NIST) [28]. It is based on generating the test signals, amplifying them, and injecting them into the tested PMUs. The injected signals are also re-acquired by the test setup and used to create the reference values to which the PMU output is compared.

PMU calibration setups similar to the one presented in [27], have been implemented and mentioned in a number of publications [29] - [35], showing that this setup can be easily implemented and provides enough accuracy for testing PMUs. Setups similar to the NIST setup [28], have been used in studies like [36] - [38].

It is generally found in these studies that the tested PMUs perform well under the steady-state conditions, but fail different tests under the dynamic conditions. It should be noted that most of the tested PMUs were built before the 2011 standard [22] was released, thus, the PMUs could have lacked the necessary algorithms to produce accurate measurements under dynamic conditions. It will be exciting to see the new generation of PMUs which should be compliant with the newest requirements.

1.2.2 Impact of wind turbines and wind power plants on Small-Signal Stability

The installed capacity of wind power has been increasing rapidly in the last years [39]. Consequently, large wind power penetration can have a significant role and impact on the security and operation of the power system [40], [41]. The effect of large wind power plants (WPPs) on small-signal stability and power system oscillations is a topic of high interest and has been investigated in a number of publications. The influence on power system oscillations of wind turbines (WTs) based on fixed speed induction generators (FSIG) and doubly-fed induction generators (DFIG) is investigated in [42], [43]. The authors of [42] found that both configurations contribute positively to the damping of inter-area oscillations, with a higher contribution from the FSIG WPPs. In [43] it is concluded that WPPs based on FSIG turbines tend to improve the damping of the inter-area oscillations. Several operating scenarios for DFIG integration into a small system are studied in [44]. It is found that the DFIGs have a positive contribution to the damping of the inter-area oscillations in most of the cases; the study shows that negative impact is obtained in certain scenarios.

WPPs based on full-scale converter interfaced WTs (FSCWTs) are included in the comparisons in [45], [46]. The authors of [45] found that the WPP based on FSCWT decreases the system damping, while the DFIGs do not have any significant impact on the damping. In [46] it is concluded that the impact on damping of WPPs based on

DFIGs of FSCWTs is identical, and that FSIG WPPs tend to improve the damping of the system. The impact on small-signal stability of WPPs based on only FSCWTs is investigated in [47]. In this paper the comparison is based on a validated dynamic model of a 3.6 MW Siemens Wind Power WT which includes all the relevant controllers for the WT to be operated in the actual power system. A number of scenarios with different wind power penetration are investigated on a seven-generator, 18-node power system model. For each scenario, the power flow in the system is kept constant in order to assess only the impact the WPP has on the damping of the power system oscillations. The study concludes that the power system oscillations are largely unaffected by different wind power penetrations level, and that there is a general decoupling between the WT mechanical system and the grid dynamics due to the power converter.

In [48] the authors investigate the effect of increased DFIG wind power penetration on a five area system. They conclude that the damping of the power system oscillations is highly dependent on which synchronous machines are removed from the system. The modal characteristics of the power system are significantly affected if generators that are dominant in the stabilization of certain modes are disconnected from the system.

The WTs that use a power converter typically function in a voltage/VAR control mode. Therefore, a number of publications investigated the effect of the WT voltage/VAR controller on the damping of inter-area oscillations. The impact on small-signal stability for DFIG in voltage/VAR control mode is investigated in [49]. It is found that in general a higher wind power penetration improves the damping of the inter-area oscillations, and that there are cases in which negative interactions are encountered. However, these negative interactions can be avoided with proper tuning of the controllers. A comparison between the voltage and power factor controlled is given in [50]. The study found that the voltage control contributes positively to the damping of the power system oscillations following the loss of a power plant.

1.2.3 Wind turbine control for Power Oscillation Damping

Converter interfaced WTs offer the possibility of controlling the active and reactive power outputs independently. This advantage makes it possible to modulate their active and reactive power outputs to help improve the damping of the power system oscillation. The idea of using converter interfaced units to improve the damping of the oscillation exists as a concept for approximately 40 years. An algorithm for modulating the active power of the Pacific HVDC Intertie was described in 1976 [51]. Later, in 1993, it was proposed to modulate both active and reactive powers of a HVDC to help damp oscillations [52].

A number of publications have investigated the impact on oscillation damping of WTs or WPPs equipped with power oscillation damping controller (POD). In [53] – [60] the POD was used to modulate the active power output (ΔP POD), while the modulation of reactive power output (ΔQ POD) was proposed in [59] – [62]. Using a combination of active and reactive power modulation was investigated in [44], [59], [60], [63] – [65]. Most of these studies have used aggregated WPP models and generally small test systems for investigating the effect of PODs on modal damping. A large power system model with more than 22 000 buses and 3104 synchronous generators is used in [62], [66] together with an aggregated WPP. In [62] it was investigated how to mitigate the impact of reduced inertia in power systems by controlling the DFIG torque reference. The study found that the small-signal stability is also improved form this control.

The study in [67] is based on a power system model with 14-generators which is divided in five areas. The study compares the results of using a WPP with detailed WT models and WPPs with a different number of aggregated WTs. The detailed model consists of 150 wind turbines, and the aggregated models use 19 WTs, three WTs, and finally a single aggregated model where the WPP is represented by one upscaled WT. The WTs are based on full scale converters and are equipped with either ΔP POD, or ΔQ POD. The study concludes that overall both controllers have similar performance, and the ΔP POD is less sensitive to the location of the WPP than a ΔQ POD which makes it a more attractive option. It is, however, noted that the active power modulation would have a higher impact on the mechanical system of the WTs than the reactive power modulation. Another conclusion is that the same contribution to the modal damping was obtained with all level of aggregation which is very important for practical power system studies.

The PODs used in the above publications are similar to the conventional power system stabilizer (PSS), consisting of a gain block, a washout filter, and a phase compensation stage represented by lead-lag blocks. Local measurements are used as input signal for the PODs.

The study in [47], [67] uses the residues of the eigenvalues of the system in order to properly tune the POD. The residue is the first order sensitivity to an eigenvalue for the feedback between the system output and input. The residue angle gives the necessary phase compensation to provide a positive damping contribution. The magnitude of the residue gives an indication of the move of the eigenvalue in the complex plane. Other publications that use this approach include [61] and [56]. The residues are also used when choosing the input/output signals in order to achieve optimal performance and robustness for a range of operating conditions of the power system. Another approach to achieve good levels of damping performance from the WPP considering a large number of operating conditions is based on particle swarm optimization. This is investigated in

[68] with the aim to achieve robust tuning of a POD based on phase compensation filters.

A different approach for damping inter-area oscillations was proposed and implemented in the early 2000s [69], [70] and the POD was named the Phasor POD. The approach was based on the idea that an oscillation has an average component and an oscillatory component, and these could be estimated provided that they are slow varying. Once the two components were obtained, it was easy to create a damping signal with any phase shift desired. This method was implemented in a thyristor controlled series compensator (TCSC) and installed in the Brazilian North-South Interconnection [71] and has shown good results. The concept was further developed to obtain an adaptive phasor POD which can use data from PMUs and WAMS instead of local measurements to produce the damping signal [72] and [73]. Furthermore, the proposed phasor POD has the ability to compensate for communication time delays, and can track the appropriate phase shift to achieve the proper damping of the power system oscillation.

The authors have also published a paper that addresses some challenges that the phasor POD can encounter [74], and was concluded that it has difficulties in extracting the information of the oscillatory modes when more than one are present in the measured signal. Another type of adaptive POD for TCSC was proposed in [75] where the oscillations are detected with the Kalman filtering method from [76], and the parameters of the POD are updated at each time step. The results presented in [75] show that a TCSC using fixed parameters fails to stabilize a power system that is operating at an off-nominal condition, while the adaptive POD does manage to stabilize the power system. A comparison between a conventional type POD and the adaptive POD proposed in [76] was shown in [77]. The PODs are used for a static VAR compensator (SVC), and a number of contingency scenarios are investigated. Wide-area measurements based on PMUs are used as inputs for both PODs in the study. It is concluded that both PODs have similar damping performance, and the adaptive POD requires a slightly higher control effort. These adaptive PODs are attractive options to manage the continuously changing and unknown operating conditions of the power system. However, it is clear that the performance of these controllers depends on the ability to correctly identify the system dynamics to which the POD is supposed to react.

1.3 Contributions

In the following, the main contributions of the presented work are listed:

- *The development of PMU test methods according to the latest standard*: A complete testing method has been developed and implemented. It consists of the necessary software to create the signals

that are used to test different aspects of the performance of the PMUs. The tests cover the steady-state requirements and the dynamic requirements defined in the standard.

- *Development of the Synchrophasor Analysis Software*: The software uses the data retrieved from the Phasor Data Concentrator (PDC) to analyse the performance of the tested PMUs. The software can compensate for different offsets in the hardware (e.g. time delay offsets, signal amplitude offsets).

- *Test PMU compliance under the IEEE C37.118.1a™-2014*: Three commercial PMUs were tested under the steady-state and dynamic conditions defined in the current standard. The tests revealed that these PMUs were not fully compliant with the requirements.

- *Investigate PMU performance under interference conditions*: The PMUs are tested under impairments which could be seen in operating power systems and are not covered by the current standard. Three scenarios are considered in this case: signals with high noise, multiple harmonics and instrument transformer saturation. These tests helped quantify the point at which the impairments limit the measurements accuracy. This information can be helpful in specifying new requirements and performance limits in future PMU standards.

- *Development of a Type 4 Full-scale converter wind turbine model*: The wind turbine model can be upscaled to represent a large WPP. The model can be linearized with the available tools in Matlab/Simulink platform and modal analysis ca be performed on it. Furthermore, the WT is represented as a phasor model and it is feasible to be used in time domain simulations that can be quite long when low frequency power system oscillations are studied.

- *Implementing a phasor POD to be used with the WPP model:* The phasor POD has been used before with FACTS devices (TCSC, SVC) to damp power system oscillations. In this PhD project, it is proposed to equip the WPPs with such a controller in order to improve the damping of the inter area oscillations. PMU measurements are used as input signals and communication latency is considered. It is shown that the phasor POD can perform well with/without latency in the input signal. A comparison is provided between the phasor POD and a conventional PSS type controller.

1.4 Thesis structure

In this section the thesis structure is introduced to provide the reader with an overview of the chapters. The project is based on a number of scientific publications which are attached to the thesis in the appendix as papers A to E. Throughout the report these papers will be referred where it is needed.

The background of the project, the state-of-the art on: PMU technology, impact of WTs on small-signal stability, and the control of WTs for power oscillation damping were presented in the prior sections. The introductory chapter is concluded with a listing of the main contributions made by the PhD project and the description of the thesis structure.

The second chapter presents an overview of the linear and eigenvalue analysis for small signal stability assessment.

The third chapter presents the development of the test methods for PMUs and the results obtained from steady-state and dynamic tests conducted on three commercial PMUs.

The fourth chapter presents the PMU performance under interference conditions and presents a summary of the results obtained from the three test scenarios.

The fifth chapter deals with the WPP based on full-scale converter.

The sixth chapter presents the impact of the WPP equipped with either the phasor POD or the conventional PSS on the inter-area oscillations.

The seventh chapter concludes the thesis.

2
OVERVIEW OF LINEAR ANALYSIS METHOD

Power system modelling and the use of eigenvalues for analysing power system oscillations are well described in literature [15], [17]. This chapter presents the fundamental concepts for small-signal stability used in this work.

2.1 Power system modelling

The dynamic behaviour of a power system can be described by a set of nonlinear ordinary differential equations [17]:

$$\dot{x} = f(x, u, t) \tag{2.1}$$

with

$$x = \begin{bmatrix} x_1 \\ x_2 \\ \vdots \\ x_n \end{bmatrix} \qquad u = \begin{bmatrix} u_1 \\ u_2 \\ \vdots \\ u_r \end{bmatrix} \qquad f = \begin{bmatrix} f_1 \\ f_2 \\ \vdots \\ f_n \end{bmatrix} \tag{2.2}$$

where n is the order of the system, r is the number of inputs, the column vector x is the state vector, and its elements $x_i \; with \; i = 1,2 \ldots n$ are the state variables. Time is represented by t, and $\dot{x} = dx/dt$. The column vector u contains the inputs to the system which are external signals that influence the performance of system. When the derivatives in (2.1) are not explicit functions of time, the system is said to be autonomous and (2.1) becomes:

$$\dot{x} = f(x, u) \tag{2.3}$$

In power system studies, generally the signals which can be observed are of interest. They are considered output variables and can be expressed in terms of the state variable and input variables as [17]:

$$y = g(x, u) \tag{2.4}$$

with

$$y = \begin{bmatrix} y_1 \\ y_2 \\ \vdots \\ y_m \end{bmatrix} \qquad g = \begin{bmatrix} g_1 \\ g_2 \\ \vdots \\ g_m \end{bmatrix} \tag{2.5}$$

where the column vector y contains the m number of output variables, and g is a vector of nonlinear functions that relates the output variables to the state and input variables.

The power system expressed in the form of (2.3) and (2.4) is suitable for time domain simulations. In order to perform modal analysis on the power system, it is desired to simplify the expression of the system. This is achieved by linearizing (2.3) around an equilibrium point (x_0, u_0) for which $\dot{x}_0 = 0$. Since only small perturbations are considered in small-signal stability, the nonlinear functions in (2.3) can be expressed in terms of Taylor's series expansion. For a detailed description on how this is achieved, the reader is kindly referred to [17]. The partial derivatives obtained from the Taylor series expansion can be written as follows [17]:

$$A = \begin{bmatrix} \frac{\partial f_1}{\partial x_1} & \cdots & \frac{\partial f_1}{\partial x_n} \\ \vdots & \ddots & \vdots \\ \frac{\partial f_n}{\partial x_1} & \cdots & \frac{\partial f_n}{\partial x_n} \end{bmatrix} \qquad B = \begin{bmatrix} \frac{\partial f_1}{\partial u_1} & \cdots & \frac{\partial f_1}{\partial u_r} \\ \vdots & \ddots & \vdots \\ \frac{\partial f_n}{\partial u_1} & \cdots & \frac{\partial f_n}{\partial u_r} \end{bmatrix}$$

$$C = \begin{bmatrix} \frac{\partial g_1}{\partial x_1} & \cdots & \frac{\partial g_1}{\partial x_n} \\ \vdots & \ddots & \vdots \\ \frac{\partial g_m}{\partial x_1} & \cdots & \frac{\partial g_m}{\partial x_n} \end{bmatrix} \qquad D = \begin{bmatrix} \frac{\partial g_1}{\partial u_1} & \cdots & \frac{\partial g_1}{\partial u_r} \\ \vdots & \ddots & \vdots \\ \frac{\partial g_m}{\partial u_1} & \cdots & \frac{\partial g_m}{\partial u_r} \end{bmatrix} \tag{2.6}$$

The linearized system is expressed in the classical state-space form as:

$$\begin{aligned} \dot{x} &= Ax + Bu \\ y &= Cx + Du \end{aligned} \tag{2.7}$$

Where $x^{n\times 1}$ is the state vector, $u^{r\times 1}$ is the input vector, and $y^{m\times 1}$ is the output vector. The system state matrix is given by $A^{n\times n}$, the input matrix is $B^{n\times r}$, the output matrix is $C^{m\times n}$, and $D^{m\times r}$ is the feed forward matrix.

2.2 Eigenvalue Analysis

The dynamic performance of the power system can be analysed by calculating the eigenvalues of the system state matrix A. The eigenvalues are given by the values of the scalar parameter λ:

$$A\phi_i = \lambda_i \phi_i, \qquad for\ i = 1,2,\dots,n \tag{2.8}$$

where the ith eigenvalue, λ_i, is the solution of

$$\det(A - \lambda_i I) = 0 \tag{2.9}$$

In (2.9) $\phi_i^{n\times 1}$ is the right eigenvector for the ith eigenvalue, and I is the identity matrix. The left eigenvector is denoted by ψ and is defined as

$$\psi_i A = \lambda_i \psi_i, \qquad for\ i = 1,2,\dots,n \tag{2.10}$$

The left and right eigenvectors are grouped in two matrices in order to make it convenient to work with all n eigenvalues:

$$\Phi = [\phi_1 \quad \phi_2 \quad \dots \quad \phi_n] \tag{2.11}$$

$$\Psi = [\psi_1^T \quad \psi_2^T \quad \dots \quad \psi_n^T]^T \tag{2.12}$$

The eigenvalues $\lambda_1, \lambda_2, \lambda_3, \dots, \lambda_n$ are grouped as diagonal elements in the diagonal matrix Λ. Following the grouping of the eigenvectors and eigenvalues it can be observed that:

$$A\Phi = \Phi\Lambda, \ \ \Psi\Phi = \mathrm{I}, \ \text{and}\ \Psi = \Phi^{-1} \tag{2.13}$$

A new state vector z is defined in order to eliminate the cross-coupling between the state variables in the original state vector x [17]. The new state vector relates to the original one in the transformed coordinates as follows:

$$x = \Phi \mathrm{z} \tag{2.14}$$

Substituting (2.14) in (2.7) and premultiplying by Φ^{-1} the state-space system in the transformed and decoupled coordinate z is obtained:

$$\begin{aligned} \dot{z} &= \Lambda z + B'u \\ y &= C'z + Du \end{aligned} \tag{2.15}$$

The time response of the ith state variable given in terms of left and right eigenvectors ψ_i, and ϕ_i, eigenvalues λ and the initial conditions for the state vector denoted by x(0) is:

$$x_i(t) = \phi_{i1}\psi_1 x(0)e^{\lambda_1 t} + \phi_{i2}\psi_2 x(0)e^{\lambda_2 t} + \cdots + \phi_{in}\psi_n x(0)e^{\lambda_n t} \qquad \textbf{(2.16)}$$

The stability of the system can be analysed with the help of eigenvalues which contain important information in terms of frequency and damping of the oscillatory modes present in the system. The time dependent characteristics of an oscillation corresponding to an eigenvalue λ_i are given by $e^{\lambda_i t}$. If the ith eigenvalue is $\lambda_i = \sigma \pm j\omega$ then the following information can be extracted:

The damped frequency of oscillation:

$$\omega_d = \mathrm{Im}(\lambda_i) = \omega \left[\frac{rad}{s}\right] \qquad \textbf{(2.17)}$$

The damping ratio of the oscillation:

$$\zeta = \frac{-\sigma}{\sqrt{\sigma^2 + \omega^2}} \qquad \textbf{(2.18)}$$

And the natural oscillation frequency:

$$\omega_n = \sqrt{\sigma^2 + \omega^2} \qquad \textbf{(2.19)}$$

It is know from classical control theory of continuous and time invariant systems that a mode corresponding to an eigenvalue λ_i is stable only if the real part of the eigenvalue is negative, that is $\sigma < 0$ [78]. The stability properties of an eigenvalue are shown in Figure 2.1 to Figure 2.5. It can be seen that when the eigenvalue has only a real part, the time response will either decrease if its value is negative, or increase if its value is positive.

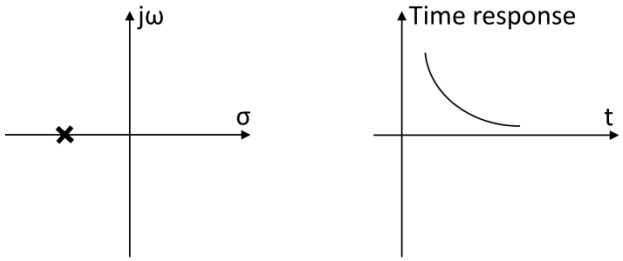

Figure 2.1: Negative real eigenvalue

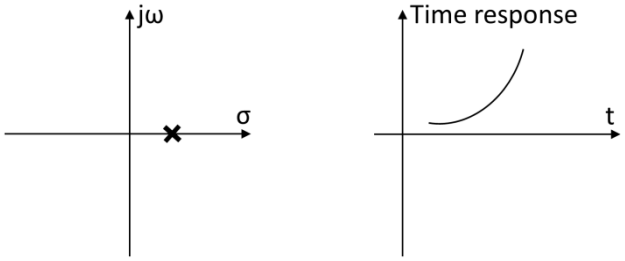

Figure 2.2: Positive real eigenvalue

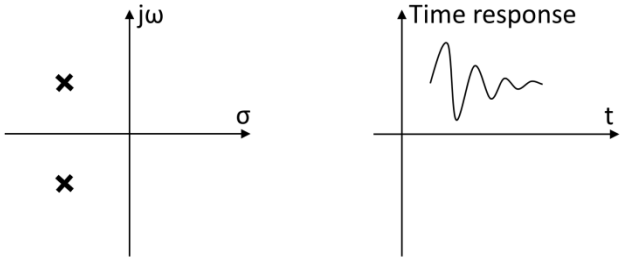

Figure 2.3: Negative complex eigenvalues pair

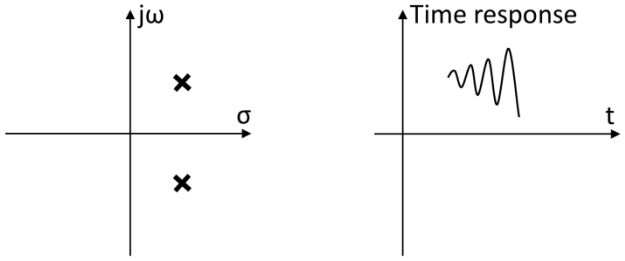

Figure 2.4: Positive complex eigenvalues pair

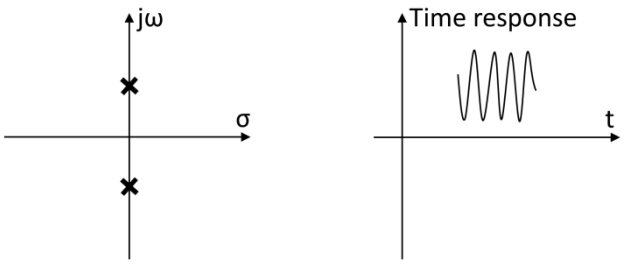

Figure 2.5: Complex eigenvalues pair on the *jω* axis

When the eigenvalue is complex it will always have a complex conjugate and together will form a pair $\lambda = \sigma \pm j\omega$. In this case the time response is an oscillation with amplitude that is decreasing when the complex pair is positioned in the left half of the complex plane as shown in Figure 2.3.When the eigenvalue pair is in the right half plane the amplitude is increasing, as shown in Figure 2.4. The oscillation amplitude remains constant when the eigenvalue pair is on the imaginary axis as shown in Figure 2.5.

In addition to the information provided by the eigenvalues, the left and right eigenvectors also contain important information about the analysed system. The right eigenvector ϕ_i describes how the activity of the ith mode is shared between the state variables, and the left eigenvector ψ_i is a measure of the contribution of the state variables on the ith mode. The product of the two eigenvectors gives the participation factors which are a measure of the importance of the state variables within the individual modes. The participation factors are calculated as follows:

$$\mathrm{p_i} = [\phi_{1i}\psi_{i1} \quad \phi_{2i}\psi_{i2} \quad \cdots \quad \phi_{ni}\psi_{in}] \qquad \textbf{(2.20)}$$

It is important to mention that the eigenvalue analysis is valid only in the region of the operating point where the system was linearized. Because power systems are nonlinear in general, a change in the operating point (due to a line trip, generator trip, change in power flow, etc.) requires the system to be linearized around the new operating point in order to correctly analyse the eigenvalues.

2.3 Numerical example

An example is presented in this section in order to illustrate the theoretical concepts presented in the previous section. The four-machine, two-area system from [17] displays some fundamental properties with respect to power system oscillations. The four generators are separated in two areas which are connected by a 220 km weak intertie line. The system has three electromechanical modes, two local modes between G_1 and G_2 in area 1, and G_3 and G_4 in area 2, and one inter area mode where generators $G_{1,2}$ oscillate against generators $G_{3,4}$.

The cases where the system is stable and unstable are shown in the following subsections. The electromechanical oscillations are excited by a 5% step in the excitation voltage reference of generator G_1, and the rotor speeds are plotted. The complex plane showing the eigenvalues of the three modes are also shown.

2.3.1 Stable case

In the stable case, there is sufficient damping for the oscillations to die out and for the system to reach its steady state after the disturbance as shown in Figure 2.6. The local area mode between G_1 and G_2 is excited by the disturbance, after which the inter-area mode dominates the response.

Figure 2.7 shows the eigenvalues of the linearized system. The local modes are marked with red circles and the inter-area mode with green circles. It can be seen that the system is stable since all eigenvalues are in the left half plane. The lines in the superimposed grid mark the constant damping ratios and frequencies. It can be seen that the frequency of the inter-area mode is around 0.6 Hz, and the damping ration of the mode is 0.17.

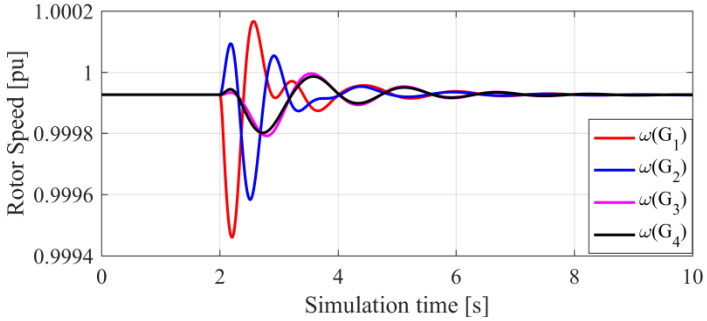

Figure 2.6: Rotor speeds in stable case

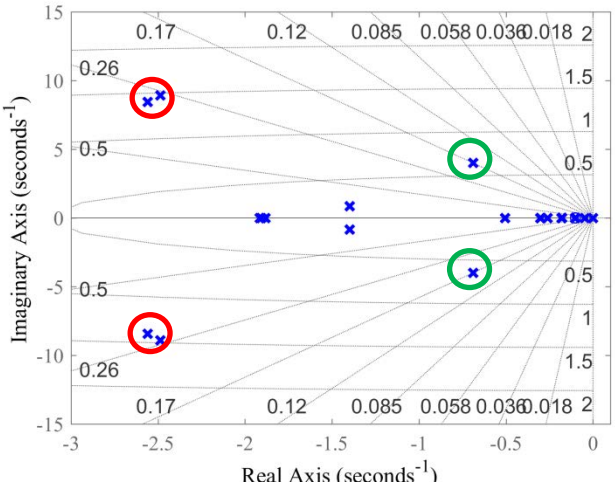

Figure 2.7: Eigenvalues in the stable case

2.3.2 Unstable case

In the unstable case, the oscillations in the rotor speeds will continue to increase after the disturbance unless action is taken by the power system protection system to restore the steady state. Figure 2.8 shows the generators rotor speeds. It can be noticed that the amplitude of the inter-area oscillations is increasing after the disturbance.

The eigenvalues of the power system are shown in Figure 2.9. It can be seen that the eigenvalues of the inter-area mode (marked with green circles) are on the right half plane, confirming that the inter-area mode is unstable in this case.

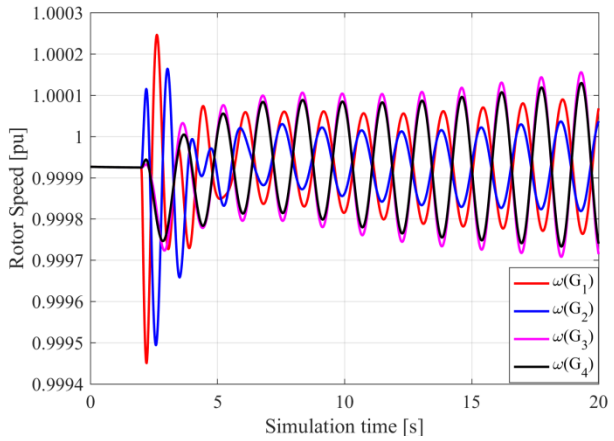

Figure 2.8: Rotor speeds in the unstable case

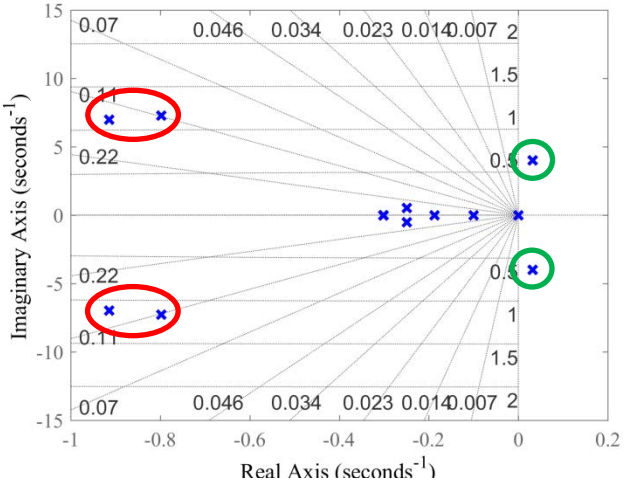

Figure 2.9: Eigenvalues in the unstable case

3
PHASOR MEASUREMENT UNITS TEST METHODS

In this chapter the development of the Phasor Measurement Unit (PMU) test methods, the analysis software, the laboratory setup and the test results are described. The IEEE Standard [22] and the IEEE Amendment [25] define the steady-state and dynamic requirements the PMU should satisfy in order to be compliant. The details and the results for both steady-state and dynamic conditions can be found in the Appendices A and B.

3.1 PMU testing architecture and test method

The first PMU standard, the IEEE 1344 [20], was completed in 1995, and a complete revision to it was the IEEE C37.118-2005 [21] which focused on the issues concerning the use of PMUs in the power system. However, the 2005 standard did not address the capability of phasor measurement units to detect power system dynamic activity. The next release was the IEEE C37.118.1-2011standard [22] which defined the requirements for PMUs measurements in steady-state and dynamic cases. This standard classified the devices in two categories, M-measurement class and P-protection class.

The M-class requires the PMUs to produce measurements with higher accuracy, and defines the required waveforms to test conditions that include various ranges for magnitude, phase angle and signal frequency as well as levels of harmonics and out-of-band signals that should be filtered out. It is intended for applications that require accurate measurements, but do not require minimal delay. The P-class relaxes the accuracy requirements because it is intended for applications requiring fast response [22].

The testing method is based on the generation of the waveforms required by the IEEE C37.118.1 standard, application to the PMU and comparison of the reported PMU data with the expected result. These waveforms are generated with the help of any mathematical computing language (e.g. Matlab), and are converted into a format that can be used with a GPS synchronized test set. In this case the IEEE C37.111-1999 COMTRADE [82] format is preferred since it is widely used for time series recording

and it is compliant to most vendors. The overall testing process is shown in Figure 3.1. More details can be found in Appendices A and B.

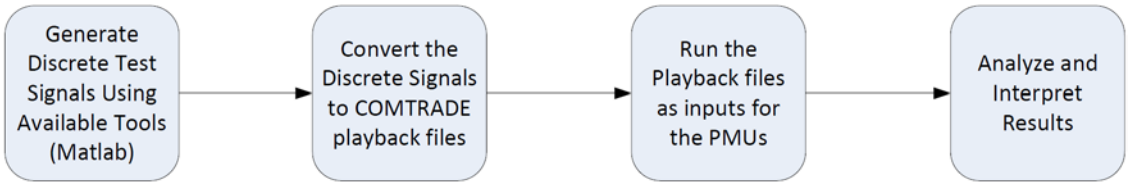

Figure 3.1: Overall PMU testing process

Mathematically, the required waveforms are created starting from the generalized phasor function which can be obtained from a sine function with amplitude and phase modifiers as:

$$X(t) = Xm[g(t)] * \cos(\omega_0 t + y(t)) \quad \textbf{(3.1)}$$

where X_m is the nominal amplitude, ω_0 is the nominal power system frequency, $g(t)$ is the amplitude modifying function and $y(t)$ is the phase modifying function. The IEEE C37.118.1 standard provides the mathematical representation of the phasors for each of the required tests. These are implemented by changing the functions $g(t)$ and $y(t)$ according to the given representation.

The phasor corresponding to the signals created with (3.1) is given by:

$$X(nT) = \left\{\frac{Xm}{\sqrt{2}}\right\}\{g(nT)\}\angle\{y(nT)\} \quad \textbf{(3.2)}$$

where nT is the reporting instant. The phasors measured and reported by the PMUs should be an estimate of $X(nT)$ value at each time instant nT.

3.2 IEEE Std. C37.118.1 Tests Identification

This section gives a brief introduction to the tests defined by the IEEE C37.118.1-2011 standard, describes what capabilities of the PMU each test is supposed to validate, and introduces the acronyms that are used throughout the rest of the report. The tests are split in two main categories, steady-state and dynamic tests.

Steady-state tests are designed to verify the capabilities of the PMUs to measure signals that do not change over time. The following descriptions apply to the M-class performance**:**

- Amplitude scan test (Ascan) – checks the ability of the PMU to correctly measure the amplitude of the input voltage and current over a wide range: 10% to 120% rated voltage; 10% to 200% rated current.

- Phase measurement test (Pscan) – checks the ability of the PMU to correctly measure the signal phase angle by varying the phase all around the circle.

- Frequency Scan test (Fscan) – verifies if the unit is capable of correctly estimating the frequency of the input signals when it is nominal and off nominal, both lower and higher.

- Harmonic Distortion test (Harm) – is aimed at validating the filtering capabilities of the PMU for each harmonic up to the 50^{th}.

- Out-of-band Interference test (Band) – checks the filtering capability of the PMU (filtering all signals that are outside the passband).

Dynamic Compliance tests are designed to evaluate the PMU performance for changing signals. The next descriptions apply to the M-class performance:

- Amplitude Modulation test (Amod) – tests the measurement bandwidth of the PMU when the amplitude of the signal is modulated with frequencies between 0.1 Hz and 5 Hz.

- Phase Modulation test (Pmod) – verifies the measurement bandwidth of the device when the phase is modulated with frequencies between 0.1 Hz and 5 Hz.

- Ramp of System Frequency (Framp) – checks the ability of the PMU to correctly make all the measurements during a ramp of frequency.

- Amplitude Step test (Astep) – checks how quickly the PMU responds to a sudden change in amplitude and that it accurately reports the signal around the change.

- Phase Step test (Pstep) – checks how quickly the PMU responds to a sudden change in phase and that it accurately reports the signal around the change.

3.3 Laboratory test setup

The hardware setup consists of a signal generator, a GPS clock, the PMUs under test and a computer running the Phasor Data Concentrator and any other necessary software. Similar hardware setups have been used before [29] - [35] due to the wide availability of the tools.

The PMU test signals are generated by a standard stand-alone test set intended for protection relay testing. It is capable of delivering 3-phase AC voltages and currents with different amplitudes and phase angles. Another of its capabilities is playing back digitized files by converting the waveforms created to test the PMUs into analog signals and amplifying them. Accurate reproduction of the signals is enabled by the 16-bit, 10 ksamples/s digital-to-analog converter (DAC) and built in amplifiers. The test set has GPS connection available and can provide synchronized start of tests. The vendor rates the synchronization error to be less than $1\,\mu s$. Further details are available in Appendices A and B**.**

A calibration check of the test set is performed in order to investigate the deviation in signal amplitude from the theoretical value and the time synchronization accuracy. The details of the procedure are given in Appendix A and a summary of the findings is available next:

- The amplitude error for Phases A and C is found to be -0.06%, and for Phase B is -0.089%. More details are available in Table II from Appendix A.

- The time synchronization of all three phases is checked. The synchronized test start is found to have a time lag of 142 μs which translates into a phase error of 2.556 degrees. No phase drift in time has been found.

The amplitude error offsets and phase error offset are used as correction factors in the Synchrophasor Test Software in order to obtain a correct comparison between the measured phasors and the theoretical ones.

An external GPS clock is part of the laboratory setup, and is used to synchronize the PMUs that are not shipped with their own antennas, and require and external signal for synchronization. The clock is rated by the vendor with a precision of $1\,\mu s$.

The Phasor Data Concentrator is collecting the data reported by the PMUs under test and archives it. The data is retrieved in CSV format and used with the Synchrophasor Test System for analysis.

3.4 Measurement evaluation

This section outlines how the measurements reported by the PMUs are evaluated. The IEEE C37.118.1 standard defines three quantities as a way of evaluating the performance of the units under test. These are the Total Vector Error (TVE), the Frequency Error (FE) and the Rate of Change of Frequency Error (ROCOF Error).

The equation for calculating the TVE is:

$$TVE = \sqrt{\frac{\left(\hat{X}_r(n)-X_r(n)\right)^2+\left(\hat{X}_i(n)-X_i(n)\right)^2}{\left(X_r(n)\right)^2+\left(X_I(n)\right)^2}} \times 100 \quad [\%] \qquad \textbf{(3.3)}$$

Where $\hat{X}_r(n)$ and $\hat{X}_i(n)$ are the measured real and imaginary parts of the phasor, and $X_r(n)$ and $X_i(n)$ are the real and imaginary parts of the reference phasor at the instance n.

The FE and RFE are calculated as:

$$FE = |f_{true} - f_{measured}| \quad [\text{Hz}] \qquad \textbf{(3.4)}$$

$$RFE = |(df/dt)_{true} - (df/dt)_{measured}| \quad [\text{Hz/s}] \qquad \textbf{(3.5)}$$

In addition to the IEEE standard [22]**,** the IEEE Synchrophasor Measurement Test Suite Specification (TSS) [83] has been published in 2014. This document defines new quantities which are useful when analysing the performance of PMUs and require these values to be provided by the test laboratories. These quantities are the Magnitude Error (ME) in percent and Phase Error (PE) in degrees which are calculated as follows:

$$\mathrm{ME} = \frac{\sqrt{\hat{\mathrm{X}}_\mathrm{r}(\mathrm{n})^2+\hat{\mathrm{X}}_\mathrm{i}(\mathrm{n})^2}-\sqrt{\mathrm{X}_\mathrm{r}(\mathrm{n})^2+\mathrm{X}_\mathrm{i}(\mathrm{n})^2}}{\sqrt{\mathrm{X}_\mathrm{r}(\mathrm{n})^2+\mathrm{X}_\mathrm{i}(\mathrm{n})^2}} \times 100 \quad [\%] \qquad \textbf{(3.6)}$$

$$\mathrm{PE(deg)} = \mathrm{atan}\left(\hat{\mathrm{X}}_\mathrm{r}(n), \hat{\mathrm{X}}_\mathrm{i}(n)\right) - \mathrm{atan}(\mathrm{X}_\mathrm{r}(n), \mathrm{X}_\mathrm{i}(\mathrm{n})) \quad [\mathrm{deg}] \qquad \textbf{(3.7)}$$

Although, FE is defined in [22] as the absolute value of the difference between the theoretical and measured frequencies of the input signal, the TSS document requires the signed value to be reported together with the absolute value. The RFE is required to be reported in a similar way. These requirements are implemented in the Synchrophasor Analysis Software described in Section 3.5.

3.5 Synchrophasor Analysis Software

The data reported by the PMUs is analyzed with a Synchrophasor Analysis Software implemented in Matlab specifically for this purpose. The aim was to obtain a flexible analysis software which can be easily modified and updated. This was achieved by

creating a structure of routines that work together. A diagram of the complete Synchrophasor Test Software is shown in Figure 3.2.

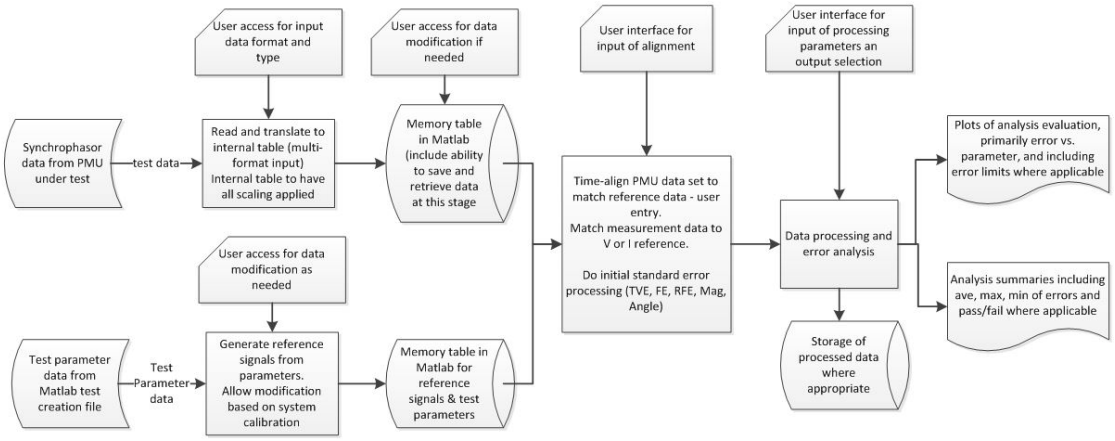

Figure 3.2: Data Flow Diagram for the Synchrophasor Test System

The main parts of the software are:

- Routines capable of loading the reported PMU data in CSV format since it is common for a Phasor Data Concentrator (PDC) to archive data in this format. The test parameter data, which hold information regarding the analyzed test, is loaded at this point. This is used in creating the appropriate reference phasors.

- The main routine which analyzes the data by comparing the reported phasors to the reference ones created with (3.2). If any corrections to the reference phasors are necessary, they are implemented at this stage (i.e. offsets in phasor amplitude and/or phase angle). The measurements are evaluated at this point using (3.3) – (3.7).

- Routines for reporting the evaluation results. The results are evaluated and plots assessing the performance of the PMUs are created at this point. These can be saved for use in reports.

3.6 Steady-state compliance test results

This section shows a selection of results for the steady-state tests conducted on three commercial PMUs from three different vendors. It is important to note that all three PMUs are of an older generation and were not built to be compliant with the IEEE C37.118.1 standard [22].

The tests conducted for this section are summarized in Table 3.1 and they cover the M-class testing requirements. Although the testing architecture and the hardware setup described in Sections 3.3 and 3.5 are perfectly capable of running and analyzing the tests for the P-class, it is more interesting to see the results for the M-class because the tests are built to challenge the PMUs measurement ranges and filtering capabilities. The results shown in this section will focus more on failed tests since these reveal the differences between PMUs better. The reporting rate of all PMUs is set to 50 samples per second, and they are all set to provide the filtering that would correspond to M-class performance.

Table 3.1: Steady-state tests description for M-class requirements

Test name	Varied quantity
Amplitude Scan	Voltage 10% - 120%
	Current 10% - 200%
Phase Scan	Angle $-\pi$ to $+\pi$
Frequency Scan	Frequency 45 – 55 Hz
Harmonic rejection	2^{nd} to 50^{th}
Out-of-band interference	10 – 100 Hz interfering frequencies

Each test consists of segments, and in each segment the varied quantity is kept constant sufficiently long for the transients in the PMUs to settle. For example, in the first test segment the amplitude of the voltage is 10%. In the second test segment, the voltage is increased to 20% and so on. The Synchrophasor Analysis software removes the period of the transients from the measurement evaluation, and only analyzes the steady-state measurement. The reported errors (TVE, FE, RFE) represent only the highest error calculated for each test segment. In this section only the result for the amplitude scan and the out-of-band rejection tests are shown. The results for the remaining tests are available in Appendix A.

3.6.1 Amplitude scan

Figure 3.3 and Figure 3.4 show the performance of the three tested PMUs under the amplitude scan test, for voltage and current respectively. Although all PMUs show high error when measuring low amplitude signals, none of the PMUs exceed the voltage TVE as it can be seen in Figure 3.3. However, Figure 3.4a shows that PMU A and PMU C are failing this test due to poor accuracy when measuring low amplitude currents. PMU A does not produce accurate measurements when currents with low magnitude (0.1 – 0.2 p.u.) are injected into the device. It shows difficulties measuring both amplitude and phase of the injected low current. Figure 3.4b shows the magnitude error to be around -0.5% at 0.1 p.u. The phase angle error is larger than one degree for the

same current level as seen in Figure 3.4c. PMU C is an interesting case because only one of its phase measurements is failing the test. Figure 3.4a shows that phase B exceeds the TVE limit. This is surprising since the PMU should have similar current transformers on all phases, and the phasor estimation method would normally be the same.

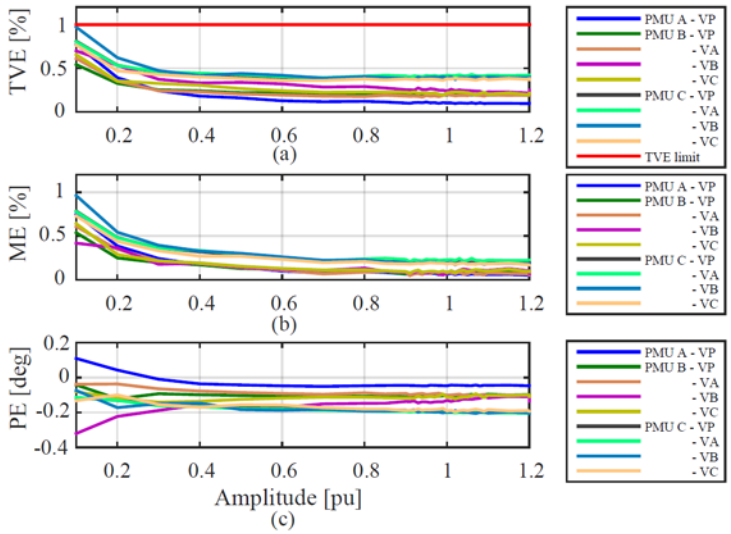

Figure 3.3: Amplitude Scan Voltage Analysis

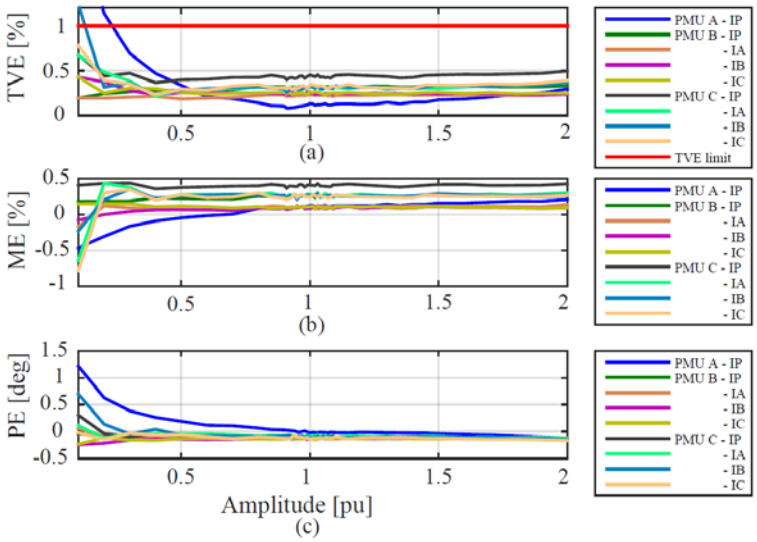

Figure 3.4: Amplitude Scan Current Analysis

3.6.2 Out-of-band rejection

The PMUs capability of rejecting the signals that are outside the pass-band and could alias into the measurements is tested in this subsection. Furthermore, testing at off-nominal frequencies can expose issues with the processing algorithms implemented in

the units. For example, Fourier filters have very high rejection at the fundamental and exact harmonic frequencies, but are less efficient away from these points. If the PMUs use fixed frequency Fourier filters, they might not be capable of properly rejecting out-of-band signals when the power system deviates from nominal. To test this aspect, the IEEE standard requires changing the center frequency of the main signal with an off-nominal frequency that is $\pm$10% of the Nyquist frequency for a given reporting rate. In this case the PMUs are set to report the measurements at 50 samples per second, thus the Nyquist frequency is 25 Hz. Hence, the off-nominal frequency values are 47.5 and 52.5 Hz.

The results of the out-of-band rejection test for the case when the frequency of the main signal is nominal (50 Hz) are shown in this subsection. More results are available in Appendix A.

Figure 3.5 shows the evaluation of the voltage measurements. It can be seen that there is a clear difference in the performance of the PMUs. While PMUs B and C filter the out-of-band signals, PMU A does not have sufficient filtering to fully reject the interfering signals. PMU A exceeds the TVE limit for interfering frequencies above 20 Hz and below 80 Hz as shown in Figure 3.5a. The out-of-band interfering signals have a detrimental effect especially on the phase measurement as shown in Figure 3.5c, which is the reason for the high TVE seen from this PMU.

Figure 3.6 shows frequency error and ROCOF error evaluation. It can be seen that PMU A estimates the frequency of the signal with the required accuracy, while PMUs B and C fail this test as shown in Figure 3.6a. Even though the RFE limit has been suspended by the IEEE amendment [25] for this test, in Figure 3.6b the limit is kept in order to provide a reference for the PMU performance. It can be seen that all devices exceed the limit.

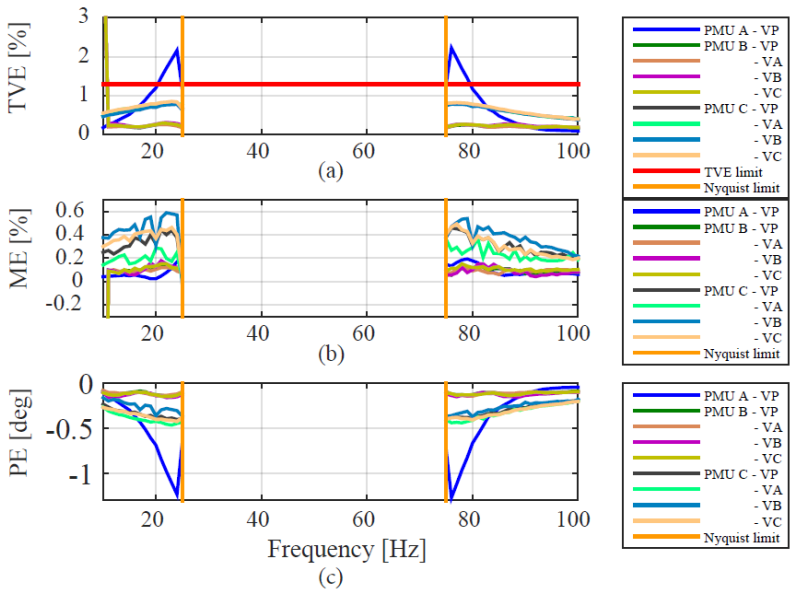

Figure 3.5: Out-of-Band rejection Voltage Analysis (signals frequency f = 50 Hz)

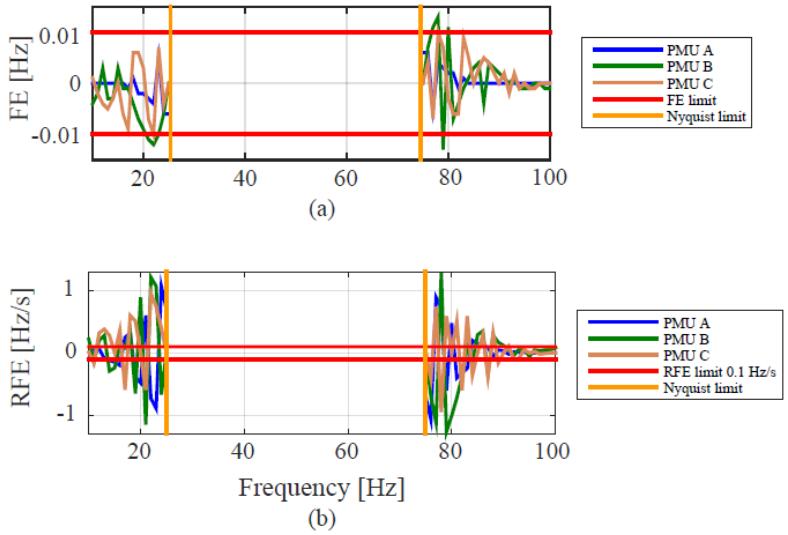

Figure 3.6: Out-of-Band rejection (signals frequency f = 50 Hz)

3.7 Dynamic compliance test results

In this section a selection of results for the dynamic tests conducted on the same PMUs is shown. This set of tests simulates different power system operating conditions such as power system oscillations, generation and load imbalance condition where the frequency can ramp up or down, or steps in the measured signals which could be caused by load switching events. More results are available in Appendix B. A short description of the tests together with the varied parameters is given in Table 3.2.

Table 3.2: Dynamic compliance test description for M-class requirements

Test name	Varied quantity
Amplitude Modulation	Phasor amplitude by 0.1 pu
Phase Modulation	Phasor angle by 0.1 rad
Frequency ramp	Frequency range 45 – 55 Hz; ramp ±1 Hz/s
Amplitude step	±0.1 pu
Phase step	±10 degrees

3.7.1 Amplitude modulation

The measurement bandwidth of the PMUs is determined with this test by modulating the amplitude of the input signals with a sinusoidal waveform. The modulation level of the sinusoidal waveform is specified in the IEEE standard to be 10% of the rated value, which will cause the phasor amplitude to oscillate between 0.9 pu and 1.1 pu. The modulator frequency range is between 0.1 Hz and 5 Hz with step increments of 0.2 Hz. The amplitude of both voltages and currents is modulated, while the phase angles are kept constant.

Figure 3.7 shows that PMU A cannot produce correct measurements over the entire range and fails this test when the modulating frequency is above 4.2 Hz. Figure 3.8 shows the reference phasor and the phasors measured by the PMUs when the modulating frequency in 5 Hz. PMU A fails to correctly measure the amplitude of the signal, while the most accurate is PMU C.

Because the phase of the signal is constant in this test, the frequency and ROCOF estimates are not affected. Hence, FE and RFE are well within limits and the results are available in Appendix B.

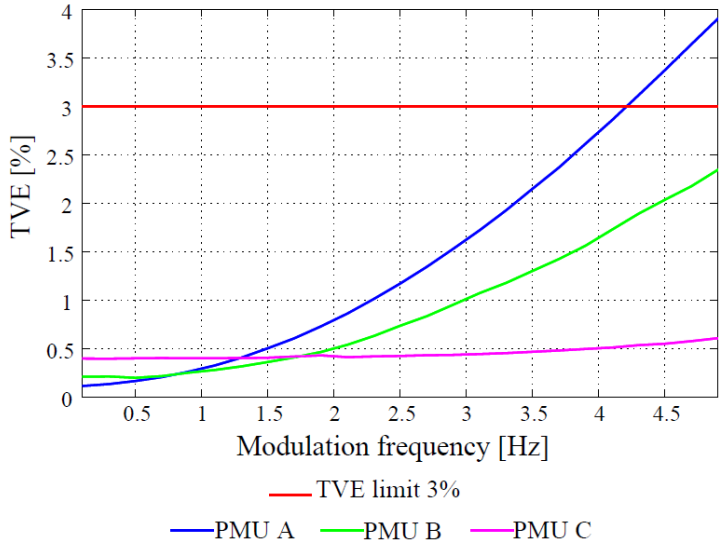

Figure 3.7: Amplitude modulation analysis

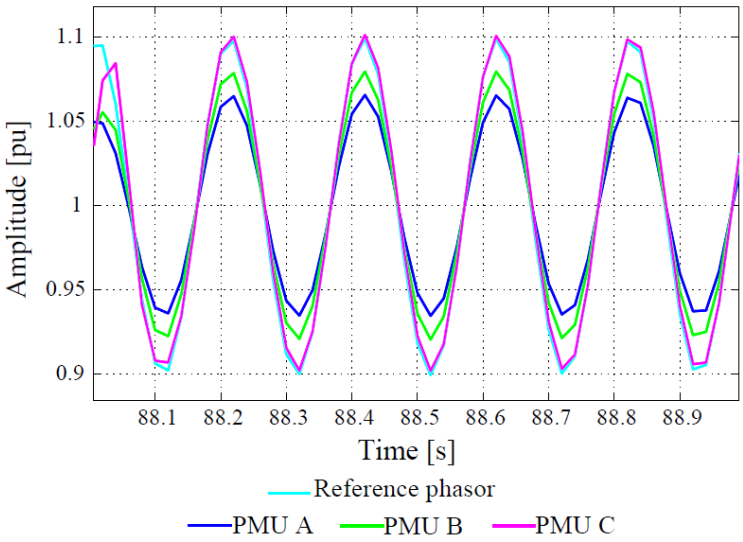

Figure 3.8: Amplitude modulation voltage phasor comparison (reference vs measured)

3.7.2 Phase modulation

The measurement bandwidth of the PMUs is verified also by modulating the phase of the input signals. In this case, the injected voltage and current waveforms have their phase modulated by 0.1 radians as required by the IEEE standard [22]. The same modulating frequency as in the previous test is applied in this case. A change in the phase angle will directly impact the frequency and ROCOF estimations since these are the first and second derivatives of the angle.

The results show that two of the tested PMUs do not have sufficient bandwidth to be compliant with the phase modulation requirements. Figure 3.9 shows that PMU A is exceeding the 3% TVE limit when the modulation frequency is above 4.5 Hz. Figure 3.10 shows a delay between the reference and measured phasor angles, and a difference between the reference and measured amplitude of oscillation which together cause the high TVE value. PMU A fails to correctly estimate the frequency of the injected signals as shown in Figure 3.11, consequently the PMU exceeds the frequency error requirement.

PMU C measures the oscillating phase angle with good accuracy, but it fails to estimate the frequency with the required accuracy when the modulating frequency of the signal is higher than 2.4 Hz as shown in Figure 3.11. The measured frequency is compared to the reference value in Figure 3.12 for a modulating frequency of 5 Hz. It is clear that PMU C fails to correctly estimate the signal frequency which is oscillating at 5 Hz. In fact, this PMU reports almost no oscillation at all.

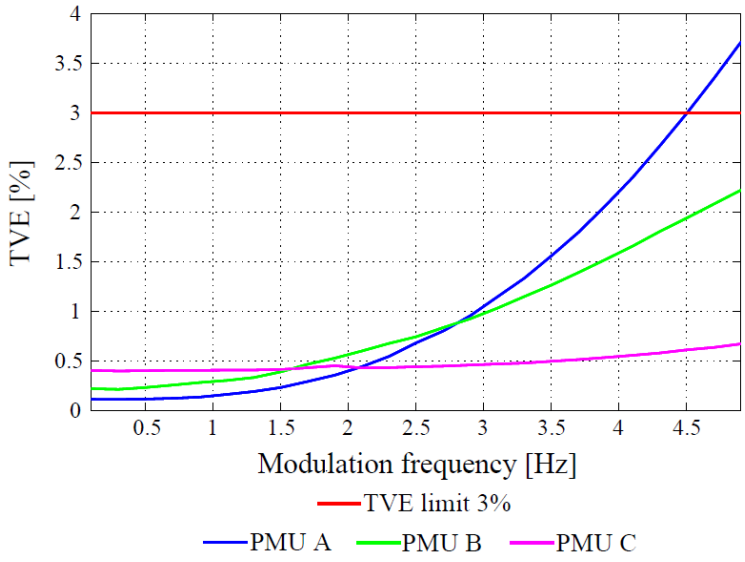

Figure 3.9: Phase modulation analysis

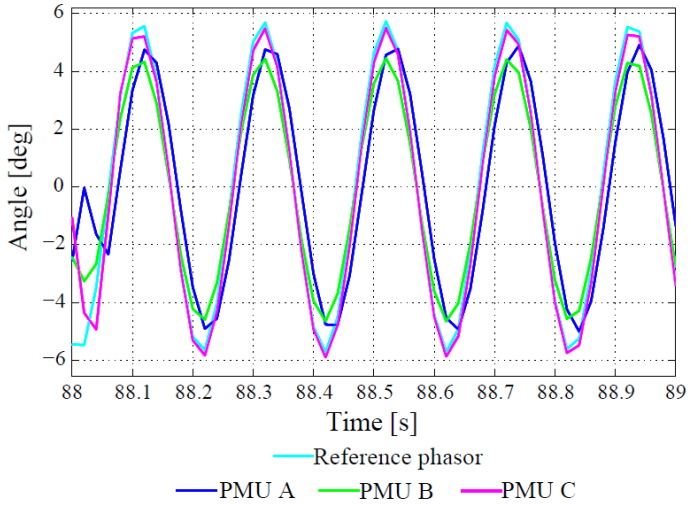

Figure 3.10: Phase modulation: voltage phase angle comparison (reference vs measured)

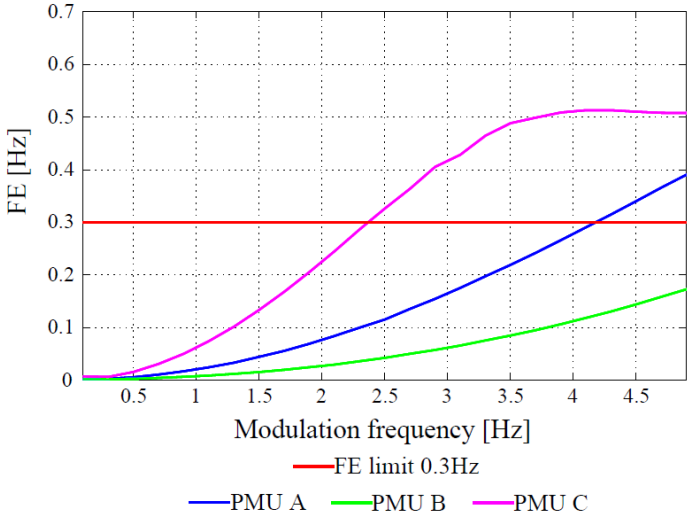

Figure 3.11: Phase modulation: Frequency Error

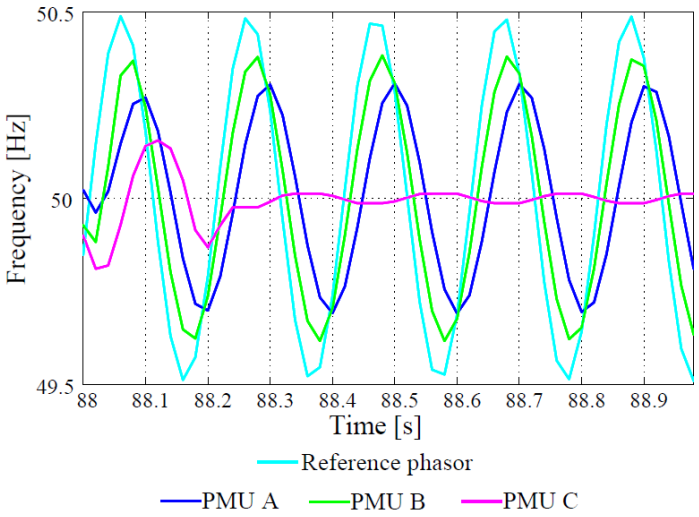

Figure 3.12: Phase modulation frequency comparison (reference vs measured)

3.8 Discussion

For the future power system, observability is of high importance and wide area measurements are needed in order to achieve it. PMUs are one of the key components since they provide time synchronized measurements of the power system operating state. Therefore, it is relevant to know the performance of these devices under different conditions. In this chapter, a laboratory test setup and methodology for testing PMUs was presented. Then, three commercially available PMUs were tested for compliance under the IEEE C37.118.1-2011 standard [22] and the IEEE C37.118.1a-2014 amendment [25]. The tests revealed that these PMUs did not satisfy the requirements to be compliant with the current standard. This was expected since the tested devices belong to an older generation of PMUs which were built before the new standard was published. Hence, it was probable the devices did not have implemented the algorithms needed to be compliant with the new requirements.

The tested PMUs failed tests from both the steady-state and dynamic requirements. It was shown that, for example, some of PMUs did not have sufficient filtering to successfully reject out-of-band interfering signals. Another problem for two of the devices was to correctly measure currents with magnitudes between 0.1 to 0.2 p.u.. The dynamic tests revealed that two PMUs did not have sufficient bandwidth to correctly measure oscillating signals (either amplitude modulated or phase modulated), and these two PMUs also produced incorrect frequency measurements in case of the phase modulation test. The tests also revealed differences in the PMU processing, for example PMU A showed poor filtering of out-of-band signals, while PMU C showed poor frequency estimation for high phase modulating frequencies (f_m > 2.4 Hz).

It can be concluded that older generation PMUs are not compliant with the current requirements because these devices were built before the new standard was released.

Therefore, the PMUs may lack the algorithms that would produce the measurements with the required accuracy. Hence, new products are needed in order to have PMUs that are compliant with the IEEE C37.118.1a-2014 amendment.

However, many of the PMUs currently installed in the power system are of the same older generation as the devices tested in this chapter. An important question is whether the measurements provided by the currently available devices can be used with the methods that have been developed or that are in a developing stage.

4

PHASOR MEASUREMENT UNITS UNDER INTERFERENCE CONDITIONS

This chapter presents the testing of the three commercial PMUs under three scenarios that occur in real power systems and are not covered by the current IEEE standard [22]: high background noise, multiple harmonics and current transformer (CT) saturation. Since these tests are performed on production PMUs, they show the overall performance limitations. Assessing the impacts of all the error contributions in a product that has not been implemented is difficult therefore, having actual results to refer to is essential in order to validate signal models. Standards are based on models and development experience, thus for the standard development cycle it is necessary to have quantified test results. The detailed testing scenarios and results can be found in the Appendix C.

4.1 Gaussian White Noise Test

The influence of white noise on signal acquisition and measurement is a classic problem that has been studied before [84]. Efforts to improve PMU measurement precision under noisy signals have been made [85]. However, the tested commercial PMUs are of an older generation, and they do not benefit from any of the new proposed methods or algorithms. The results of this test are relevant because most of the PMUs currently installed in the power system are also of an older generation, and it can be expected to have similar performance as the ones tested here.

In this test, white noise is added to the fundamental frequency component of the voltage and current waveforms. The Signal-to-Noise Ratio (SNR) is gradually decreased, thus increasing the noise level, and the error is evaluated with (3.3) - (3.7). The results of such an SNR sweep will give a good understanding of the PMU precision under noisy signals.

It was reported by [86] that the SNR at the distribution level is around 60 dB. This value was obtained by collecting and analysing the noise and harmonic content of signals from the distribution grid. This measurement is used as reference point in creating the tests and interpreting the results.

The same method described in Chapter 3.1 is used for creating the test signals which in this case are described by:

$$x(n) = Acos(2\pi(f_0 + \Delta f)nT + \varphi) + w(n) \quad \textbf{(4.1)}$$

Where *A* and φ are the amplitude and initial angle of signal waveforms. The nominal frequency of the signals f_0 is 50 Hz in this case, and Δf is the deviation from the nominal frequency. *w(n)* is the zero mean white noise with the power spectral density PSD of $\rho^2 W/Hz$ [87].

The SNR expressed in decibels (dB) is used to calculate the power of the added noise as:

$$P_{noise,dB} = P_{x,dB} - SNR_{dB} \quad \textbf{(4.2)}$$

where $P_{x,dB}$ is the average power of signal x with *w(n)=0*, and is calculated as [88]:

$$P_x = \lim_{n\to\infty} \frac{1}{2N+1} \sum_{n=-N}^{N} |x(n)|^2 \quad \textbf{(4.3)}$$

where N is the number of sample points of signal x.

The standard deviation used to calculate the term *w(n)* is:

$$\rho = \sqrt{10^{\frac{P_{noise,dB}}{10}}} \quad \textbf{(4.4)}$$

The power system frequency is usually deviating below or above nominal. Testing the PMUs at signals with off-nominal frequencies covers a real power system scenario, and can reveal weaknesses in the PMU processing algorithms. For example, Fourier filters have very high rejection at the fundamental and exact harmonic frequencies. When the power system deviates from nominal frequency, such filters are less efficient and might not give adequate rejection and compromise the accuracy of the measurements. This is tested by changing the center frequency of the voltages and currents. The IEEE standard [22] requires testing out-of-band rejection with an off-nominal frequency that is ±10% of the Nyquist frequency for a given reporting rate. All the tested PMUs are set to report 50 samples per second, and for this rate the Nyquist frequency is 25 Hz and thus the deviation used in these tests is $\Delta f = \pm 2.5$ Hz.

An example of the voltage signal with noise injected in the tested PMUs is shown in Figure 4.1, and the test parameters are summarized in Table 4.1.

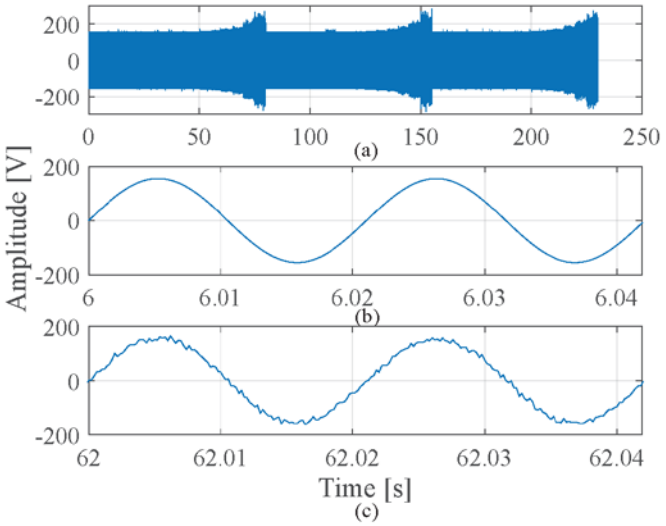

Figure 4.1: Phase A Voltage Signal: (a) envelope of signal showing the increased amplitude at the 3 test frequencies due to the injected noise; (b) detailed view f_0 = 47.5 Hz, SNR = 80 dB; (c) detailed view f_0 = 47.5 Hz, SNR = 25 dB;

Table 4.1: White Noise Test Parameters

V [Vrms]	110		
I [Arms]	5		
f [Hz]	47.5	50	52.5
SNR [dB]	10 - 80 with 5 dB step increments		

4.1.1 White noise test results

The measurement is evaluated according to the IEEE C37.118.1a amendment by calculating the TVE, FE and RFE (3.3)-(3.5). Both this test and the Out-of-Band test defined in IEEE C37.118.1 are evaluating the filtering capabilities of the PMUs. Therefore, the 1.3% TVE, 0.01 Hz and 0.1% RFE limits defined in the standard are used to analyse the measurements for this test.

The voltages and currents TVE show that all devices are within limits for high and medium SNRs. For signal-to-noise ratios around 30 dB and lower, the 1.3% limit is exceeded and the error continues to increase as seen in Figure 4.2.

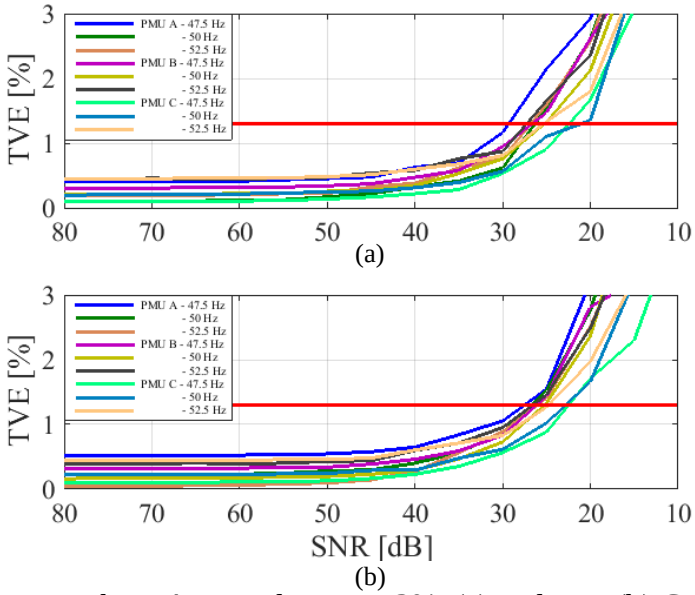

Figure 4.2: Phase A; TVE limit = 1.3%; (a) Voltage; (b) Current

Figure 4.3 shows that the frequency estimation algorithm of the PMUs is more sensitive to noisy signals. It also shows that there is a difference between the processing algorithms of the PMUs since PMU A is more affected by noise exceeding the 0.01 Hz limit at around 45 dB, where the other two devices have an accuracy of 5 mHz.

Figure 4.4 shows that the ROCOF is even more affected by noise, with PMU A being the first to exceed the limit at about 63 dB, while the other two PMUs still meet the requirement at 56 dB.

The overall results show that frequency and ROCOF measurements are more affected by noise which is to be expected since they are the first and second derivatives of the phase angle. It can be concluded that the outcome of the tests specified by the standard will remain unaffected as long as the SNR remains above 65 dB.

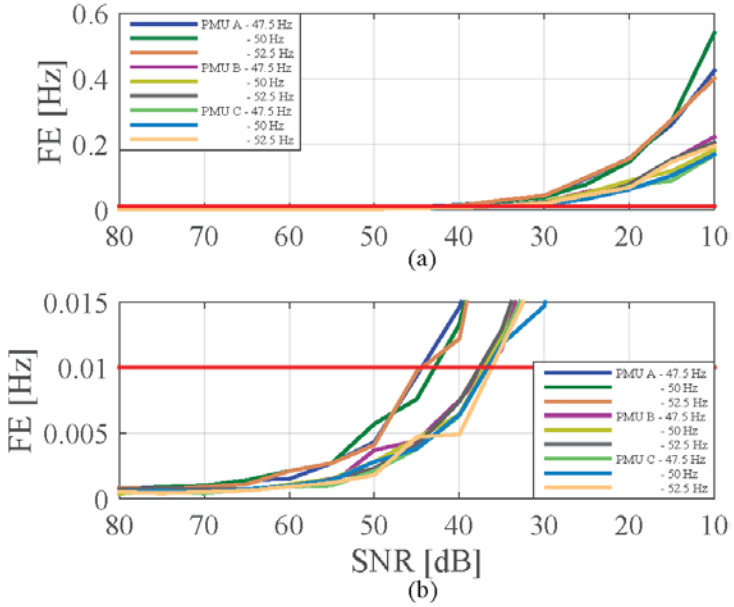

Figure 4.3: Frequency Error; (a) Maximum error; (b) detail of (a) showing the error limit

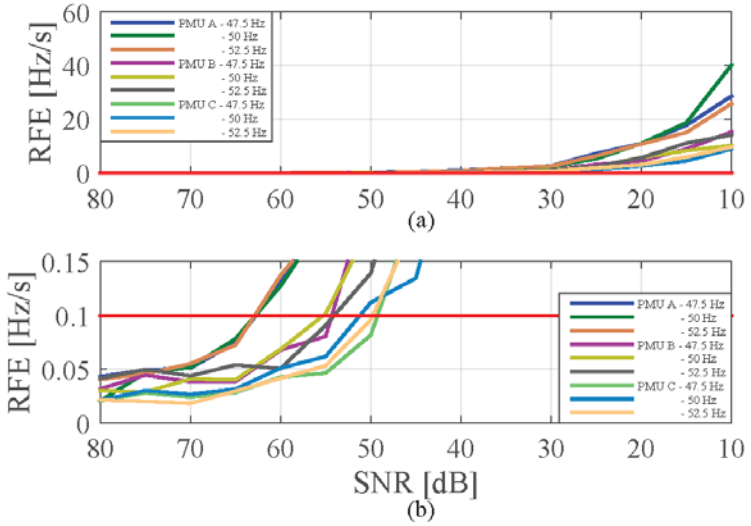

Figure 4.4: ROCOF Error; (a) Maximum error; (b) detail of (a) showing the error limit

4.2 Multiple Harmonics Rejection Test

The IEEE standard [22] requires testing harmonic interference rejection from the second harmonic up to the fiftieth. Power systems often contain multiple harmonics with varying amplitude in both voltages and currents. These may be present in grids with renewable energy such as wind farms, especially with wind turbines with Doubly-Fed Induction Generators (DFIG) and full-load converter configurations [89]. Typically, low order harmonics (5^{th}, 7^{th}, 11^{th}, and 13^{th}) have been reported in [90] for wind parks with DFIG turbines. Another phenomenon that causes multiple harmonics to be present is transformer inrush [91], [92].

For this test, all cases are run both at nominal and off-nominal ($\Delta f = \pm 2.5$ Hz) system frequency to check rejection as described in the previous section. The voltage and current signals injected in the PMUs contain single harmonics as specified in the standard, and multiple harmonics between 2^{nd} and 7^{th} with varying amplitude. The details of the harmonic content can be found in Appendix C.

The outcome of this test demonstrates that these PMUs provide sufficient filtering to successfully suppress harmonic interference for both single and multiple harmonic contents, also when the frequency deviates from nominal. Figure 4.5 and Figure 4.6 show the voltage and current TVE are well within the limits for signals at off-nominal frequency containing multiple harmonics and single harmonics respectively. More results are available in Appendix C.

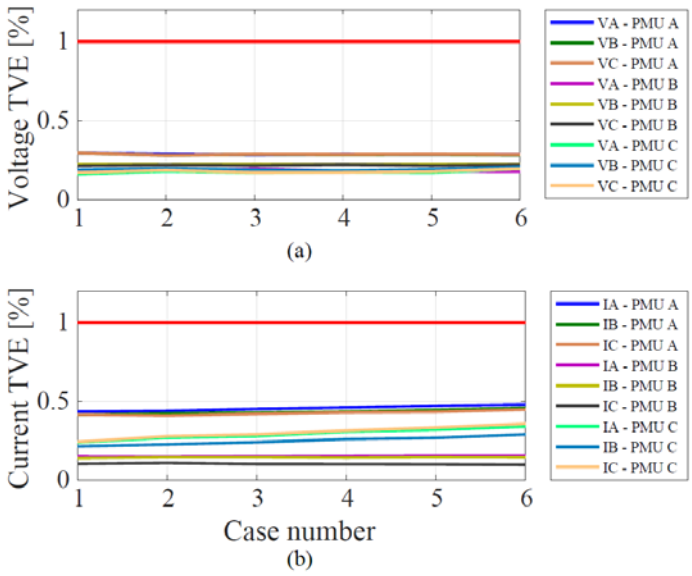

Figure 4.5: Multiple harmonic rejection: (a) Voltage analysis; (b) Current analysis; Signal frequency f = 52.5 Hz

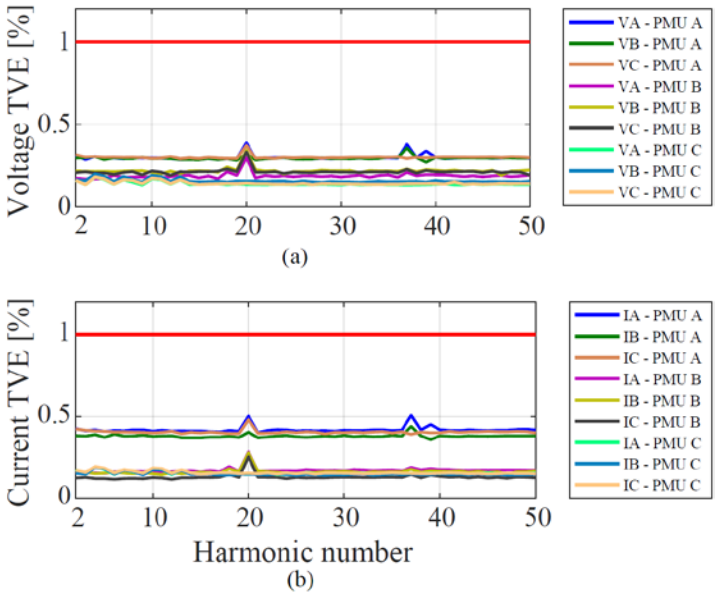

Figure 4.6: Single harmonic rejection; (a) Voltage analysis; (b) Current analysis; Signal frequency f = 52.5 Hz

4.3 Current Transformer Saturation Test

PMUs connect to the high currents in the transmission network via current transformers (CTs). The core of the CTs can saturate if the measured current exceeds the normal operation capability of the device thus producing a highly distorted signal [93]. To avoid this, the IEEE C37.110-2007 Guide for CTs for protective Relaying [94] provides guidelines on protection CTs choice and installation. However, the expected accuracy of this type of CT at rated current is only 3%, and even though they will handle currents up to 20 times the rated value without losing more than 10% in accuracy, these are not in the focus of PMU measurements. The PMU standard specifies measurement accuracy at 1% TVE for most tests. CTs should be in this accuracy range or better in order to take full advantage of the PMU measurement precision. Closer in the range of PMU operation is the metering CT category defined in IEEE C57.13 standard for instrument transformers [95]. These devices guarantee accuracies between 0.3% and 1.2% for a current range of 10%-100%. However, there is no requirement regarding over-current capability of these devices, nor regarding the saturation of their cores.

Besides high currents caused by faults or overloading, CT core saturation can be caused by a DC current component flowing in the circuit [96] - [98]. Power converters are widely used in the renewable energy sector, and these converters can give rise to a DC component if their DC compensation sensor fails [99].

This test aims to determine how a saturated current waveform affects the accuracy of the PMU measurements. To achieve this, waveforms simulating CT saturation are

created and played back into the PMUs. More details on creating the saturated waveforms are available in Appendix C.

The level of saturation is quantified by the saturation factor K_S which is increased in steps during the test and the measurement is evaluated at each step. The waveform is not saturated for $K_S \leq 1$, and starts to saturate when K_S becomes larger than one. Figure 4.7 shows a comparison between the ideal current (blue line) and the real current (red line) which is distorted during core saturation. The real current type waveforms are injected into the PMUs. The amplitude of the current is scaled according to what PMU current inputs can handle.

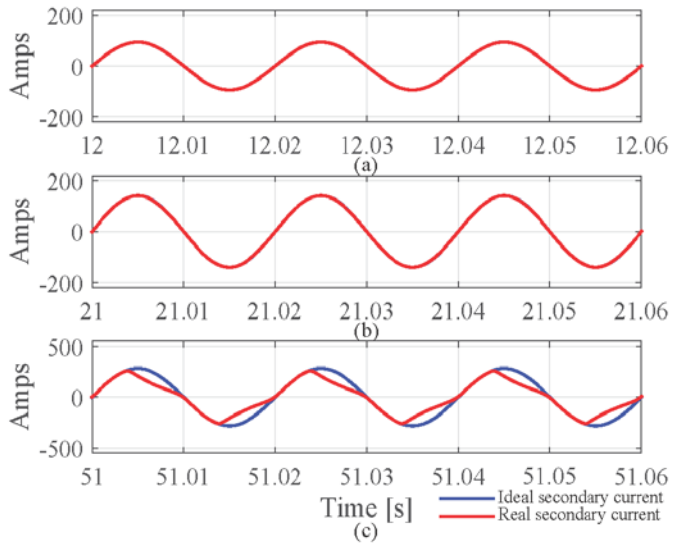

Figure 4.7: Ideal vs real secondary current for: (a) $K_S = 0.65$; (b) $K_S = 1$; (c) $K_S = 2$

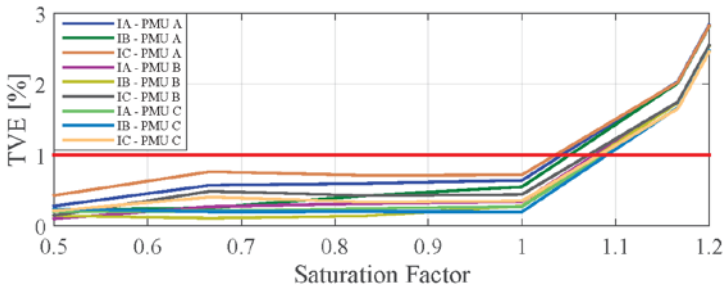

Figure 4.8: CT saturation test; current TVE

Figure 4.8 shows that PMU measurement fails at a fairly low level of CT core saturation ($K_S = 1.1$). Saturation can be prevented by correct choice and installation of CTs. However, it can still occur during faults or if a DC current flows in the circuit. Detecting such an event and flagging the data as bad data could prove useful if the PMU

measurements are used in control algorithms. This might be difficult as saturation usually occurs very fast.

4.4 Discussion

This chapter presented the performance of three PMUs under three plausible power system interference conditions. All PMUs were configured for M-class since it is expected to produce the most precise measurements. The tests showed that the PMUs are within the required accuracy for phasor measurement when the injected signals have a SNR higher than 40 dB. The frequency and ROCOF measurements are more affected by noise and they fail at about 55 dB SNR for frequency and 65 dB SNR for ROCOF measurements. Improved processing methods or better filtering would be required for acceptable results if PMUs are used in environments with high noise.

The tests also showed that the PMUs provide sufficient filtering to reject multiple harmonics, just the same as single harmonics both in nominal and off-nominal frequency conditions. All quantities reported by the PMUs were within the required limits, which indicates that testing for single harmonic rejection, as the standard requires, is sufficient for verifying the compliance of the PMUs with the harmonic rejection test.

PMU measurements are highly affected by CT core saturation. The tests revealed that a low level of CT saturation (Ks = 1.1) causes the PMU measurement to exceed the limits. A pattern can be seen in this case, the amplitude flattens and the angle of the phasors increases, but this is not distinct enough to clearly identify CT saturation only from the data. It could be better detected from the raw measurements inside the PMU and then indicated with an error flag transmitted with the data.

The results may prove useful for PMU and phasor application development. For example, an application could detect high noise with the aid of a tracking filter and use the information to relax trigger points. This would make the application more robust. CT saturation showed a small signature which is probably not distinct enough to help flag the event, especially since saturation will typically occur very fast. Finally, the PMUs proved to reject harmonics very well, therefore it is likely this area is well covered by the current requirements.

5

WIND TURBINE MODEL FOR SMALL-SIGNAL STABIILTY ANALYSIS

This chapter presents a Type 4 full-scale converter wind turbine (FSCWT) phasor model implemented in the Matlab/Simulink platform for small-signal stability studies. Typically the phasor simulation is used in Simulink to study low frequency electromechanical oscillations of power systems that consist of a large number of generators and motors. In addition, it can also be applied to any linear system [100]. The phasor method replaces the sinusoidal quantities of currents and voltages with phasors expressed in complex or polar form. More details about the model and results described in this chapter are available in Appendix D.

5.1 Wind Turbine Model

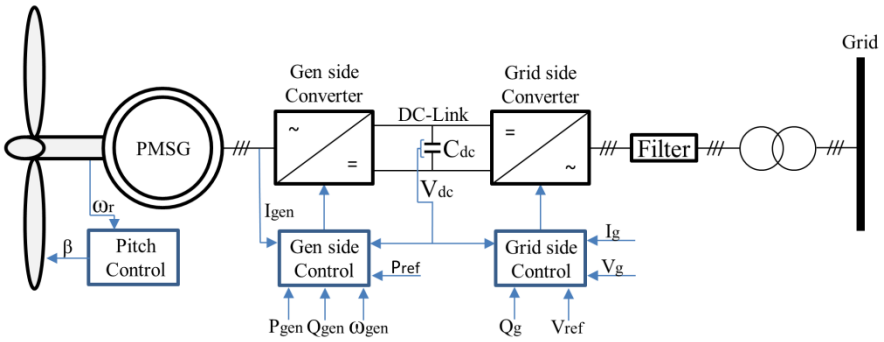

Figure 5.1: Wind turbine concept

The wind turbine concept for this study is based on a Permanent Magnet Synchronous Generator (PMSG) and connects to the grid through a full-scale converter as shown in Figure 5.1. The WT blades are pitch controlled and it has variable-speed operation to maximize the active power output. In this study it is represented by a reduced order, phasor model suitable for dynamic power system studies. The model can be used as a single wind turbine or as an aggregated model of a wind power plant (WPP). When used as a WPP, only the main interaction between the power system and the WPP is considered.

A block diagram showing the overall connections of the phasor model implemented in Simulink is shown in Figure 5.2 and is followed by a description of the subsystems.

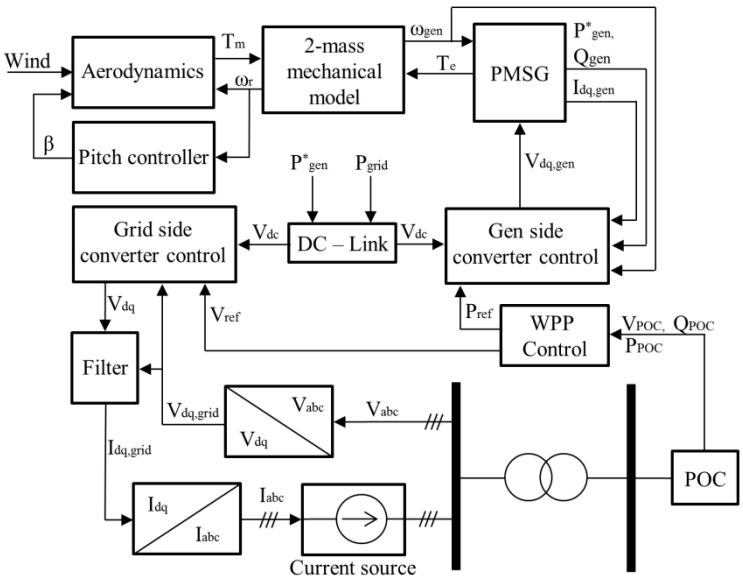

Figure 5.2: Block diagram of the phasor type model

The Aerodynamics model implements a variable wind speed turbine which includes wind speed, power coefficient C_p, pitch angle β, and tip speed ratio λ, and calculates the mechanical torque output using the equations presented in [101] and Appendix D. The torque output is in per unit, based on the power rating of the generator.

The mechanical model is implemented as a third order two mass model which includes the rotor and generator inertia constants, shaft stiffness and damping as in [102]. The differential equations are presented here, while the block diagram is available in Appendix D.

$$\dot{\omega_r} = \frac{1}{2H_t}[-K_{sf}\theta_{sf} - D(\omega_r - \omega_{gen}) - T_m] \quad \textbf{(5.1)}$$

$$\dot{\omega_g} = \frac{1}{2H_g}[K_{sf}\theta_{sf} + D(\omega_r - \omega_{gen}) + T_m] \quad \textbf{(5.2)}$$

$$\dot{\theta}_{sf} = \omega_r - \omega_{gen} \quad \textbf{(5.3)}$$

where ω_r and ω_{gen} are the wind turbine rotor and generator speeds, θ_{sf} is the shaft twist angle, D is the shaft damping coefficient, and K_{sf} is the shaft stiffness. The wind turbine rotor and generator inertia constants are represented by H_t and H_g respectively.

The PMSG implements a second order electrical model of a permanent magnet synchronous generator in the dq rotor reference frame with all the quantities in the rotor frame referred to the stator [100]. The following assumptions are made in this model [103]:

- The flux variation induced by the rotor magnets in the stator phases is sinusoidal, and so are the electromotive forces.
- The variation of the inductance as a function of rotor position is sinusoidal
- Cogging torque, magnetic saturation and iron losses are neglected

Only the dq-axis differential equations in matrix form are shown in (5.4), the block diagram is available in Appendix D. Note that the PMSG model in Simulink library is using the motor convention instead of the generator convention. The wind turbine model and its control are based on the motor convention.

$$\begin{bmatrix} \dot{I}_{d,gen} \\ \dot{I}_{q,gen} \end{bmatrix} = \begin{bmatrix} -\frac{R_s}{L_{sd}} & \frac{L_{sq}}{L_{sd}}\omega_s \\ -\frac{L_{sd}}{L_{sq}}\omega_s & -\frac{R_s}{L_{sq}} \end{bmatrix} \begin{bmatrix} I_{d,gen} \\ I_{q,gen} \end{bmatrix} + \begin{bmatrix} \frac{1}{L_{sd}} & 0 \\ 0 & \frac{1}{L_{sq}} \end{bmatrix} \begin{bmatrix} V_{d,gen} \\ V_{q,gen} \end{bmatrix} \qquad \textbf{(5.4)}$$

where $I_{d,gen}, I_{q,gen}$ are the d-axis and q-axis currents, $V_{d,gen}, V_{q,gen}$ are the dq-axis stator voltages, R_s is the stator resistance, and L_{sd}, L_{sq} are the d-axis and q-axis inductances.

The DC-link circuit transfers the active power generated by the generator to the grid side converter, and from this converter it is injected into the grid. The DC-link capacitor voltage V_{dc} is kept at its rated value by the grid side converter. The details about the dynamic modeling and block diagram are available in Appendix D.

The controller of the generator side converter drives the generator to obtain the optimum efficiency depending on wind conditions such as low wind for example by following a Maximum Power Point Tracking (MPPT) algorithm as the one in [104]. The converter can also adjust the generator's active power according to a power reference set by the wind park control if for example power regulation is required.

A number of generator control strategies can be implemented which are based on controlling the electrical torque and active power production by acting on the q-axis stator current [105] if the d-axis is aligned with the magnet flux. By acting on the d-axis stator current component, the generator can be controlled to run at unity power factor, by compensating for its reactive power demand. While this strategy normally minimizes the converter rating, it does not directly control the voltage at the generator terminals,

and may cause over-voltages in case of over-speeds. However, the wind turbine speed is controlled by changing the pitch angle of the blades in order to avoid the turbine spinning faster than its rated value. Therefore, the unity power factor strategy is chosen in this model.

The stator dq-current components cannot be controlled independently because of the cross-coupling effects shown in (5.4). These effects are canceled by feed-forward compensation. The controlled stator voltage components, including the decoupling feed-forward compensation, are calculated as:

$$\begin{bmatrix} V_{d,gen} \\ V_{q,gen} \end{bmatrix} = \begin{bmatrix} R_s & -L_{sq}\omega_s \\ L_{sd}\omega_s & R_s \end{bmatrix} \begin{bmatrix} I_{d,gen} \\ I_{q,gen} \end{bmatrix} + \begin{bmatrix} K_{Pd} + \dfrac{K_{Id}}{s} \\ K_{Pq} + \dfrac{K_{Iq}}{s} \end{bmatrix} \begin{bmatrix} i_{d,ref} - I_{d,gen} \\ i_{q,ref} - I_{q,gen} \end{bmatrix} \quad \textbf{(5.5)}$$

where K_P and K_I are the proportional and integral gains of the dq-axis PI current controllers, $i_{d,ref}, i_{q,ref}$ are current references for d and q-axis respectively, and the rest of the variables have been defined below (5.4). According to (5.4) and (5.5), (5.6) can be given:

$$\begin{bmatrix} \dot{I}_{d,gen} \\ \dot{I}_{q,gen} \end{bmatrix} = \begin{bmatrix} K_{Pd} + \dfrac{K_{Id}}{s} \\ K_{Pq} + \dfrac{K_{Iq}}{s} \end{bmatrix} \begin{bmatrix} i_{d,ref} - I_{d,gen} \\ i_{q,ref} - I_{q,gen} \end{bmatrix} \quad \textbf{(5.6)}$$

It can be seen from (5.5) that the converter is controlled by acting on its stator voltage dq-axis components, which in return defines the dq-axis stator current components as in (5.4). The active power control is performed through $V_{q,gen}$, and the reactive power control is performed through $V_{d,gen}$.

The $V_{d,gen}$ controller consists of an outer loop that determines the d-axis current reference $i_{d,ref}$ from (5.5). This is achieved by calculating the error between the reference reactive power (which is zero for unity power factor operation) and the measured reactive power, and using a PI to adjust the current reference. An inner loop regulates $I_{d,gen}$ according to $i_{d,ref}$ by acting on the stator voltage $V_{d,gen}$. The $V_{q,gen}$ controller also consists of and outer and inner loop working on the same principle.

The grid side converter control maintains the DC-link capacitor voltage V_{dc} at its rated value, which assures the active power flow from the generator to the grid. It also controls the reactive power exchange with the grid thus maintaining the voltage and power factor. The principle of operation is similar to the generator side converter, by

controlling the direct and quadrature (dq) axis current components. In this case the d-axis is aligned with the grid voltage, which gives:

$$V_{grid} = V_{d,grid} + j0; \quad \textbf{(5.7)}$$

The dc-link capacitor voltage V_{dc} is controlled by the d-axis current component while the reactive power and voltage are controlled by the q-axis current component. The control consists of outer loops that determine the dq-current references, and inner loops that control the currents to follow these references.

The RL filter connects the grid side converter to the wind turbine transformer. In this case the filter is modeled in the dq-frame, with the d-axis aligned to the grid voltage. More details are available in Appendix D.

The wind turbine model is used with three phase power systems consisting of synchronous generators and loads. Therefore, it is necessary to transform the three phase voltages and currents to the dq rotating reference frame. This takes place in the **ABC to dq** blocks, which also implement a Phase-Locked Loop (PLL) that computes the angle of the grid voltage phasor and uses it to align the internal dq-reference frame.
A controlled **Current source** is used to interface the WT to the power system.

The WPP Controller is an outer corrective control system that controls the power and voltage outputs of the WPP at the Point of Connection (POC). The controller takes as inputs the measured active and reactive powers (P_{POC} and Q_{POC}) and the voltage (V_{POC}), and sends a power reference and a voltage reference to the aggregated WPP model. The controls implemented in this model are based on [47] and [106]. More details are available in Appendix D.

The WPP collector system models the cables used to connect individual turbines to the grid. Because the model presented in this chapter is of an aggregated WPP, the exact placement of the wind turbines is not known. Therefore, an approximation of the collector system is made as in [47]. The collector system is modeled as a T-equivalent with the entire capacitance lumped as a shunt, and with half of the resistance and inductance connected in series and distributed on each side.

5.2 Study Case Results

The study case is based on the classic Kundur's two area system to which the WPP phasor model is connected to bus 5 as shown in Figure 5.3. For this analysis all the

generators are equipped with Power System Stabilizers (PSS), and all the generator parameters and PSS tuning is implemented as shown in [17].

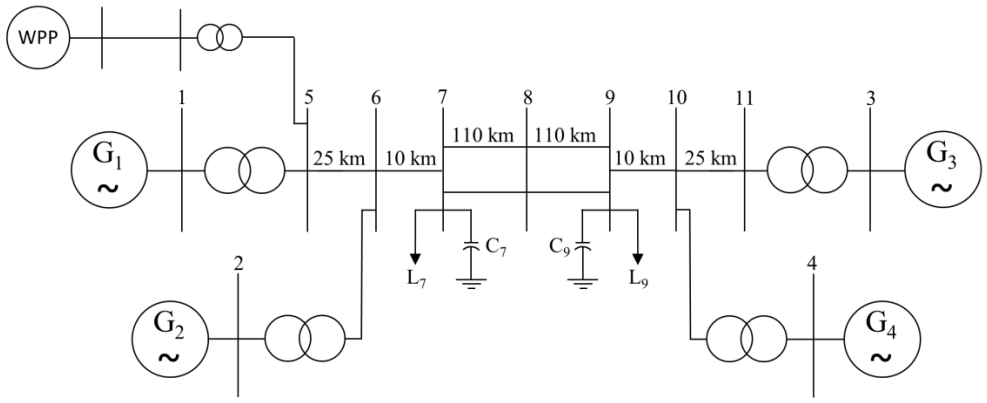

Figure 5.3: Study case power system

The analysis is performed in Matlab/Simulink, where the synchronous generators and the rest of the power system are implemented using the SimPowerSystems [107]. The WPP model presented in this chapter is included in the system, and the entire system is simulated using the phasor method.

The linearization is performed using the Simulink Control Design [108], directly on the entire initialized power system. This tool uses exact linearization for functions that have an analytical first derivative, while numerical perturbation is used for elements that cannot be linearized analytically, e.g. look-up tables.

The study is carried out in two steps:

- First, the modal analysis of the classical two area system is carried out in order to test if the power system is linearized correctly, and to validate the results by comparing to the values in [17].

- Second, the WPP is included in the power system and the wind power capacity is increased from 30 MW to 560 MW in five steps. It is important to note that as the wind power injection is increased, the power set-point of generator G_1 is reduced in order to keep the power flows and the loading of the other generators unchanged. Significant change in power flow or dispatch of the existing units can affect the modal characteristics of the power system [81]. This should be avoided if the influence of the WPP on power system oscillations is to be correctly investigated.

5.2.1 Case study with no wind power

For this case, the WPP is not included in the network model. A power flow calculation is executed in Simulink, and the power system network is initialized. The entire model is then linearized using the Linear Analysis tool from the Simulink Control Design toolbox. The eigenvalues of the linearized model are calculated and presented in Table 5.1. There is one inter-area mode present in the system, where the generators G_1 and G_2 from Area 1 swing against the generators G_3 and G_4 from Area 2. There are also two local modes present, where the generators in each area swing against each other. These results are similar to the ones in [17].

Table 5.1: Modal characteristics of the power system without wind power

Eigenvalue/(Frequency in Hz, Damping Ratio)		
Inter-area mode	**Area 1 local mode**	**Area 2 Local Mode**
-0.689 ± j4 (f=0.65, ζ=0.17)	-2.56 ± j8.42 (f=1.4, ζ=0.291)	-2.49 ± j8.9 (f=1.47, ζ=0.269)

5.2.2 Case study with wind power

For this study, the WPP is connected to bus 5 which is the high voltage bus of generator G_1, as shown in Figure 5.3. The wind power injected into the power system is increased in five steps, from 30 MW to 560 MW. For each step increase in the wind power, the reference set-point of G_1 is reduced, the power system is initialized with the new values, and the model is linearized. The eigenvalues in Table 5.2 show that the WPP has little effect on the inter-area mode with only a slight increase in the damping noticed as the wind power penetration is increased.

The interaction of the WPP with the power system oscillations is evaluated with the aid of participation factors shown in Table 5.3. These are normalized according to the state variable which has the highest participation. It can be seen that in this case generator G_3 has the highest participation in the inter-area mode, and the participation of the WPP mechanical system is very little compared to the synchronous generators. This result confirms there is a general decoupling between the grid dynamics and the mechanical part of the WT in the case of a full-load converter configuration. It is also important to mention that in this study the WPP is operated within limits. If any of the components were to hit their limits the analysis might not be valid. This is because modal analysis is based on Taylor expansion in which the system is described in terms of deviation from the steady state. If a limit is reached, this description is no longer valid.

Table 5.2: Modal characteristics of the power system with wind power penetration

Wind Power [MW]	Eigenvalue/(Frequency in Hz, Damping Ratio)		
	Inter-area mode	**Area 1 local mode**	**Area 2 Local Mode**
30	-0.692 ± j3.99 (f=0.64, ζ=0.171)	-2.6 ± j8.35 (f=1.39, ζ=0.297)	-2.49 ± j8.9 (f=1.47, ζ=0.269)
50	-0.694 ± j3.99 (f=0.64, ζ=0.171)	-2.62 ± j8.3 (f=1.39, ζ=0.301)	-2.49 ± j8.9 (f=1.47, ζ=0.269)
100	-0.699 ± j3.97 (f=0.64, ζ=0.173)	-2.67 ± j8.18 (f=1.37, ζ=0.311)	-2.49 ± j8.9 (f=1.47, ζ=0.269)
200	-0.707 ± j3.94 (f=0.63, ζ=0.176)	-2.74 ± j7.92 (f=1.33, ζ=0.327)	-2.49 ± j8.89 (f=1.47, ζ=0.27)
560	-0.704 ± j3.79 (f=0.61, ζ=0.182)	-2.6 ± j7.02 (f=1.19, ζ=0.347)	-2.49 ± j8.89 (f=1.47, ζ=0.27)

Table 5.3: Participation factors for the inter-area mode with 560 MW wind power

State variable	Participation factor
δ (G_1)	0.32
δ (G_2)	0.15
δ (G_3)	1
δ (G_4)	0.87
δ_r (WPP)	$<10^{-2}$

As mentioned before, the modal analysis is based on a linear method and is only valid around an operating point. Hence, it is usually complemented with dynamic simulations of the nonlinear system. Furthermore, time domain simulations of both the nonlinear and linear systems can be compared in order to verify whether the model has been linearized correctly. Figure 5.4 shows the rotor responses of generators G_1 and G_3 following a 1% step change in the excitation voltage of generator G_1, which excites the power system oscillations from which the inter-area mode is clearly visible. The responses of the linear and nonlinear models overlap validating the linear model.

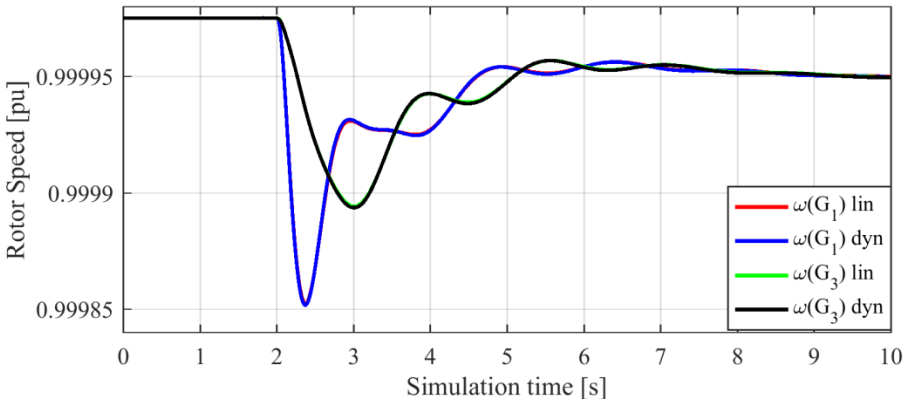

Figure 5.4: Rotor responses of generators G_1 and G_3 with 560 MW wind power

5.3 Discussion

In this chapter a phasor model of a full-scale wind turbine was implemented. The aim was to use the model as an aggregated WPP together with power system models which include synchronous generators for time domain dynamic simulations and for small-signal stability studies. The WPP model takes into account the aerodynamics of the turbine, pitch angle of the blades, and uses a two-mass model for the drive train. The electrical part consists of a PMSG model, converter model with the appropriate controls, and the RL filter model.

The WPP is integrated in the classic four-machine, two-area system and the modal characteristics of the entire system are analyzed with and without wind, using the tools available in Simulink. It is found that the WPP, with different levels of wind power penetration, has little impact on the eigenvalues of the power system. Furthermore, the analysis of the participation factors showed that the synchronous generators have the highest impact on the power system oscillations, while the mechanical system of the WPP is basically decoupled from the rest of the grid by the power converter. These findings are supported by previous research which has investigated the impact of a validated dynamic WT model, provided by one of the vendors for the studies [47].

6
INTER-AREA POWER OSCILLATION DAMPER

In this chapter the WPP model presented in Chapter 5 is equipped with power oscillation dampers (PODs) in order to help improve the damping of the inter-area oscillations. For comparison, two types of PODs are implemented: an adaptive phasor POD based on [69], [70], [72], [73], which has been used in FACTS devices such as TCSC and SVCs, and a POD based on the conventional PSS type which typically consists of a gain block, a washout filter block, and lead-lag phase compensation blocks. More details about the models and results presented in this chapter are available in Appendix E.

6.1 Phasor Power Oscillation Damper

The signal measured during an oscillation consists of two components: a constant or slowly varying component, and an oscillatory component. The phasor POD approach focuses on extracting the oscillatory component as a space phasor which is rotating with the frequency of the oscillation. The space phasor is represented in a dq-rotating frame which has the same frequency. The measured signal is expressed as:

$$S(t) = S_{av}(t) + S_d(t)\cos\varphi(t) - S_q(t)\sin\varphi(t) \qquad \textbf{(6.1)}$$

where S_{av} is the average component, and S_d, S_q are the oscillatory components in the dq- rotating frame, and $\varphi(t) = \omega t + \varphi_0$. Here, φ_0 is the angle at which the phasor is locked to the dq-frame, and ω is the rotating frequency of the phasor.

A recursive least squares (RLS) algorithm is used to estimate the average and oscillatory components [72]. A parameter vector Θ and a regression matrix ϕ are defined as follows:

$$\Theta = \begin{bmatrix} S_{av}(t) & S_d(t) & S_q(t) \end{bmatrix}^T \qquad \textbf{(6.2)}$$

$$\phi = [1 \quad cos\varphi(t) \quad -sin\varphi(t)]^T \qquad \textbf{(6.3)}$$

For each computation time step the RLS algorithm updates the value of the parameter vector $\Theta(t)$ from its previous estimate $\Theta(t-1)$. The steps of the RLS algorithm are the following [79]:

- Calculate the prediction error:

$$\varepsilon(t) = S(t) - \phi(t)\Theta(t-1) \quad \textbf{(6.4)}$$

- Calculate the RLS gain vector $K_d(t)$:

$$K_d(t) = \frac{C(t-1)\phi^T(t)}{v + \phi(t)C(t-1)\phi^T(t)} \quad \textbf{(6.5)}$$

- Update the covariance matrix C(t):

$$C(t) = \frac{[I - K_d(t)\phi(t)]\, C(t-1)}{v} \quad \textbf{(6.6)}$$

- Update the parameter vector $\Theta(t)$:

$$\Theta(t) = \Theta(t-1) + K_d(t)\varepsilon(t) \quad \textbf{(6.7)}$$

where v in (6.5) and (6.6) is the forgetting factor which is in the range of (0 1]. If the estimated parameters would be constant, then the forgetting factor would be set to $v = 1$ which corresponds to 'no forgetting'. In this case, the parameters are assumed to be slowly varying in time, hence $v < 1$. The covariance matrix $C(t)$ is the identity matrix multiplied by a large number ($10^3 I$), and the parameter vector $\Theta(t)$ is initialized with zeros.

The overall block diagram of the phasor POD is shown in Figure 6.1. The RLS algorithm block uses (6.2) to (6.7) and outputs the estimated components S_{av}, S_d, and S_q. The block also uses information about the frequency of the oscillating mode. Usually, the inter-area oscillation modes are known in advance by the transmission system operators. Hence, prior knowledge about the power system where the POD is to be installed is an advantage. Otherwise, the oscillating modes can be found by analysing the available measurements. An example of a new method that can be used to identify the frequency and damping of the oscillatory modes from the measurements is presented in [109]. The latency compensation, phase shift and transformation to time domain blocks are described next.

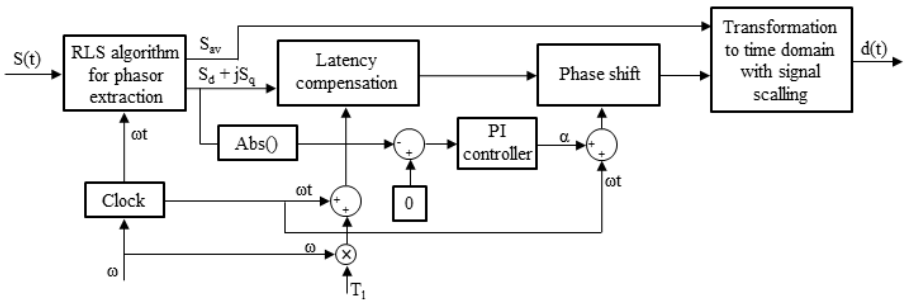

Figure 6.1: Block diagram of phasor POD

The **latency compensation** block: PMU measurement latency is a time delay (T_l) which from a phasor point of view translates into a phase lag between the signal measured at the PMU location in the power system and the signal received by the POD. Since the phasor POD expresses the phasor in the rotating dq-frame, the latency can be compensated for by rotating the dq-frame to d'q'-frame with an angle $\theta = \omega T_l$, as follows [72]:

$$\begin{bmatrix} S'_d \\ S'_q \end{bmatrix} = \begin{bmatrix} \cos\theta & -\sin\theta \\ \sin\theta & \cos\theta \end{bmatrix} \begin{bmatrix} S_d \\ S_q \end{bmatrix} \quad \textbf{(6.8)}$$

Remote PMU measurements are used as input signals for the POD. As required by the IEEE C37.118.1-2011 standard [22], the PMU is GPS synchronized and the samples sent by the PMUs are time-stamped. At the receiving end, the control centre uses a GPS clock to time stamp the signals received from the PMUs with a microsecond precision. The two time stamps are used to calculate the latency in the communication infrastructure and associated hardware [80]. Thus, the value of T_l associated with each sample is known and the value of the compensating angle θ can be calculated.

The **phase shift** block in Figure 6.1 further rotates the d'q'-frame to d"q"-frame with the angle α:

$$\begin{bmatrix} S''_d \\ S''_q \end{bmatrix} = \begin{bmatrix} \cos\alpha & -\sin\alpha \\ \sin\alpha & \cos\alpha \end{bmatrix} \begin{bmatrix} S'_d \\ S'_q \end{bmatrix} \quad \textbf{(6.9)}$$

The amplitude of the oscillation in the dq-frame is represented by the estimated phasor magnitude $|S_d + jS_q|$. This value is non-oscillatory and always positive, and the aim is to drive the phasor magnitude to zero in order to damp the oscillations. This is achieved with a PI controller which takes as input the difference between a zero reference and the magnitude of the estimated phasor and in turn produces the phase shift angle α(t) as follows [72]:

$$\alpha(t) = -K_p\left|S_d(t) + jS_q(t)\right| - K_i \int \left|S_d(t) + jS_q(t)\right| dt \qquad \textbf{(6.10)}$$

where K_p and K_i are the proportional and integral gains of the PI controller.

The latency compensated and phase shifted phasor is then transformed back into a time domain signal as:

$$d(t) = [\cos\varphi(t) \quad -\sin\varphi(t)] \begin{bmatrix} S_d^{''} \\ S_q^{''} \end{bmatrix} \qquad \textbf{(6.11)}$$

The damping signal $d(t)$ is scaled using the estimated average component $S_{av}(t)$ and used as input for the PODs.

6.2 Case study 1

The first case study is based on the Kundur's four-machine, two-area system shown in Figure 6.2. The generators are represented by transient models and are equipped with the IEEE DC1A exciter. All the system parameters are listed in [17]. The aggregated WPP model is connected to bus 5.

As in Chapter 5, the analysis is performed in Matlab/Simulink, using SimPowerSystems to model the system and Simulink Control Design to linearize the system and perform the modal analysis.

The WPP is equipped with either the phasor POD or the conventional PSS type controllers to help improve the damping of the inter-area oscillations. The POD controller acts on the power reference given by the WPC block shown in Figure 5.2, hence the damping signal modulates the active power output of the WPP.

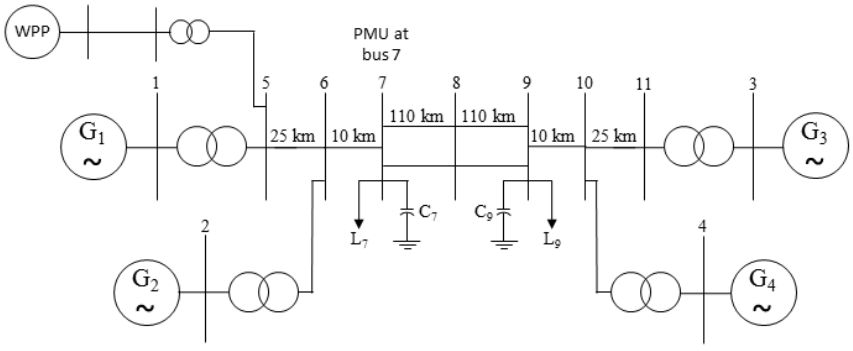

Figure 6.2: Test system 1: four-machine, two-area system with WPP

The block diagram of the active power control in the WPC with the added controller is shown in Figure 6.3. Note that for comparison, the **POD controller** block in Figure 6.3 will implement in turns, the phasor POD and the conventional PSS.

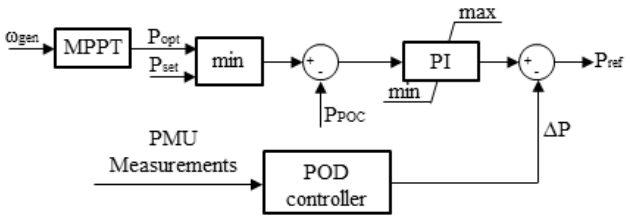

Figure 6.3: WPC active power control with POD

A PMU is installed at bus 7 as shown in Figure 6.2, and it is configured to send measurements at 60 samples per second. The line current measured by the PMU is used as input signal for the POD controller.

The WPP is set to inject 400 MW into the power system. The power output of the synchronous generator is balanced with the power output of the WPP so the power flow in the system remains unchanged. It is known that the modal characteristics of the power system can change if there is a significant change in the power flow of the system [81]. This is undesired since we are only interested in the impact of the WPP on the damping of the power system oscillations.

Only the main findings are presented in this chapter, while more details can be found in Appendix E.

6.2.1 Case without latency in the PMU measurements

The eigenvalues of the power system with no wind power penetration are shown in Table 6.1. It can be seen that the inter-area mode has very low damping in this case.

The contribution of the WPP on the damping of the inter-area oscillation when it is equipped with the phasor POD is shown in Table 6.2. It is very important to mention that the eigenvalues are positive because the system is now discrete due to the sampling rate introduced by the PMU measurements. Therefore, the eigenvalues are related to the unity circle in the z-plane. It can be seen that the damping ratio of the inter-area mode has increased from 0.005 to 0.167. Moreover, the damping ratio of the area one local mode which is the mode between generators G_1 and G_2 has also increased. This is because the WPP is connected to bus five in area one, hence it has an impact on the oscillatory mode in this area. The system eigenvalues for the case when the WPP is

equipped with the conventional PSS are shown in Table 6.3. It can be seen that the two POD controllers have similar performances in damping the inter-area oscillations.

Table 6.1: Test system modal characteristics without wind power

Eigenvalue/(Frequency in Hz, Damping Ratio)		
Inter-area mode	**Area 1 local mode**	**Area 2 Local Mode**
-0.0175 ± j3.58 (f=0.57, ζ=0.005)	-0.591 ± j6.65 (f=1.06, ζ=0.089)	-0.555 ± j6.88 (f=1.1, ζ=0.08)

Table 6.2: Test system modal characteristics with WPP and phasor POD

Eigenvalue/(Frequency in Hz, Damping Ratio)		
Inter-area mode	**Area 1 local mode**	**Area 2 Local Mode**
0.984 ± j0.076 (f=0.74, ζ=0.167)	0.98 ± j0.101 (f=0.99, ζ=0.146)	0.984 ± j0.113 (f=1.09, ζ=0.08)

Table 6.3: Test system modal characteristics with WPP and conventional PSS

Eigenvalue/(Frequency in Hz, Damping Ratio)		
Inter-area mode	**Area 1 local mode**	**Area 2 Local Mode**
0.981 ± j0.087 (f=0.86, ζ=0.165)	0.984 ± j0.102 (f=0.99, ζ=0.106)	0.984 ± j0.114 (f=1.11, ζ=0.08)

6.2.2 Case with latency in the PMU measurements

In this subsection the impact of the measurement latency on the efficiency of the PODs is investigated. The study runs through a latency sweep with the range between 0 ms and 116 ms. The latency of the communication infrastructure is typically limited to milliseconds, but in unusual cases it can increase to hundreds of milliseconds [110], [111].

Figure 6.4 shows the active power flow from area one to area two in the 220 km long intertie line. At second number two a 1% step increase in the excitation voltage of generator G_1 excites the inter-area mode. The WPP, equipped with the conventional PSS, acts to damp the inter-area oscillations. It can be seen that as the latency increases, the damping decreases. The critical point in this case is between 83 ms and 100 ms, after which the WPP causes the oscillations to increase in amplitude causing the system

to become unstable. This shows that if the conventional PSS type controller is to be used together with WPP and remote PMU measurements, the latency should be taken into account. The lead-lag blocks of the controller can be designed to provide good phase compensation for a number of latency values. However, the phase compensation will work in the range that it was designed for.

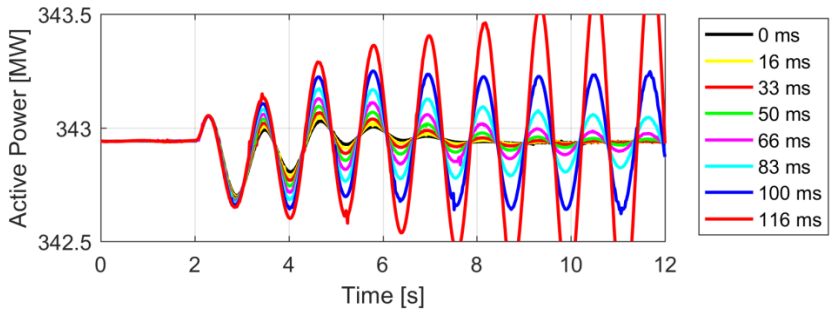

Figure 6.4: Intertie active power flow; conventional PSS latency sweep

Figure 6.5 shows the intertie power flow for the case when the WPP is equipped with the phasor POD. The same step is applied to the generator G_1 excitation voltage at second number two. It can be seen that the phasor POD has the same efficiency over the entire range of latencies. The latency information provided by the time-stamping of the measurements is used by the POD to calculate the appropriate compensation.

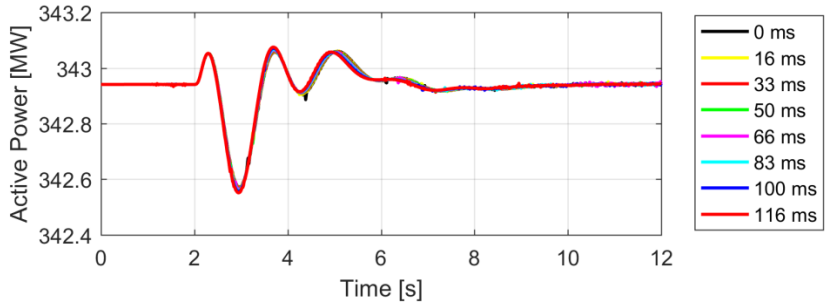

Figure 6.5: Intertie active power flow; phasor POD latency sweep

6.3 Case study 2

The second case study is based on a seven-generators, 18-node system shown in Figure 6.6. The generators are aggregated machines, each representing a smaller or larger number of units. The system has also six loads and their distribution causes a power flow of 1900 MW from north to south on lines l_{38} and l_{48}. The parameters of the generators, lines, and loads are given in [47]. An aggregated WPP is connected to the high voltage bus of generator G_2.

The modal characteristics of the seven-generator system without wind power penetration are detailed in Table 6.4, and in the complex s-plane in Figure 6.7. Four inter-area modes are identified, out of which three have low damping. The WPP equipped with the PODs will aim to improve damping ratio of the inter-area mode denoted by λ_1.

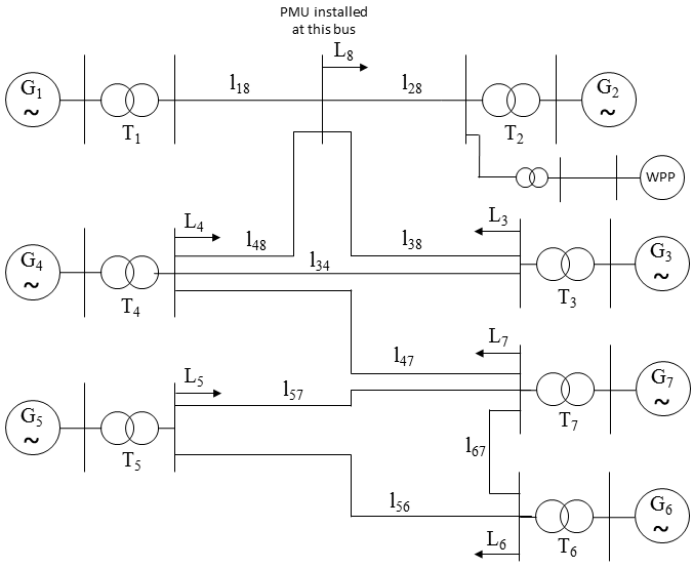

Figure 6.6: Test system 2, seven-machine, 18-node system

Table 6.4: Modal characteristics of test system 2 without wind power

Eigenvalue	λ / (frequency in Hz, Damping ratio)	Mode description
λ_1	-0.265 ± j3.64 / (f=0.58, ζ=0.07)	Inter-area mode between $G_{1,2} – G_{3-7}$
λ_2	-0.89 ± j8.22 / (f=1.31, ζ=0.108)	Inter-area mode between $G_4 – G_6$
λ_3	-0.685 ± j9.78 / (f=1.56, ζ=0.07)	Inter-area mode between $G_4 – G_7$
λ_4	-0.506 ± j7.34 / (f=1.17, ζ=0.07)	Inter-area mode between $G_1 – G_2$

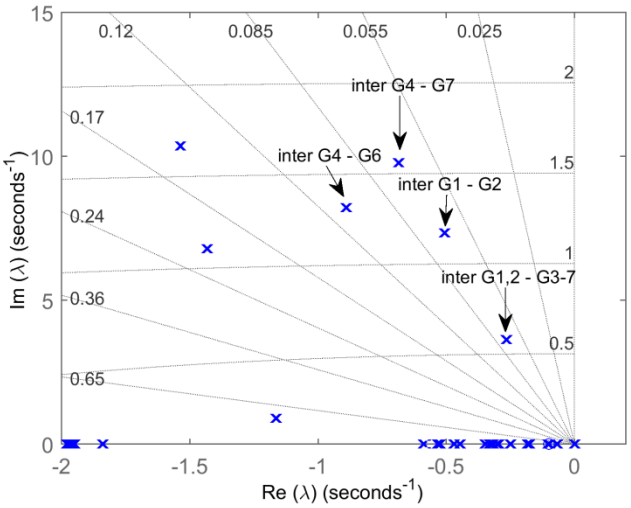

Figure 6.7: Eigenvalues of the 7-generator system

For this case study the WPP is set to produce 1000 MW. The power output of generator G_2 is adjusted to accommodate the wind power injection so that the power flow in the system remains unchanged. A PMU is installed at the bus that connects lines l_{38} and l_{48}, and it reports the measurements at 50 samples per second. The POD input signal is the active power flow measured in line l_{38}.

6.3.1 Case without PMU measurement latency

The inter-area oscillations are excited by a three-phase short circuit applied midway on the line l_{48}. The fault is cleared after 146 ms. Figure 6.8 shows the dynamic response of the nonlinear system in which the active power flow in line l_{48}, before and after the short-circuit is observed. The plot shows a comparison between the cases where there is no contribution from the WPP, and when the WPP is equipped with the phasor POD and the conventional PSS. It is clear that the WPP improves the damping of the inter-area mode. The detailed eigenvalues are shown in Table 6.5.

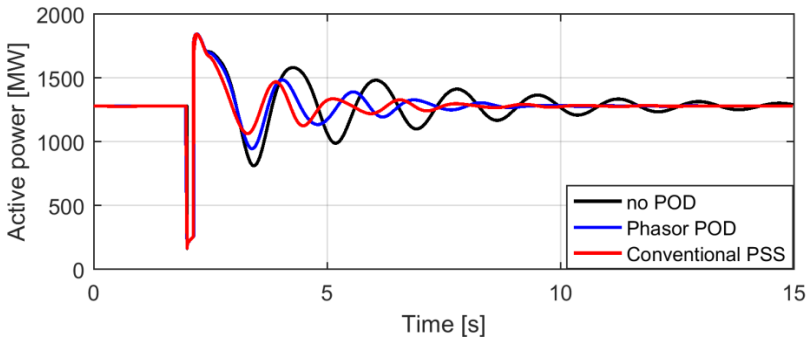

Figure 6.8: Inter-area oscillations with no PMU latency

Table 6.5: Test system eigenvalues with WPP contribution

Eigenvalue	WPP with phasor POD λ / (frequency in Hz, Damping ratio)	WPP with conventional PSS λ / (frequency in Hz, Damping ratio)
λ_1	0.985 ± j0.0859 / (f=0.7, ζ=0.131)	0.985 ± j0.0859 / (f=0.7, ζ=0.135)
λ_2	0.97 ± j0.161 / (f=1.32, ζ=0.108)	0.97 ± j0.145 / (f=1.19, ζ=0.127)
λ_3	0.968 ± j0.192 / (f=1.56, ζ=0.07)	0.97 ± j0.174 / (f=1.42, ζ=0.083)
λ_4	0.98 ± j0.142 / (f=1.15, ζ=0.067)	0.982 ± j0.126 / (f=1.02, ζ=0.078)

Note that the eigenvalues are analyzed in the z-plane which is why they have positive real parts. It can be seen that the performances of the phasor POD and conventional PSS are very similar and that the damping ration of λ_1 is increased from 0.07 to 0.13.

6.3.2 Case with PMU latency

In this section the performances of the phasor POD and conventional PSS controllers are investigated in a number of scenarios where the input signal is delayed when compared to the signal measured at the PMU location. To provide a good idea about the difference in performance, the latency is varied between 0 ms and 140 ms.

The impact of the latency on the conventional PSS is studied first. Figure 6.9 shows the active power flow in line l_{48}. It can be seen that the WPP equipped with the conventional PSS manages to stabilize the system as long as the latency does not exceed 100 ms. After this value, the WPP impact becomes detrimental since not only it does not provide sufficient damping, but it actually contributes to the increase in amplitude of the oscillation causing the system to become unstable.

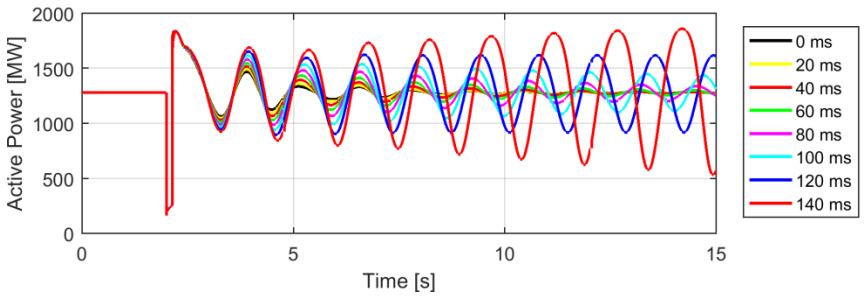

Figure 6.9: Active power flow in line l_{48}; conventional PSS performance under latency

The performance of the phasor POD is studied under the same latency range. Figure 6.10 shows that the phasor POD keeps the same performance for the entire latency range. Unlike the conventional PSS type which uses a fixed phase compensation value

given by the tuning of the lead-lag blocks, the phasor POD uses the time delay available with each sample of the input signal to adjust the position of the dq-frame, thus compensating for the delay.

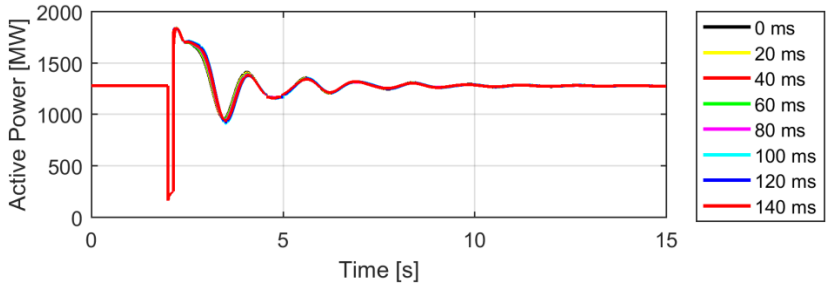

Figure 6.10: Active power flow in line l_{48}; phasor POD performance under latency

6.4 Discussion

In this chapter the WPP was used to help improve the damping ratio of inter-area oscillations in power systems. To achieve this, the WPP was equipped with a power oscillation damping controller. For comparison, two types of controllers were chosen. First, a phasor POD was implemented and tested with the WPP. The phasor POD was used before together with FACTS devices to damp inter-area oscillations in power system, and was proven to be a good combination. Unlike the TCSC which can be installed at a specific point in the power system, the WPP depends on the wind resources. It is therefore, interesting to investigate the possibility of using the phasor POD together with wind power plants. In this study the WPP was shown to help improve the inter-area oscillation damping when equipped with the phasor POD. Next, the WPP was equipped with a conventional PSS type controller, and it was also found to help improve the damping of the power system oscillations.

Remote PMU measurements were used as input signals for the two types of PODs. Initially, it was considered that there is no delay between the signal that reaches the POD and the signal measured in the power system at the PMU location. In this case, both PODs showed similar performance in the seven-generator system, with no clear advantage of one over the other. The advantage of using a POD that can easily compensate for time delay became clear when the input signal latency was gradually increased. In this case, the conventional PSS showed to be less and less efficient as the latency increased. Once the signal latency exceeded 100 ms, the conventional PSS could not damp the power system oscillations. In fact the controller was causing the WPP to help increase the amplitude of the oscillations. This happened because the fixed phase shift of the lead-lag blocks was eventually not enough to assure the output of the

controller will help damp the oscillations. The phasor POD, however, showed that it can maintain its efficiency for the entire range of latencies involved in this study.
Even though the phasor POD has the advantage of easily compensating for PMU time delays, which makes it suitable to be used together with WAMS, more research is needed to ensure the controller is actually robust enough to be used in the actual power systems.

7 CONCLUSION

The work presented in this thesis can be divided into two main parts. In the first part PMU test methods were developed to verify the PMU compliance according to the latest requirements. The laboratory test setup for PMU validation was assembled using widely available hardware, and the necessary software for creating the tests and evaluating the measurements was developed as part of the PhD project. In addition to the tests defined in the standard, the PMU performance was investigated under impairments which can be seen in an actual power system: high noise, multiple harmonics and instrument transformer saturation. The second part of the project looks into full-scale converter WTs (Type 4) and WPP models suitable for small-signal stability analysis, and explores the possibility of using the WPP to improve the damping of inter-area oscillations. The WPP is equipped, in turns, with two types of PODs for comparison: a phasor POD and a conventional PSS type. Remote PMU measurements are used as input signals for the PODs and data communication latency is considered.

7.1 Results

The PMU test setup was used to test three commercial PMUs from three different vendors. The PMU measurements were evaluated according to the latest requirements (IEEE C37.118.1a-2014 amendment). It was found that the tested PMUs failed a number of tests for both steady-state and dynamic conditions. For example, one of the devices was not filtering out-of-band interfering signals which in turn affected the phase of the phasor measurement causing the TVE to exceed the allowed limit. Two of the PMUs were showing difficulties in producing correct measurements when the injected currents were between 10% and 20% of the rated value. One of these two PMUs showed a particular interesting result since it was producing correct measurements on two of the phases, and incorrect result on the third phase. This is unexpected since the PMUs would most likely use the similar hardware for all its current phases, and the same processing algorithm would most likely be used for the acquired measurements.

The dynamic tests were a challenge for the tested PMUs. The tests revealed that two of the units had difficulties in measuring oscillating signals, especially when the phase angle was the oscillating quantity. These devices failed to correctly estimate the main frequency of the injected signal. The frequency ramp and the step tests also revealed issues with the PMUs. All devices showed a delay in the frequency measurement in

case of the frequency ramp. Moreover, one of the devices had issues with the amplitude estimation of the phasors.

The performance of the PMUs was also explored under impairments that can be seen in a real power system. The noise tests showed that these units would produce accurate results for a signal to noise ratio above 65 dB. Below this level, the ROCOF estimation will be the first to show high error, followed by the frequency estimation and finally the phasor measurement. The measurements were also affected by CT saturation which was causing the high errors almost as soon as the CT would start to saturate. Although, it is not an issue directly related to the PMU, in such conditions, wrong measurements can reach different power system control applications. Therefore, it would be beneficial to have a way of flagging these measurements as incorrect. Finally, multiple harmonics can be present in the power system. The tested PMUs proved to have sufficient filtering to successfully reject multiple and single harmonics at both nominal and off-nominal frequencies.

For small-signal analysis studies, a phasor model of a type 4 wind turbine was implemented. The model can be used as a single WT or as an aggregated WPP. The advantage of a phasor model WT is that it reduces simulation time, and it is still accurate for studying low frequency oscillations in a power system involving a large number of generators. Furthermore, the phasor model can be linearized by the available tools together with the entire initialized power system model. This is useful for small-signal stability studies which are based on modal analysis of the linearized system. The implemented model was tested together with the classic two-area, four-generator system. The wind power penetration was increased in steps and the impact of the WPP on the modal characteristics was investigated. It was found that the implemented model did not have a significant effect on the oscillatory modes of the power system. Moreover, the participation factors showed that the WPP mechanical system does not have a high participation when compared to the synchronous generators. These results are similar to previous findings that have been published in this field.

The WPP is equipped with PODs to contribute to the damping of the inter-area oscillations. For comparison two types of PODs are implemented: a phasor POD and a conventional PSS. Both PODs use remote PMU measurements as input signals. The typical latency in the communication infrastructure for phasor measurements is of a few milliseconds. However, situations can rise where the latency increases to hundreds of milliseconds. To investigate the performances of the two PODs, the input signals are subjected to a range of latencies between 0 ms and 140 ms. The results show that the conventional PSS, which uses a fixed phase shift chosen at the design stage, does perform well as long as the latency is not too high. For latencies higher than 100 ms, this controller causes the WPP to sustain or even amplify the power system oscillations.

The phasor POD, benefits from a latency compensation stage which uses the information provided by the time-stamping of the PMU measurements, at the PMU location and at the control center to correct the input signal. The advantage is that the latency for each communicated sample is known due to the GPS synchronization of the PMUs and control center. The results show that the phasor POD performs similar over the entire latency range used in this study.

7.2 Future work

In this section several topics that have been identified as suitable candidates for future research are presented:

- The test results presented in Chapter 3 are based on older PMUs and it was shown that these devices are not compliant with the current standard. Companies are working on producing units that are capable of satisfying all the requirements. It would be interesting and useful to compare newer devices with the ones that are already available in order to see the differences. These tests could prove to be useful to power system operators which invest in such equipment.

- A more detailed assessment of the PODs used with the WPP seems necessary. It is clear that each of the POD type investigated has its own advantages. The classical PSS is simple and it is widely used with synchronous generators. However, using it together with WAMS might prove challenging. The phasor POD is based on estimating the oscillatory and average components of the measured signal, and has the advantages of easily compensating for latency in the input signal. The next step would be to use real-time digital simulators , such as RTDS, to implement this type of controller, and use it together with WT models to investigate their effects on inter-area oscillations. The RTDS, for example, has a PMU model implemented which can be used for measurements in the model.

- The RTDS also offers the possibility of hardware in loop testing. An actual commercial PMU could be used in assessing the impact of the WPPs on power system oscillations.

- Finally, field tests would give a good understanding regarding the use of a phasor POD with wind turbines. Many PMUs have been installed in the system already and these could be used to provide measurements for the POD.

REFERENCES

[1] International Energy Outlook 2016, May 2016. [Online]. Available: https://www.eia.gov/outlooks/ieo/pdf/wolrd.pdf.

[2] U.S.-Canada Power System Outage Task Force, “Final Report on the August 14, 2003 Blackout in the United States and Canada: Causes and Recommendations,” U.S. Department of Energy, Washington DC, USA, Tech. Rep. April, 2004.

[3] European Commission, “A Roadmap for moving to a competitive low carbon economy in 2050,” 2011.

[4] F. Li, W. Qiao, H. Sun, H. Wan, J. Wang, Y. Xia, Z. Xu, and P. Zhang, “Smart Transmission Grid: Vision and Framework,” *IEEE Trans. Smart Grid*, vol. 1, no. 2, pp. 168-177, Sep. 2010.

[5] H. Johannsson, A. H. Nielsen, and J. Østergaard, “Wide-Area Assessment of Aperiodic Small Signal Rotor Angle Stability in Real-Time,” *IEEE Trans. Power Syst.*, vol. 28, no. 4, pp. 4545-4557, Nov. 2013.

[6] M. Glavic and T. Van Cutsem, “Wide-Area Detection of Voltage Instability from Synchronized Phasor Measurements. Part I: Principle,” *IEEE Trans. Power Syst.*, vol. 24, no. 3, pp. 1408-1416, Aug. 2009.

[7] M. Glavic and T. Van Cutsem, “Wide-Area Detection of Voltage Instability from Synchronized Phasor Measurements. Part I: Simulation Results,” *IEEE Trans. Power Syst.*, vol 24, no. 3, pp. 1417-1425, Aug. 2009.

[8] A. G. Phadke, J. S. Thorp and M. G. Adamiak, "A New Measurement Technique for Tracking Voltage Phasors, Local System Frequency, and Rate of Change of Frequency," in *IEEE Trans. Power App. Syst.*, vol. PAS-102, no. 5, pp. 1025-1038, May 1983.

[9] A. G. Phadke and J. Thorp, *Synchronized Phasor Measurements and Their Applications.* Springer Verlag, 2008.

[10] A. Phadke and R. De Moraes, “The Wide World of Wide-Area Measurement,” *IEEE Power Energy Mag.*, vol. 6, no. 5, pp. 52-65, Sep. 2008.

[11] S. Skok, I. Ivankovic, and Z. Cerina, “Applications Based on PMU Technology for Improved Power System Utilization,” in *IEEE PES General Meeting*, Jun. 2007, pp. 1-8.

[12] D. Novosel, V. Madani, B. Bhargava, K. Vu, and J. Cole, “Dawn of the grid synchronization,” *IEEE Power Energy Mag.*, vol. 6, no. 1, pp. 49-60, Jan. 2008.

[13] M. Klein, G. J. Rogers and P. Kundur, "A fundamental study of inter-area oscillations in power systems," *IEEE Trans. Power Syst.*, vol. 6, no. 3, pp. 914-921, Aug 1991.

[14] P. Pourbeik, P. S. Kundur and C. W. Taylor, "The anatomy of a power grid blackout - Root causes and dynamics of recent major blackouts," *IEEE Power Energy Mag.*, vol. 4, no. 5, pp. 22-29, Sept.-Oct. 2006.

[15] G. Rogers, “Power System Oscillations,” in *Power Electronics and Power Systems*, 2nd ed., Kluwer Academic Publisher, 2000.

[16] D. Wilson, J. Bialek and Z. Lubosny, "Banishing blackouts [power system oscillations stability]," in *Power Engineer*, vol. 20, no. 2, pp. 38-41, April-May 2006.

[17] P. Kundur, *Power System Stability and Control*, New York, NY, USA, McGraw-Hill, 1994.

[18] S.M. Ustinov, J.V. Milanović, V.A. Maslennikov, “Inherent dynamic properties of interconnected power systems,” *International Journal of Electrical Power & Energy Systems*, vol. 24, no. 5, Jun. 2002, pp. 371-378.

[19] A. G. Phadke, "Synchronized phasor measurements-a historical overview," *IEEE/PES Transmission and Distribution Conference and Exhibition*, 2002, pp. 476-479 vol.1.

[20] IEEE Standard for Synchrophasers for Power Systems," in *IEEE Std 1344-1995(R2001)*, 1995.

[21] IEEE Standard for Synchrophasors for Power Systems," in *IEEE Std C37.118-2005 (Revision of IEEE Std 1344-1995)*, pp.1-57, 2006.

[22] IEEE Standard for Synchrophasor Measurements for Power Systems," in *IEEE Std C37.118.1-2011 (Revision of IEEE Std C37.118-2005)* , vol., no., pp.1-61, Dec. 28 2011.

[23] IEEE Standard for Synchrophasor Data Transfer for Power Systems," in *IEEE Std C37.118.2-2011 (Revision of IEEE Std C37.118-2005)* , vol., no., pp.1-53, Dec. 28 2011.

[24] K. E. Martin, "Synchrophasor Measurements Under the IEEE Standard C37.118.1-2011 With Amendment C37.118.1a," in *IEEE Transactions on Power Delivery*, vol. 30, no. 3, pp. 1514-1522, June 2015.

[25] IEEE Standard for Synchrophasor Measurements for Power Systems -- Amendment 1: Modification of Selected Performance Requirements," in *IEEE Std C37.118.1a-2014 (Amendment to IEEE Std C37.118.1-2011)* , vol., no., pp.1-25, April 30 2014.

[26] J. Depablos, V. Centeno, A. G. Phadke and M. Ingram, "Comparative testing of synchronized phasor measurement units," *IEEE Power Engineering Society General Meeting, 2004.*, 2004, pp. 948-954 Vol.1.

[27] K. E. Martin, T. Faris, and J. Hauer, "Standardized testing of phasor measurement units," in *Proc. Fault Disturbance Anal. Conf.*, Apr. 2006, pp. 1-22.

[28] G. Stenbakken and M. Zhou, "Dynamic Phasor Measurement Unit Test System," *2007 IEEE Power Engineering Society General Meeting*, Tampa, FL, 2007, pp. 1-8.

[29] K. Narendra, D. R. Gurusinghe, and A.D. Rajapakse, "Dynamic Performance Evaluation and Testing of Phasor Measurement Unit (PMU) as per IEEE C37.118.1 Standard," *Presented at the Doble Client Committee Meetings Int. Protect. Testing Users Group, Chicago, IL, USA.*

[30] D.R. Gurusinghe, A.D. Rajapakse, and K. Narendra, "Evaluation of Steady-State and Dynamic Performance of a Synchronized Phasor Measurement Unit," in *Proc. IEEE Elect. Power Energy Conf., London, ON, Canada,* 2012, pp. 57-62.

[31] D.R. Gurusinghe, A.D. Rajapakse, and K. Narendra, "Testing and Enhancement of Dynamic Performance of a Phasor Measurement Unit," *IEEE Trans. Power Del.*, vol. 29, no. 4, August 2014.

[32] K.E. Martin, J.F. Hauer, and T.J. Faris, "PMU Testing and Installation Considerations at the Bonneville Power Administration," in *Proc. IEEE PES General Meeting, Tampa, FL,* 2007, pp. 1-6.

[33] K. Narendra, Z. Zhang, J. Lane, B. Lackey, and E. Khan, "Calibration and Testing of Tesla Phasor Measurement Unit (PMU) Using Doble F6150 Test Instrument," *iREP Symposium-Bulk Power System Dynamics and Control –VII, Revitalizing Operational Reliability*, August, 2007.

[34] R. Garcia-Valle, G. Yang, K. E. Martin, A. H. Nielsen, and J. Ostergaard, "DTU PMU laboratory development-Testing and validation," in *Proc. Innovative Smart Grid Technologies Conference Europe (ISGT Europe),* 2010, pp. 1-6.

[35] M. S. Almas, J. Kilter, and L. Vanfretti, "Experiences with steady-state PMU compliance testing using standard relay testing equipment," in *Proc. IEEE*

Electric Power Quality and Supply Reliability Conference (PQ), 2014, pp.103-110.

[36] G. Stenbakken, and T. Nelson, "Static Calibration and Dynamic Characterization of PMUs at NIST," in *Proc. IEEE PES General Meeting*, Tampa, FL, *2007*, pp 1-4.

[37] Z. Huang, B. Kasztenny, V. Madani, K. Martin, S. Meliopoulos, D. Novosel, and J. Stenbakken, "Performance Evaluation of Phasor Measurement Systems," in *Proc. IEEE PES General Meeting*, Pittsburgh, PA, *2008*, pp.1-7.

[38] P. Komarnicki, C. Dzienis, Z. A. Styczynski, J. Blumschein, and V. Centeno, "Practical experience with PMU system testing and calibration requirements," in *Proc. IEEE PES General Meeting*, Pittsburgh, PA, 2008, pp. 1-5.

[39] Global wind energy Report 2015, April 2016. [Online]. Available: http://www.gwec.net/publications/global-wind-report-2/

[40] P. Ledesma, J. Usaola, and J. Rodriguez, "Transient stability of a fixed speed wind farm," *Renewable Energy*, vol. 28, no. 9, pp. 1341-1355, Jul 2003.

[41] V. Akhmatov, H. Knudsen, A. H. Nielsen, J. K. Pedersen, and N. Kjølstad Poulsen, "Modelling and transient stability of large wind farms," *International Journal of Electrical Power and Energy Systems*, vol. 25, no. 2, pp. 123–144, Feb 2003.

[42] O. Anaya-Lara, F. Hughes, N. Jenkins, and G. Strbac, "Influence of windfarms on power system dynamic and transient stability," *Wind Engineering*, vol. 30, no. 2, pp. 107-127, Mar 2006.

[43] J.G. Slootweg, and W.L. Kling, "The impact of large scale wind power generation on power system oscillations," *Elect. Power Syst. Res.*, vol. 67, no. 1, pp. 9-20, Oct 2003.

[44] N. R. Chaudhuri and B. Chaudhuri, "Impact of wind penetration and HVDC upgrades on dynamic performance of future grids," in *IEEE PES General Meeting*, San Diego, CA, 2011, pp. 1-8.

[45] E. Hagstrom, I. Norheim, K. Uhlen, "Large-scale wind power integration in norway and impact on damping in the Nordic grid", *Wind Energy*, vol. 8, no. 3, pp. 375-384, 2005.

[46] C. Samarasinghe and D. Vowles, "Wind generation investigation project – effect of wind generation on small signal stability," The National Grid, TRANSPOWER New Zealand, Tech. Rep. Investigation 8, Mar. 2008.

[47] T. Knuppel, J. N. Nielsen, K. H. Jensen, A. Dixon and J. Ostergaard, "Small-signal stability of wind power system with full-load converter interfaced wind turbines," *IET Renewable Power Generation*, vol. 6, no. 2, pp. 79-91, Mar. 2012.

[48] N. Modi, T. K. Saha and N. Mithulananthan, "Effect of wind farms with doubly fed induction generators on small-signal stability — A case study on Australian equivalent system," in *IEEE PES Innovative Smart Grid Technologies*, Perth, WA, Nov. 2011, pp. 1-7.

[49] G. Tsourakis, B. M. Nomikos, C.D. Vournas, “Effect of wind parks with doubly fed asynchronous generators on small-signal stability,” *Elect. Power Syst. Res.*, vol. 79, no. 1, Jan 2009, pp. 190-200.

[50] E. Vittal, M. O'Malley and A. Keane, "Rotor Angle Stability With High Penetrations of Wind Generation," *IEEE Trans. Power Syst.*, vol. 27, no. 1, pp. 353-362, Feb. 2012.

[51] R. L. Cresap and W. A. Mittelstadt, "Small-signal modulation of the Pacific HVDC intertie," *IEEE Trans. Power App. Syst.*, vol. 95, no. 2, pp. 536-541, Mar 1976.

[52] T. Smed and G. Andersson, "Utilizing HVDC to damp power oscillations," in *IEEE Trans. Power Del.*, vol. 8, no. 2, pp. 620-627, Apr 1993.

[53] F. M. Hughes, O. Anaya-Lara, N. Jenkins and G. Strbac, "A power system stabilizer for DFIG-based wind generation," *IEEE Trans. Power Syst.*, vol. 21, no. 2, pp. 763-772, May 2006.

[54] N. Kshatriya, U. D. Annakkage, F. M. Hughes and A. M. Gole, "Optimized Partial Eigenstructure Assignment-Based Design of a Combined PSS and Active Damping Controller for a DFIG," *IEEE Trans. Power Syst.*, vol. 25, no. 2, pp. 866-876, May 2010.

[55] Z. Miao, L. Fan, D. Osborn and S. Yuvarajan, "Control of DFIG based wind generation to improve inter-area oscillation damping," in *IEEE PES General Meeting - Conversion and Delivery of Electrical Energy in the 21st Century*, Pittsburgh, PA, 2008, pp. 1-7.

[56] L. Sigrist and L. Rouco, "Design of damping controllers for doubly fed induction generators using eigenvalue sensitivities," in *IEEE/PES Power Systems Conference and Exposition*, Seattle, WA, 2009, pp. 1-7.

[57] G. Tsourakis and C. Vournas, "A controller for wind generators to increase damping of power oscillations," in *Proc. of IEEE International Symposium on Circuits and Systems*, Paris, 2010, pp. 2195-2198.

[58] G. Tsourakis, B. M. Nomikos and C. D. Vournas, "Contribution of Doubly Fed Wind Generators to Oscillation Damping," *IEEE Trans. Energy Convers.*, vol. 24, no. 3, pp. 783-791, Sept. 2009.

[59] J. L. Dominguez-Garcia, O. Gomis-Bellmunt, F. Bianchi, A. Sumper, and A. Sudria-Andreu, “Power System stabiliser capability of offshore wind power plants,” in *Proc of the EWEA*, Copenhagen, 2012, pp. 29-32.

[60] L. Fan, H. Yin and Z. Miao, "On Active/Reactive Power Modulation of DFIG-Based Wind Generation for Interarea Oscillation Damping," *IEEE Trans. Energy Convers.*, vol. 26, no. 2, pp. 513-521, June 2011.

[61] A. Adamczyk, R. Teodorescu and P. Rodriguez, "Control of Full-Scale Converter based Wind Power Plants for damping of low frequency system oscillations," in *IEEE Trondheim PowerTech*, Trondheim, 2011, pp. 1-7.

[62] D. Gautam, V. Vittal, R. Ayyanar and T. Harbour, "Supplementary control for damping power oscillations due to increased penetration of doubly fed induction generators in large power systems," in *IEEE/PES Power Systems Conference and Exposition*, Phoenix, AZ, 2011, pp. 1-6.

[63] R. D. Fernandez, R. J. Mantz and P. E. Battaiotto, "Contribution of wind farms to the network stability," *2006 IEEE PES General Meeting*, Montreal, Que., Jun. 2006, pp. 1-6.

[64] R.D. Fernández, R.J. Mantz, and P.E. Battaiotto, “Potential contribution of wind farms to damp oscillations in weak grids with high wind penetration,” *Renewable and Sustainable Energy Reviews*, vol. 12, no. 6, pp. 1692-1711, Aug. 2008.

[65] C. Martinez, G. Joos and B. T. Ooi, "Power system stabilizers in variable speed wind farms," *2009 IEEE PES General Meeting*, Calgary, AB, 2009, pp. 1-7.

[66] D. Gautam, L. Goel, R. Ayyanar, V. Vittal and T. Harbour, "Control Strategy to Mitigate the Impact of Reduced Inertia Due to Doubly Fed Induction Generators on Large Power Systems," *IEEE Trans. Power Syst.*, vol. 26, no. 1, pp. 214-224, Feb. 2011.

[67] T. Knuppel, J. N. Nielsen, K. H. Jensen, A. Dixon and J. Ostergaard, "Power oscillation damping capabilities of wind power plant with full converter wind turbines considering its distributed and modular characteristics," in *IET Renewable Power Generation*, vol. 7, no. 5, pp. 431-442, Sept. 2013.

[68] A. Mendonca and J. A. P. Lopes, "Robust tuning of power system stabilisers to install in wind energy conversion systems," *IET Renewable Power Generation*, vol. 3, no. 4, pp. 465-475, December 2009.

[69] L. Angquist, “Method and a Device for Damping Power Oscillations in Transmission Lines,” U.S. Patent 6 559 561, May 6, 2003.

[70] L. Angquist and C. Gama, "Damping algorithm based on phasor estimation," in *Proc. of IEEE PES Winter Meeting*, Columbus, OH, 2001, vol.3, pp. 1160-1165.

[71] C. Gama, L. Angquist, G. Ingerstrom, M. Noroozian, “Commissioning and operative experience of TCSC for damping power oscillation in the Brazilian North-South Interconnection,” CIGRE 2000 session, Paris, pp 1-6.

[72] N. R. Chaudhuri, S. Ray, R. Majumder and B. Chaudhuri, "A New Approach to Continuous Latency Compensation With Adaptive Phasor Power Oscillation Damping Controller (POD)," *IEEE Trans. on Power Syst.*, vol. 25, no. 2, pp. 939-946, May 2010.

[73] N. R. Chaudhuri, B. Chaudhuri, S. Ray, and R. Majumder, “Wide-area phasor power oscillation damping controller: a new approach to handling time-varying signal latency,” *IET Gener. Transm. Distrib.*, vol. 4, no. 5, pp. 620-630, May 2010.

[74] N. R. Chaudhuri, S. Ray, R. Majumder and B. Chaudhuri, "A case study on challenges for robust wide-area phasor POD," *2009 IEEE Power & Energy Society General Meeting*, Calgary, AB, 2009, pp. 1-6.

[75] R. Sadikovic, P. Korba and G. Andersson, "Self-tuning controller for damping of power system oscillations with FACTS devices," *2006 IEEE Power Engineering Society General Meeting*, Montreal, Que., Jun. 2006, pp. 1-6.

[76] P. Korba, M. Larsson and C. Rehtanz, "Detection of oscillations in power systems using Kalman filtering techniques," *Proceedings of 2003 IEEE Conference on Control Applications, 2003. CCA 2003.*, 2003, pp. 1-5.

[77] N. R. Chaudhuri, A. Domahidi, B. Chaudhuri, R. Majumder, P. Korba, S. Ray, and K. Uhlen, "Power oscillation damping control using wide-area signals: A case study on Nordic equivalent system," *IEEE PES T&D 2010*, New Orleans, LA, USA, 2010, pp. 1-8.

[78] E. Hendricks, O. Jannerup, and P.H. Sorensen, *Linear Systems Control – Deterministic and stochastic methods.* The Technical University of Denmark, Ørsted, DTU section of Automation, 2005.

[79] K. J. Astrom and B. Witternmark, *Adaptive Control*, 2nd ed. Reading, MA: Addison-Wesley, 1995.

[80] P. Korba, R. Segundo, A. Paice, B. Berggren, and R. Majumder, “Time delay compensation in power system control,” E. U. Patent EP08 156 785, May 23, 2008.

[81] D. Wilson, J. Bialek and Z. Lubosny, "Banishing blackouts [power system oscillations stability]," *Power Engineer*, vol. 20, no. 2, pp. 38-41, April-May 2006.

[82] IEEE Standard Common Format for Transient Data Exchange (COMTRADE) for Power Systems," *IEEE Std C37.111-1999*, vol., no., pp.1-55, Oct. 15, 1999.

[83] IEEE Synchrophasor Measurement Test Suite Specification--Version 2," in *IEEE Synchrophasor Measurement Test Suite Specification--Version 2* , vol., no., pp.1-43, Sept. 28 2015.

[84] C. Offelli and D. Petri, "Weighting effect on the discrete time Fourier transform of noisy signals," *IEEE Trans. Instrum. Meas.*, vol. 40, no. 6, pp. 972–981, Dec. 1991.

[85] D. Macii, D. Petri, and A. Zorat, "Accuracy Analysis and Enhancement of DFT-Based Synchrophasor Estimators in Off-Nominal Conditions," *IEEE Trans. Instrum. Meas.*, vol. 61, no. 10, pp. 2653–2664, Oct. 2012.

[86] L. Zhan, Y. Liu, J. Culliss, J. Zhao, and Yilu Liu, "Dynamic Single-Phase Synchronized Phase and Frequency Estimation at the Distribution Level," *IEEE Trans. Smart Grid*, vol. 6, no. 4, pp. 2013-2022, July 2015.

[87] C. R. Mason, *The Art and Science of Protective Relaying*. 2nd ed., John Wiley, New York, 1986.

[88] J. G. Proakis and D. G. Manolakis, Digital Signal Processing, Principles, Algorithms, and Applications. 3rd ed., Prentice-Hall Inc., New Jersey, 1996.

[89] B. Badrzadeh, M. Gupta, N. Singh, A. Petersson, L. Max, and M. Hogdahl, "Power system harmonic analysis in wind power plants—Part I: Study methodology and techniques," in *Proc. IEEE Ind. Appl. Soc. Annual Meeting*, Las Vegas, NV., Oct. 2012, pp.1-11.

[90] S. Liang, Q. Hu, and W. Lee, "A survey of harmonic emissions of a commercial operated wind farm," in *Proc. IEEE Industrial and Commercial Power Systems Technical Conf.*, Tallahassee, FL, USA, May 2010, pp. 1-8.

[91] L. F. Blume, G. Camilli, S.B. Farnham, and H.A. Peterson, "Transformer Magnetizing Inrush Currents and Influence on System Operation," *AIEE Trans.*, vol. 63, no. 6, pp. 366-375, Jun. 1944.

[92] H. S. Bronzeado, P.B. Brogan, R. Yacamini, "Harmonic Analysis of Transient Currents During Sympathetic Interaction," *IEEE Trans. Power Syst.* , vol. 11, no. 4, pp. 2081-2056, Nov. 1996.

[93] E. C. Segatto and D. V. Coury, "A power transformer protection with recurrent ANN saturation correction," in *Proc. IEEE PES General Meeting, vol.2*, 12-16 June 2005, pp. 1341-1346.

[94] IEEE Guide for the Application of Current Transformers Used for Protective Relaying Purposes, IEEE Std C37.110™-2007.

[95] IEEE Standard Requirements for Instrument Transformers, IEEE Std C57.13™-2008.

[96] J. G. Kappenman, V. D. Albertson, and N. Mohan, “Current Transformer and Relay Performance in the Presence of Geomagnetically-Induced Currents,” *IEEE Trans. Power App. Syst.*, vol. PAS-100, no. 3, pp. 1078–1088, Mar. 1981.

[97] F. Bachinger, A. Hackl, P. Hamberger, Leikermoser, G. A. Leber, H. Passath, and M. Stoessl, “Direct current in transformers: Effects and compensation,” in CIGRE Session, SC A2, Paris, Aug. 2012, pp. 1-5.

[98] K. Draxler and R. Styblíková, “Effect of Magnetization on Instrument Transformers Errors,” *J. Electr. Eng.*, vol. 61, no. 7/s, pp. 50–53, 2010.

[99] G. Buticchi, E. Lorenzani, and G. Franceschini, “A DC Offset Current Compensation Strategy in Transformerless Grid-Connected Power Converters,” *IEEE Trans. Power Del.*, vol. 26, no. 4, pp. 2743–2751, Oct. 2011.

[100] MATLAB documentation center. [Online]. Available: https://www.mathworks.com/help/

[101] S. Heier, *Grid integration of wind energy conversion systems*, John Wiley & Sons, 1998.

[102] N. W. Miller, W. W. Pric, and J. J. Samches-Gasca. (2003, Oct.). Dynamic modeling of GE 1.5 and 3.6 Wind Turbine-Generators. GE-Power System Energy Consulting. [Online]. Available: https://pdfs.semanticscholar.org/4be9/52ff4ee3203db24ed461f8064abb00b8fa4e.pdf

[103] D. Grenier, L. A. Dessaint, O. Akhrif, Y. Bonnassieux and B. Le Pioufle, "Experimental nonlinear torque control of a permanent-magnet synchronous motor using saliency," *IEEE Trans. Ind. Elect.*, vol. 44, no. 5, pp. 680-687, Oct 1997.

[104] S. M. Muyeen, J. Tamura, and T. Murata, *Stability augmentation of a grid connected wind farm, Green Energy and Technology*, Springer-Verlag, 2009.

[105] S. Morimoto, Y. Takeda and T. Hirasa, "Current phase control methods for permanent magnet synchronous motors," *IEEE Trans. Power Elect.*, vol. 5, no. 2, pp. 133-139, Apr 1990.

[106] A. D. Hansen and I. D. Margaris. (2014). Type IV Wind Turbine Model DTU Wind energy. [Online]. Available: http://orbit.dtu.dk/en/publications/type-iv-wind-turbine-model(99b55843-deb3-49b9-b564-e664bc25fa99).html

[107] MATLAB documentation center, SimPowerSystems™ 6.6 – User’s Guide, 2016.

[108] MATLAB documentation center, Simulink Control Design™ 4.4– User’s Guide, 2016.

[109] J. A. de la O Serna, J. M. Ramirez, A. Zamora Mendez and M. R. A. Paternina, "Identification of Electromechanical Modes Based on the Digital Taylor-Fourier Transform," in *IEEE Transactions on Power Systems*, vol. 31, no. 1, pp. 206-215, Jan. 2016.

[110] J. Y. Cai, Zhenyu Huang, J. Hauer and K. Martin, "Current Status and Experience of WAMS Implementation in North America," *2005 IEEE/PES Transmission & Distribution Conference & Exposition: Asia and Pacific*, Dalian, 2005, pp. 1-7.

[111] G. T. Heydt, C. C. Liu, A. G. Phadke and V. Vittal, "Solution for the crisis in electric power supply," *IEEE Comput. Appl. Power*, vol. 14, no. 3, pp. 22-30, Jul 2001.

A
STEADY-STATE PMU COMPLIANCE TEST UNDER C37.118.1A-2014

This paper has been presented at the IEEE PES Innovative Smart Grid Technologies (ISGT) Europe Conference in Ljubljana, Slovenia and has been published as part of the conference proceedings

Steady-State PMU Compliance Test under C37.118.1a™-2014

Radu Ghiga*, Qiuwei Wu*, Kenneth Martin†, Walid El-Khatib*, Lin Cheng‡ and Arne H. Nielsen*
*Center for Electric Power and Energy Engineering
Technical University of Denmark, Kgs. Lyngby 2800, Denmark
Emails: rghiga@elektro.dtu.dk, qw@elektro.dtu.dk and wzel@elektro.dtu.dk
†Senior Consultant at Electric Power Group, Los Angeles, California
Email: kenm8421@yahoo.com
‡Department of Electrical Engineering, Tsinghua University, Beijing 100084, China
Email: chenglin@mail.tsinghua.edu.cn

***Abstract*—This paper presents a flexible testing method and the steady-state compliance of PMUs under the C37.118.1a amendment. The work is focused on the changes made to the standard for the harmonic rejection and out-of-band interference tests for which the ROCOF Error limits have been suspended. The paper aims to provide an indication whether these limits should be reinstated or not. The test platform consists of a test signal generator capable of providing three phase voltages and currents, and playing back digitized files, PMUs under test, and a PMU test result analysis kit. Three PMUs from different vendors were tested simultaneously in order to provide a fair comparison of the devices. The results for the steady state tests are discussed in the paper together with the strengths and weaknesses of the PMUs and of the test setup.**

I. Introduction

PMUs are considered one of the key technologies for wide area power system protection control and monitoring systems [1]. Therefore, these units are increasingly being developed in order to improve their performance. PMU data can be used for multiple applications. Some of them include oscillation monitoring, fault detection, state estimation and model validation [2]. The reliability of these applications is based on the accuracy of the PMUs for a correct synchrophasor and frequency estimation. In this case, it is essential to understand the technical performance of these devices and to validate the measured data before using them on a larger scale.

Previous work done in the field includes different testing methods such as the one described in [3] which was developed for the compliance testing with the 2005 standard [4]. Steady-state tests according to the 2011 standard have been published before [5].

This paper extends the previous work regarding testing and validation presented in [6] by updating the test platform with the latest requirements presented in the IEEE C37.118.1a amendment. The steady-state tests vary different parameters of the input signals such as voltage and current amplitude, phase and frequency. The filtering capabilities of the units are tested by injecting harmonics and signals that are outside the bandwidth of the PMUs. The phasor estimation of the units is evaluated by the Total Vector Error (TVE). The Frequency Error (FE) shows estimated frequency accuracy of the devices under test. The harmonic and out of band interfering signals tests are modified by the amendment to the standard which suspended the ROCOF Error (RFE) limit for these two tests. The paper shows the impact of these signals on the PMUs measurements, and gives suggestions regarding the limits suspended by the IEEE C37.118.1a amendment.

The paper is organized as follows: Section II provides information regarding the hardware, methodology and the performed tests. Section III presents the results, and finally Section IV concludes the paper, summarizing the contribution of the work.

II. PMU Testing Architecture and Methodology

This section of the paper provides information of the laboratory hardware used for testing the PMUs and describes the methodology.

A. Test Bed Description

To generate the PMU input signals a standard stand alone test set for protection relays is used. It is capable of delivering 3-phase AC voltages and currents that are synchronized to the UTC with a rated time synchronization error of less than $1\mu s$.

The Total Vector Error (TVE) of the PMUs should be calculated within 1% of the nominal signal [7]. In order to achieve such precision, the test equipment should be able to produce signals with an accuracy at least ten times higher than that [8]. This translates into a precision of at least 0.1%. The test set has a rated amplitude precision of 0.02% which is within the required range. The nominal voltage level for these tests is 70 Vrms and the nominal current level is 5 Arms.

A calibration of the test set is carried out in order to verify what is the deviation in voltage amplitude from the theoretical value. For this test a signal file is created in Matlab that generates six amplitudes, including the value considered nominal (100 V peak) further on in the testing. Each of them is kept constant for 30 seconds in order to provide enough time for measurements. Due to space limitation, only the measurements for the nominal amplitude are shown in Table II.

978-1-5090-3358-4/16/$31.00 ©2016 IEEE

Four digital voltmeters with specifications shown in Table I are used to read the voltage output of the test set, and their average reading was used as a correction. It can be seen that two of the meters agree closely, while the other two are somewhat different. Due to this, it is hard to tell whether the readings are correct or incorrect. Therefore, uncertainty is defined as the maximum deviation of each meter from the average. The Test Set error (%TS error) is the deviation of the average measured voltage from the output set by the test file. Each TS Error is used as a correction factor for the amplitude of each phase. The standard deviation of the measurement is given by the S.D. and S.D. pu rows in the Table II.

The time synchronization check is carried out with an oscilloscope which is triggered on the 1 PPS signal obtained from a GPS clock receiver. The three phases are checked simultaneously, and a time lag of $142\mu s$ is found which translates into a phase error of 2.556 degrees. The test did not show any phase drift in time. Consequently, the angle of the reference phasor is corrected with 2.556 degrees.

The test set has the capability of playing back digitized files by converting the waveforms into analog signals and amplifying them. Its 16-bit, 10 ksamples/s digital-to-analog converter (DAC) and built-in amplifiers, enable accurate reproduction of the waveforms, including harmonics and interfering frequencies. Multiple devices can be tested simultaneously using the same input signal, providing a fair PMU performance analysis. Details about the methodology of the testing procedure are available in the next subsection.

B. Testing procedure

The test process is based on the generation of waveforms required by the C37.118.1 standard, application to the PMU and comparison of the reported PMU data with the expected result. The idea is simple and robust since a PMU estimates a synchrophasor equivalent for a given AC waveform. By taking a phasor equivalent model and producing the AC waveform that it represents with high accuracy as an electrical signal then injecting it into a PMU, the resulting synchrophasor estimate should match the original phasor model. The overall steps of the process are shown in Fig 1.

Matlab is used to create data points reproducing a specific phasor model designed to test a certain aspect of the PMU measuring capability. The phasor model is converted into the equivalent 3-phase AC signal. A discrete time representation

TABLE I: Voltmeters Used in Calibration Test

	Multimeters	Rated accuracy
M1	Agilent U1242B	$\pm 1\% + 5$ (% of reading + No. of Least Significant Digit)
M2	Agilent U1242B	$\pm 1\% + 5$ (% of reading + No. of Least Significant Digit)
M3	Agilent U3606A	$\pm 0.22\% + 0.12\%$ (% of reading + % of range)
M4	Agilent U3606A	$\pm 0.22\% + 0.12\%$ (% of reading + % of range)

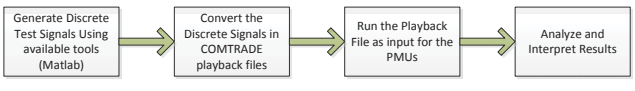

Fig. 1: Overall testing Process

TABLE II: Amplitude Calibration Results

	Phase A	Voltage Phase B	Phase C
% of nominal		100	
V (RMS)		70.7106	
M1	70.6100	70.5900	70.6100
M2	70.6100	70.5900	70.6100
M3	70.7210	70.7090	70.7250
M4	70.7160	70.7010	70.7180
Average	70.6643	70.6417	70.6658
%M1	-0.0767	-0.08139	-0.0788
%M2	-0.0767	-0.08139	-0.0788
%M3	0.0803	0.0870	0.0838
%M4	0.0732	0.0757	0.0739
%Uncertainty	0.0803	0.0870	0.0838
S.D.	0.0626	0.0664	0.0644
S.D. pu	0.00088	0.00094	0.00091
% TS Error	-0.06566	-0.0893	-0.0635

of the test signal is therefore obtained and saved as a .mat file. The .mat file does not generally transfer to a signal generator, it is converted using Matlab to the IEEE C37.111 COMTRADE format since it is widely used for time series recording and is compliant to most vendors.

Once the test data is loaded into the test set it can be played back using a time synchronized start. The output sampling is accurately synchronized, with a rated time error of less than $1\mu s$. The PMU data is recorded during the full duration of the test using a commercially available Phasor Data Concentrator (PDC).

The block diagram of the full testing procedure is shown in Fig 2.

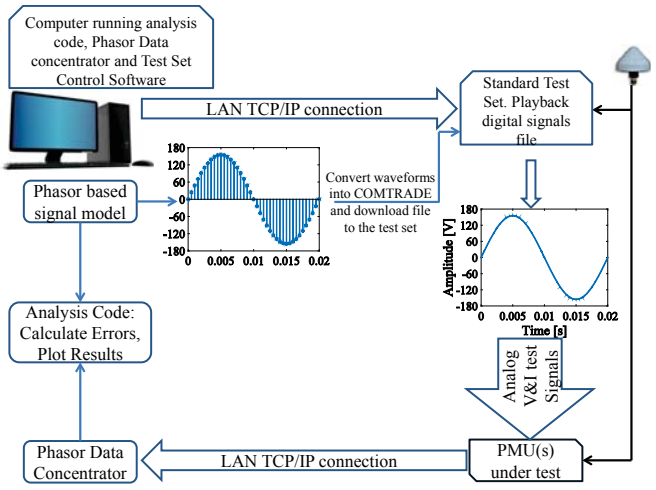

Fig. 2: Block Diagram of the Test Platform

C. Reference Phasor Definition, Measurement Evaluation and Test description

A generalized phasor function can be obtained from a sine function with amplitude and phase modifiers as:

$$X(t) = X_m[g(t)] * cos(\omega_0 t + y(t)) \quad (1)$$

Where X_m is the nominal amplitude, ω_0 is the nominal power system frequency, g(t) is an amplitude modifying function and

y(t) is a phase modifying function. The corresponding phasor value is:

$$X(nT) = \{X_m/\sqrt{2}\}\{g(nT)\}\angle\{y(nT)\} \quad (2)$$

Where nT is the reporting instant. The phasor values reported by the PMU should be an estimate of this value for each given instant in time.

Frequency and ROCOF are defined as:

$$f(t) = \frac{1}{2\pi}\frac{d(\omega_0 t + y(t))}{dt} \quad (3)$$

$$ROCOF(t) = \frac{df(t)}{dt} \quad (4)$$

The analysis software uses these equations to build the reference phasor to which the TS Error for amplitude shown in Table II and the phase delay of 2.556 degrees corrections are applied.

The TVE, FE and RFE are defined by C37.118.1 standard and are well known [7]. Thus, the equations will not be presented here again. There are two new quantities defined in the Test Suite Specification document [9]. The magnitude error (ME), which gives information regarding the amplitude error of the measured phasor, and is defined as,

$$ME(\%) = \frac{\sqrt{\hat{X}_r(n)^2 + \hat{X}_i(n)^2} - \sqrt{X_r(n)^2 + X_i(n)^2}}{\sqrt{X_r(n)^2 + X_i(n)^2}} x100\% \quad (5)$$

And the Phase Error (PE) which shows the error in the angle estimation of the phasor, and is defined as,

$$PE(deg) = atan(\hat{X}_r, \hat{X}_i) - atan(X_r, X_i) \quad (6)$$

Where $\hat{X}_r$ and $\hat{X}_i$ are the measured real and imaginary parts of the phasor and X_r and X_i are the real and imaginary parts of the reference phasor.

The implemented steady state tests are shown in the following table:

TABLE III: Steady-state tests description for M-class requirements

Test Name	Varied quantity
Amplitude scan (Ascan)	Voltage 10% - 120% Current 10% - 200%
Phase Scan (Pscan)	Angle - π to + π
Frequency Scan (Fscan)	Frequency 45 - 55 Hz
Harmonic rejection (Harm)	2^{nd} to 50^{th}
Out-of-Band (Band)	10 - 100 Hz interfering frequencies

III. Test Results

This section presents the results for steady-state compliance tests listed in Table III for the M-performance class and a PMU reporting rate of 50 samples/s. Each time a parameter is varied, the three PMUs are allowed to settle and enough time is given in order to record at least 200 data points. The transient interval is removed from the analysis and the evaluation is carried out on all data points of the settled measurements. The TVE, FE, and RFE shown in this section represent the maximum value of the analysis interval. The limits are shown on the plots with a red line at the values defined by standard [7] and amendment [10] for the specific test.

1) Amplitude Scan Test: The test varies the amplitude of the three phase voltages and currents input according to Table III. All PMUs show high TVE values when the amplitude of the input signal is 0.1 p.u. This is caused by the amplitude of the measured phasor rather than its angle as shown in Fig. 3b and Fig. 3c.

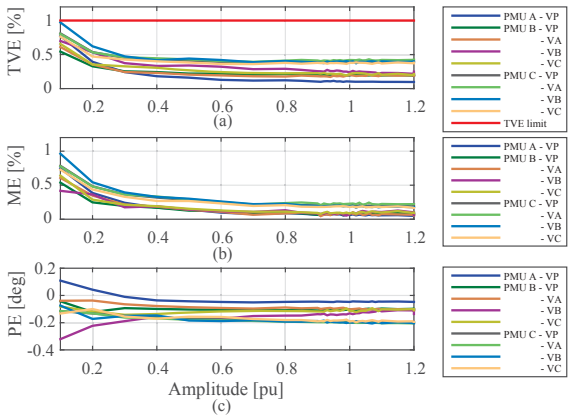

Fig. 3: Amplitude Scan Voltage: a) Total Vector Error; b) Magnitude Error (measured-reference); c) Phase Error (measured-reference)

The test reveals differences for current measurements. Fig. 4a shows that PMU A is the most accurate at rated current value. However, it exceeds the limit for current amplitudes below 0.3 p.u. Fig. 4c shows that PMU A is reporting an incorrect phase angle for low input currents. One possible explanation is the design of the current transformers in PMU A which cannot accurately measure low amplitude currents.

A curious case is PMU C. Phase B current measurement exceeds TVE and the reason is incorrect angle estimation shown in Fig. 4b. However, the other two phases are within limits. This is surprising since all three phases should have similar current transformers and the phasor estimation algorithm should be the same. In contrast, Phase A shows high magnitude error and low phase error, Fig. 4b and Fig. 4c.

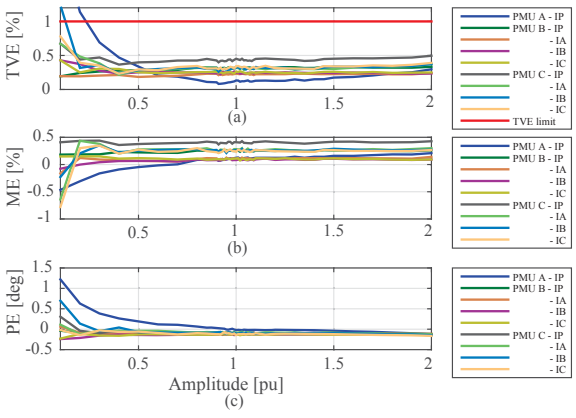

Fig. 4: Amplitude Scan Current: a) Total Vector Error; b) Magnitude Error (measured-reference); c) Phase Error (measured-reference)

2) Phase Scan Test: The test uses an input signal with an off-nominal frequency. This way the PMU is reporting a changing angle. The C37.118.1 standard recommends as frequency offset $|f_{in} - f_0| < 0.25Hz$. For this test, the chosen offset is 0.12Hz. The accuracy of the voltage and current measurements is well within the limit for all PMUs as shown in Fig. 5.

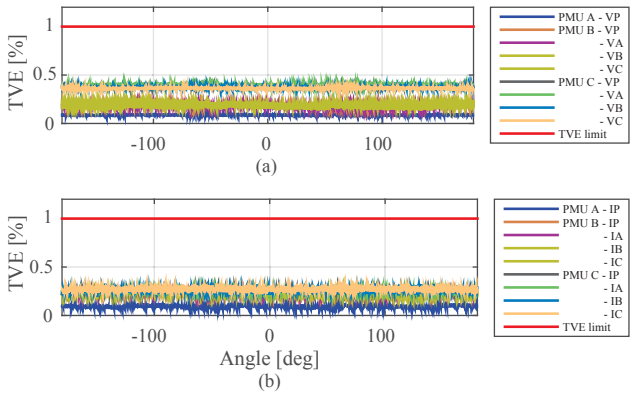

Fig. 5: Phase Scan Total Vector Error a) Voltage; b) Current

3) Frequency Scan Test: The test varies the input signal frequency from 45 Hz up to 55 Hz for both voltages and currents with a step increase of 0.1 Hz. Fig 6a shows that PMU B exceeds the TVE limit at 45 Hz. This is due to incorrect amplitude estimation seen in Fig. 6b. The vendor specifies that the limit of the off-nominal frequency that this device can handle is 45 Hz. Therefore, one possible explanation is that at exactly this frequency, the PMU does not have the bandwidth to measure correctly. PMU C exceeds the TVE limit when the signal frequency is 55 Hz. This can be explained by the higher phase error this PMU has at 55 Hz compared to the others as shown in Fig. 6c.

A frequency-phase bias can be seen for all PMUs in both voltages and current measurements in Fig. 6c and Fig. 7c. One reason could be that the test set has a frequency phase bias caused by the reconstruction filters. It can be noticed that the slopes by which the angles vary are different for each PMU. This would suggest that the estimation algorithms of the devices also have some kind of frequency phase bias since the input waveforms are the same for all three PMUs. It is difficult to point out the real reason without extended testing.

The frequency error is within limits for all devices as shown in Fig. 8a. Concerning ROCOF Error, PMU B exceeds the limit at exactly 45 Hz, similar to the TVE results probably because of the above mentioned reason.

4) Harmonic rejection Test: This test shows if the accuracy of the PMUs is decreased when measuring signals containing harmonics. Harmonics from second up to 50th are injected one by one into the input signal. The reference signal is kept at constant amplitude and frequency.

Fig. 9 shows that all PMUs estimate the voltage and current phasors with the required accuracy. In case of PMU C, the 19th harmonic seems to have a large impact increasing the TVE to 0.9%. Although not shown here due to space limitations, the 19th harmonics affects both phasor amplitude and angle.

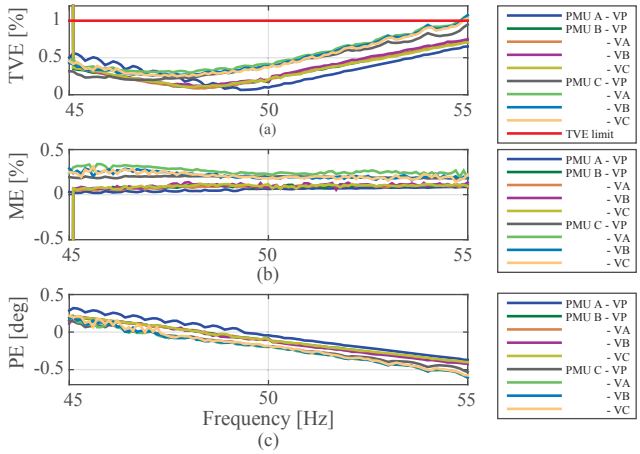

Fig. 6: Frequency Scan Voltage: a) Total Vector Error; b) Magnitude Error (measured-reference); c) Phase Error (measured-reference)

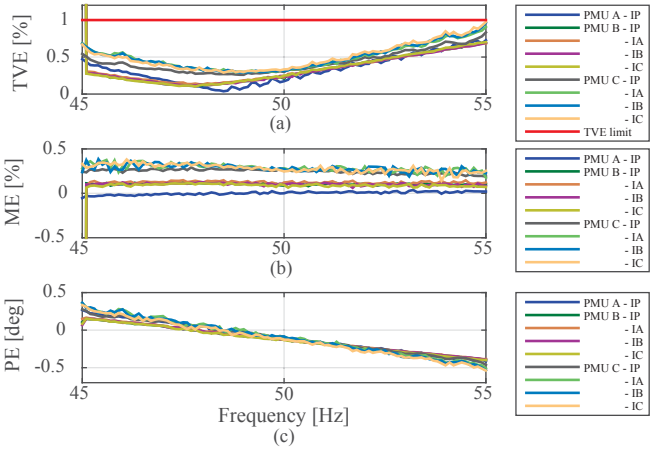

Fig. 7: Frequency Scan Current: a) Total Vector Error; b) Magnitude Error (measured-reference); c) Phase Error (measured-reference)

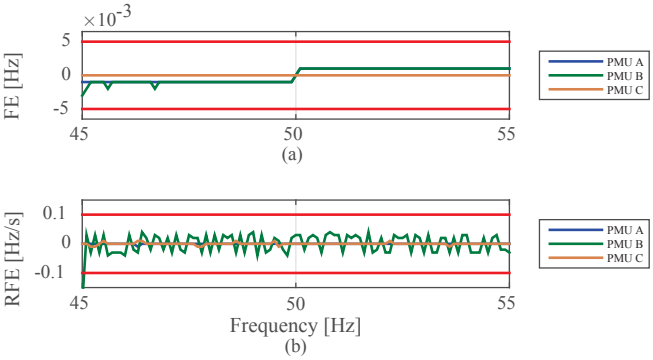

Fig. 8: Frequency Scan: a) Frequency Error; b) ROCOF Error

Unfortunately a reason for this is not obvious, and lack of knowledge about the PMU's algorithms makes it difficult to provide an explanation.

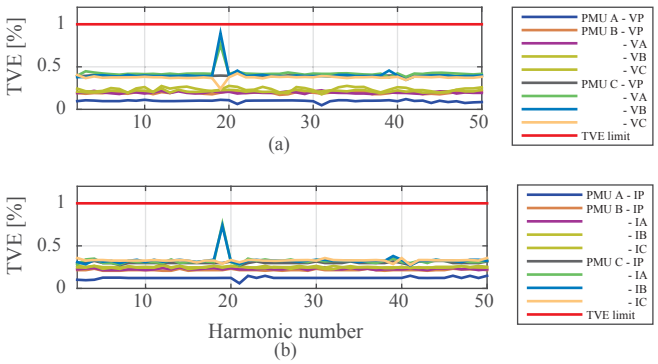

Fig. 9: Harmonic rejection Test: a) Voltage TVE; b) Current TVE

Frequency and ROCOF errors are well within the limits for all devices. The amendment C37.118.1a-2014 [10] suspends the limit for the RFE. However, based on the results shown in Fig. 10b, it seems that the PMUs are capable of delivering good ROCOF estimations when facing signals with harmonics. The authors' opinion, based on shown results, is that the RFE limit could be revised and reinstated.

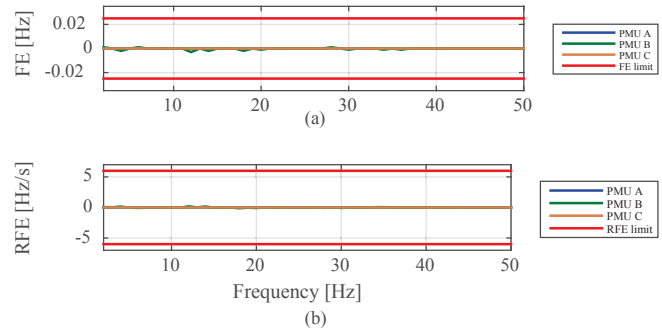

Fig. 10: Harmonic rejection Test: a) Frequency Error; b) ROCOF Error

5) Out-of-Band Test: This test is designed to inject into the PMUs a single frequency sinusoid added to the fundamental. The interfering frequency is varied over a range of 10 Hz to 100 Hz in steps of 1 Hz, and the PMUs should completely filter the interfering signals.

In order to test the filtering when the frequency is off nominal, the standard [7] requires to be varied by $\pm 5\%$ of the reporting rate which gives 47.5 Hz and 52.5 Hz for 50 samples per second. Due to space limitations, only the results for voltage TVE, FE, and RFE at 47.5 and 50 Hz will be shown in this paper. The Nyquist Cutoff is shown on the plots by the orange vertical lines. Frequencies inside the passband are excluded from the analysis.

Fig. 11 shows a clear difference between the tested devices. PMU A is particularly sensitive to the interfering signals which have a high influence on the angle measurement of the device

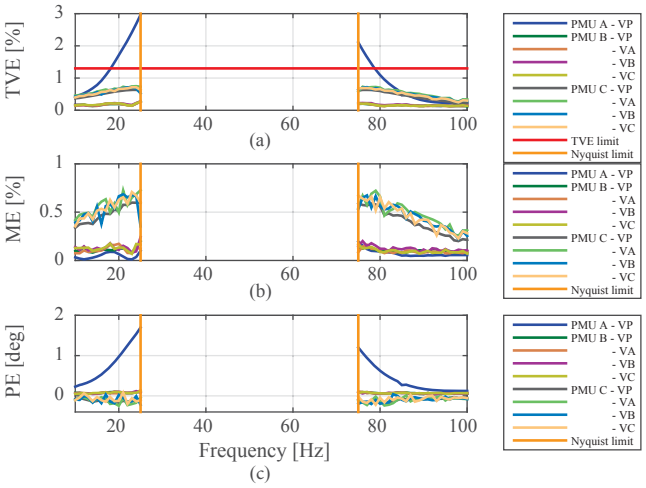

Fig. 11: Out-of-Band Test - Voltage; signal frequency 47.5 Hz: a) Total Vector Error; b) Magnitude Error (measured-reference); c) Phase Error (measured-reference)

as seen in Fig. 11c. PMUs B and C both show a good angle estimation, while the magnitude error of PMU C is higher than the others, Fig. 11b.

Fig. 12 shows there is a change in the performance of the PMUs when the fundamental signal frequency is 50 Hz. The phase error of PMU A is now negative and somewhat lower. However, the TVE still exceeds the limit. Fig. 12b shows that PMU C has noticeable differences between the magnitude error of its phases. The calculated magnitude error for phase A is around 0.2% while for phase B is reaches 0.6%. It would have been expected for all phases of a PMU to show similar results, however it seems this is not always the case.

Fig. 13 shows the frequency error limit is exceeded by all PMUs. This is expected considering the mathematical relationship between frequency and phase angle, which is affected by the interfering signals. The error is further amplified when the ROCOF is calculated as the time derivative of the frequency. Therefore, it is expected to see high values for RFE as shown in Fig. 14. The amendment has suspended the RFE limit, however, it is shown in Fig. 14 in order to provide a comparison with the targeted value.

IV. Conclusion

This paper reviewed the steady-state compliance of three commercial PMUs under the C37.118.1a amendment. The evaluation method is simple and robust, and the equipment is off the shelf which makes it widely available. The analysis software is written entirely in Matlab and can be easily modified to accommodate future changes. A calibration check of the test set output is performed and correction factors are calculated for amplitude and angle which are then applied to the reference phasor in order to match the theoretical value to the ones injected into the PMUs.

The paper offers a view on the limits suspended by the amendment to the standard. The results indicate that the PMUs

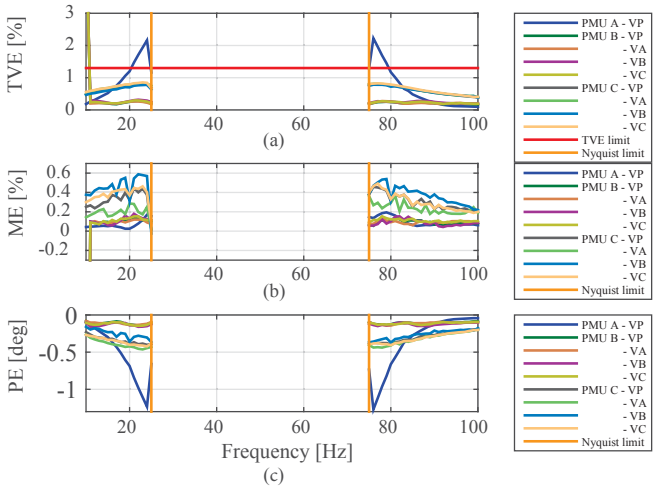

Fig. 12: Out-of-Band Test - Voltage; signal frequency 50 Hz: a) Total Vector Error; b) Magnitude Error (measured-reference); c) Phase Error (measured-reference)

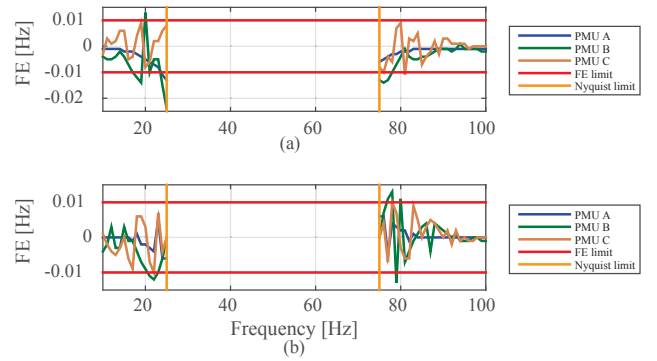

Fig. 13: Out-of-Band Test - Frequency Error: a) signal frequency 47.5 Hz; b) signal frequency 50 Hz

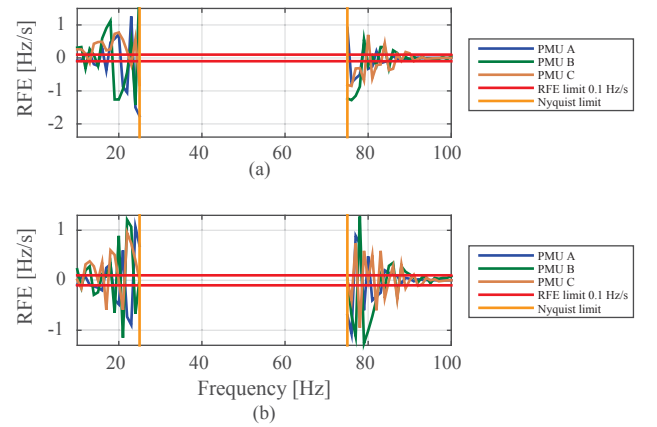

Fig. 14: Out-of-Band Test - ROCOF Error: a) signal frequency 47.5 Hz; b) signal frequency 50 Hz

are capable of estimating ROCOF within the standard limit in which case the requirements for harmonic rejection RFE could be reinstated. Still, better filtering is needed before ROCOF measurements under out-of-band interference can comply to the standard limit. For now the limit is suspended to allow qualification of such PMUs.

Concerning the hardware setup, the frequency scan test revealed a frequency phase bias. This should be investigated further to discover the real cause. A possible explanation is that the standard relay test set is causing this due to its reconstruction filters which probably do not have constant phase delay in the pass-band. If this proves to be true, either a hardware or software solution should be implemented.

Acknowledgment

The authors would like to thank the Nordic Energy Research (Norden) which supports the Smart transmission grid operation and control (StronGrid) project and made this research possible.

References

[1] A. Bose, "Smart transmission grid applications and their supporting infrastructure", IEEE Trans on Smart Grid, vol. 1, pp. 1119, 2010.

[2] D. E. Bakken, A. Bose, C. H. Hauser, D. E. Whitehead, and G. C. Zweigle, "Smart generation and transmission with coherent, real-time data", Proceedings of the IEEE, vol. 99, no. 6, pp. 928951, 2011.

[3] K. Martin, T. Faris, J. Hauer, "Standardized Testing of Phasor Measurement Units", Fault and Disturbance Analysis Conference 2006, Georgia Tech, Atlanta, GA.

[4] IEEE C37.118-2005, IEEE Standard for Synchrophasors in Power Systems.

[5] Almas, Muhammad Shoaib, Jako Kilter, and Luigi Vanfretti. "Experiences with steady-state PMU compliance testing using standard relay testing equipment." Electric Power Quality and Supply Reliability Conference (PQ), 2014. IEEE, 2014.

[6] Garcia-Valle, R., Yang, G. Y., Martin, K. E., Nielsen, A. H., & Ostergaard, J. (2010, October). DTU PMU laboratory developmentTesting and validation. In Innovative Smart Grid Technologies Conference Europe (ISGT Europe), 2010 IEEE PES (pp. 1-6). IEEE.

[7] IEEE Standard for Synchrophasor Measurements for Power Systems - IEEE Std C37.118.1™-2011.

[8] IEEE Guide for Synchronization, Calibration, Testing, and System Protection and Control - IEEE C37.242™-2013.

[9] "IEEE Synchrophasor Measurement Test Suite Specification", IEEE-SA Conformity Assessment Program, December 2014.

[10] Amendment 1: Modification of Selected Performance Requirements - IEEE Std C37.118.1a™-2014 (Amendment to IEEE Std C37.118.1™-2011).

[11] Martin, Kenneth E., John F. Hauer, and Tony J. Faris. "PMU testing and installation considerations at the Bonneville power administration." Power Engineering Society General Meeting, 2007. IEEE. IEEE, 2007.

B
DYNAMIC PMU COMPLIANCE TEST UNDER C37.118.1A-2014

This paper has been presented at the IEEE PES General Meeting Conference in Denver, CO, USA and has been published as part of the conference proceedings

Dynamic PMU Compliance Test under C37.118.1a™-2014

R. Ghiga, Q. Wu, K. Martin, W. Z. El-Khatib, L. Cheng and A. H. Nielsen

***Abstract*—This paper presents a flexible testing methodology and the dynamic compliance of PMUs as per the new C37.118.1a amendment published in 2014. The test platform consists of test signal generator, a Doble F6150 amplifier, PMUs under test, and a PMU test result analysis kit. The Doble amplifier is used for providing three phase voltage and current injections to the PMUs. Three PMUs from different vendors were tested simultaneously in order to provide a fair comparison of the devices. The new 2014 amendment comes with significant changes over the C37.118.1 - 2011 standard regarding the dynamic tests.**

I. Introduction

PMUs are increasingly being developed in order to improve their performance. These units are considered to be among the key technologies for wide area power system protection control and monitoring [1]. The measurement data obtained from PMUs could be used to create improved control algorithms for the future power systems. Therefore, it is important to test the accuracy of the measurements in dynamic conditions since the power system itself is dynamic.

The IEEE standard for Synchrophasor Measurements for Power Systems IEEE C37.118.1-2011 [2] defines the tests that simulate different conditions of the power system such as oscillations, switching of loads and frequency ramps. The amendment to C37.118.1a [3] was published in 2014 and comes with significant changes regarding the dynamic compliance tests which consist of less strict limits for quantities like Total Vector Error (TVE), Frequency Error (FE) and Rate of Change of Frequency Error (RFE).

Dynamic compliance of PMUs is a subject that has been addressed in previous work such as [4], while [5] although published before the 2011 standard [2], provided an insight about dynamic testing.

The paper is organized as follows: Section II provides information regarding the hardware, methodology and the performed tests. Section III presents the results of dynamic compliance tests for PMUs from three different vendors, and finally Section IV concludes the paper with summarizing the contribution of the work.

R. Ghiga, Q. Wu, W. Z. El-Khatib and A. H. Nielsen are with the Center for Electric Power and Energy Engineering, Technical University of Denmark, Kgs. Lyngby 2800, Denmark; Emails: rghiga@elektro.dtu.dk, qw@elektro.dtu.dk,wzel@elektro.dtu.dk and ahn@elektro.dtu.dk

K. Martin is Senior Consultant at Electric Power Group, Los Angeles, California; Email: kenm8421@yahoo.com

L. Chen is with the Department of Electrical Engineering, Tsinghua University, Beijing 100084, China; Email: chenglin@mail.tsinghua.edu.cn

II. PMU Testing Architecture and Methodology

This section of the paper presents the laboratory hardware used for testing the PMUs and describes the methodology of the testing.

A. Test Bed Description

To generate the PMU input signals, a Doble F6150 Power System Simulator is used. Normally, this device serves as a standard stand alone test set for protection relays. This Power System Simulator is capable of delivering 3-phase AC voltages and currents with different amplitudes.

The PMUs inputs are connected directly to the test set without using additional amplifiers which reduces accuracy issues. Multiple devices can be tested simultaneously using the same input signal, providing a fair performance analysis.

As the standard [2] requires, the measurement errors of the PMUs should be calculated within 1% of the nominal signal. In order to achieve such precision, the test equipment should be able to produce signals with an accuracy around ten times higher than that as mentioned in [6]. Supposedly, the chosen simulator is capable of a precision up to 0.02% which is sufficient for this job. The Doble F6150 Power System Simulator can output signals with varying frequency, modulated amplitude and modulated phase, and it can step both phase or amplitude which covers the entire dynamic test range.

B. Testing procedure

The test process is based on the generation of waveforms required by the C37.118.1a amendment, application to the PMU and comparison of the reported PMU data with the expected result. The idea is simple and robust since a PMU estimates a synchrophasor equivalent for a given AC waveform. By taking a phasor equivalent model and producing the AC waveform that it represents with high accuracy as an electrical signal then putting it into a PMU, the resulting synchrophasor estimate should match the original phasor model.

Transient effects due to parameter change, would distort the measurements. Therefore, the tests allow enough settling time, and the sample points of transients are discarded from the analysis.

C. Reference Phasor Definition, Measurement Evaluation and Test description

A generalized phasor function can be obtained from a sine function with amplitude and phase modifiers as in (1):

$$X(t) = X_m[g(t)] * cos(\omega_0 t + y(t)) \quad (1)$$

Where X_m is the nominal amplitude, ω_0 is the nominal power system frequency, g(t) is an amplitude modifying function and y(t) is a phase modifying function. The corresponding phasor value is:

$$X(nT) = \{X_m/\sqrt{2}\}\{g(nT)\}\angle\{y(nT)\} \quad (2)$$

Where nT is the reporting instant. The phasor values reported by the PMU should be an estimate of this value for each given instant in time. Frequency and ROCOF are defined in (3):

$$f(t) = \frac{1}{2\pi}\frac{d(\omega_0 t + y(t))}{dt}; \quad ROCOF(t) = \frac{df(t)}{dt} \quad (3)$$

The measurement evaluation is specified in the IEEE C37.118.1 [2] and it consists of the Total Vector Error given by (4),

$$TVE = \sqrt{\frac{(\hat{X}_r(n) - X_r(n))^2 + (\hat{X}_i(n) - X_i(n))^2}{(X_r(n))^2 + (X_i(n))^2}} \quad (4)$$

Where $\hat{X}_r$ and $\hat{X}_i$ are the measured real and imaginary parts of the phasor and X_r and X_i are the real and imaginary parts of the reference phasor.

Similarly, frequency measurement error (FE) and Rate Of Change Of Frequency Error (RFE) are defined by the standard as (5) and (6),

$$FE = |f_{true} - f_{measured}| = |\Delta f_{true} - \Delta f_{measured}| \quad (5)$$

$$RFE = |(df/dt)_{true} - (df/dt)_{measured}| \quad (6)$$

where $f_{measure}$ is the frequency estimated by the PMU while f_{true} is the frequency of the test signal from the Doble F6150 Power System Simulator.

The dynamic compliance tests are shortly described in the following table:

TABLE I: Dynamic tests description

Test Name	Varied quantity
Amplitude modulation (Amod)	Phasor amplitude by 0.1 pu
Phase modulation (Pmod)	Phasor Angle by 0.1 rad
Frequency Ramp (Framp)	Frequency $\pm 1 Hz/s$ Range 45 - 55 Hz
Amplitude step (Astep)	± 0.1 pu
Phase Step (Pstep)	± 10 degrees

III. Test Results

This section presents the results for dynamic compliance tests listed in Table for the M-performance class and 50 Hz reporting rate of the PMUs. The limits for TVE, FE and RFE are shown on the plots with a red line at the values defined by amendment [3] for the specific test.

1) Amplitude Modulation Test: This is one of the tests designed to determine the measurement bandwidth of the PMUs, by modulating the amplitude of the input signals (voltages and currents) with a sinusoidal waveform with a 10% modulation level. Therefore, the amplitude of the phasor should oscillate between 0.9 and 1.1 p.u. The modulation frequency range, as stated by the amendment [3] is between 0.1 Hz - 5 Hz with increments of 0.2 Hz. Fig 1a shows that

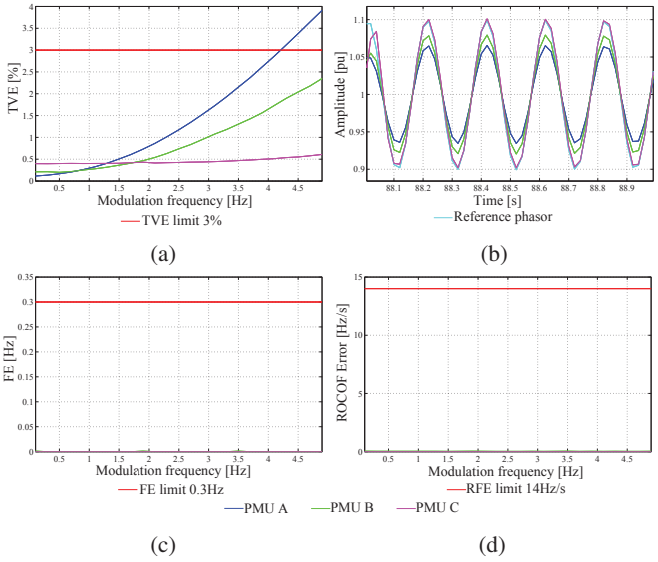

Fig. 1: Amplitude Modulation Test: a) PosSeq voltage TVE; b) PosSeq voltage amplitude at f_m = 5 Hz; c) FE; d) RFE

PMU A satisfies the measurement bandwidth TVE compliance up to a modulation frequency of 4.2 Hz, beyond which it exceeds the 3% limit. Although the performance of PMU B decreases as the modulation frequency increases, the TVE is within the required limit. PMU C is measuring the inputs signals with almost constant accuracy throughout the entire modulation range. Fig 1b shows the section of the test signal where the modulation frequency is 5 Hz. It can be seen that the difference between PMU A measurement and reference amplitude is significant. This causes the TVE to exceed the 3% limit. The magenta line of PMU C is almost identical with the reference signal.

Figs 1c and 1d show that all units are measuring the frequency with high accuracy. Furthermore, only the line of PMU C is visible because it is overwriting the lines of the other two units.

2) Phase Modulation Test: This is the second test designed to verify the measurement bandwidth of the PMUs. The phase of the input signal is modulated by 0.1 radian (5.729 degrees) and the modulation frequency is the same as for the previous test. Fig 2a shows that PMU A is exceeding the 3% limit beyond 4.5 Hz modulation frequency. This is due to the offset between the reference value and the measurement of PMU A visible in Fig 2b. The other two units satisfy the TVE compliance for phase modulation.

The frequency error is shown in Fig 2c. PMU C is the first one to exceed the threshold beyond 2.4 Hz. PMU A satisfies the compliance up to 4.2 Hz modulation frequency. PMU B manages to estimate the input signal frequency with enough accuracy from start to finish. Fig 2d shows the RFE. PMUs A and B manage to provide measurements within the required limits while unit C is exceeding the threshold close to 5 Hz modulation frequency.

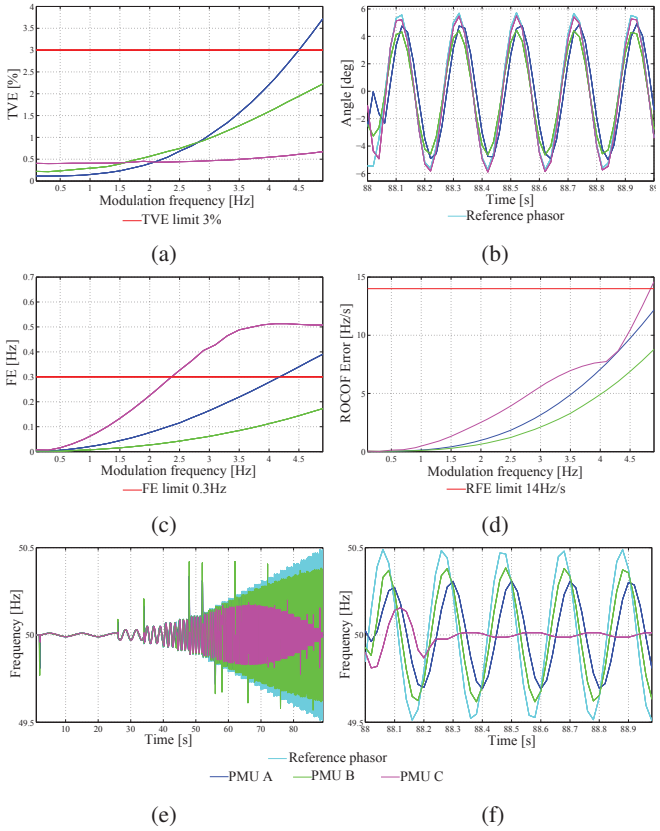

Fig. 2: Phase Modulation Test: a) PosSeq Voltage TVE; b) PosSeq Voltage amplitude at f_m = 5 Hz; c) FE; d) RFE; e) Frequency; f) Frequency at f_m = 5 Hz

The test modulates the phase of the input signals and the frequency $F = d(phase)/dt$ and it varies with the phase. Fig 2e shows the frequency measurement of the PMUs for the entire modulation range. PMU C does not manage to produce the correct measurements for the signal frequency which is why it exceeds the FE limit. Fig 2f shows the measurements and reference for 5 Hz modulation frequency. It is clear that PMU C performs poorly since it reports almost no oscillation at all. Furthermore, this figure shows that there is a delay in frequency measurement for all units.

3) Amplitude Step Test: This test in focusing on the ability of the phasor measurement unit to measure positive and negative amplitude steps that occur in dynamic power systems due to switching actions. These changes are analyzed for the available PMUs and the obtained results are presented in this section. A phasor is not expected to be accurate during highly non-linear event like a step change input. Therefore, the TVE may be high and exceed limits during the step. The test measures response time, which is the interval of time from which the TVE leaves the steady-state limit until it returns within that limit. It also checks that the response is aligned with the actual step in time (delay time) and that it does not take on extreme values during the transition (overshoot). All limits for the mentioned quantities are defined in the amendment [3].

For ease of use and understanding the time when the step occurs is chosen as t = 0s. Therefore, the steady state prior the step is referred by negative time, while the transients and steady state after the amplitude increase are on the positive side. Moreover, the delay time can have both positive or negative values due to this reference point in time. For this test the amplitude of the signal is stepped with 0.1 pu as shown in Fig 3a.

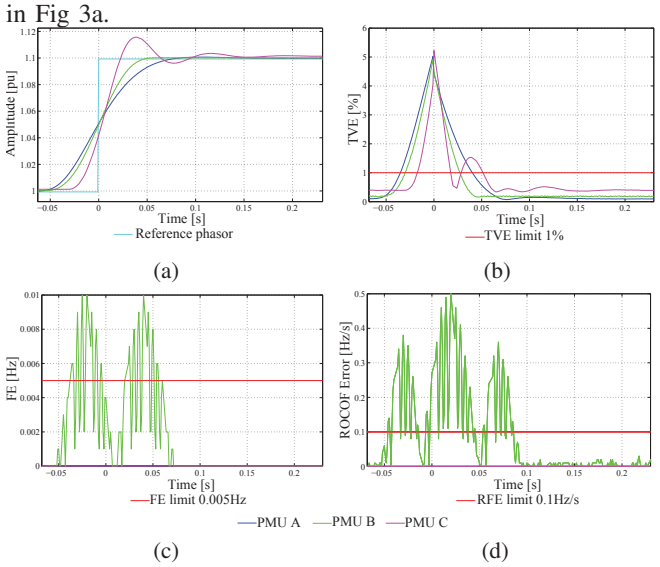

Fig. 3: Positive Amplitude Step Test: a) PosSeq Voltage amplitude; b) PosSeq Voltage TVE; c) FE; d) RFE

It can be seen that each device reacts differently to a step change. The following table presents the calculated response time, delay time, over and undershoot as well as the limits specified in C37.118.1a.

TABLE II: Positive Amplitude Step, Overshoot and Undershoot compliance under C37.118.1a for M-class performance

Fs	50 Hz			
	Overshoot		Undershoot	
	Calculated [%]	Limit [%]	Calculated [%]	Limit [%]
PMU A	1.4	10	0	10
PMU B	1.04		0	
PMU C	16.4		3.19	

TABLE III: Positive Amplitude Step Response and Delay Times compliance under C37.118.1a for M-class performance

Fs	50 Hz							
	Response Time [ms]						Delay Time [ms]	
	TVE		FE		RFE			
PMU A	75	140	0	280	0	280	-1.14	5
PMU B	57		98		132		-0.4	
PMU C	68		0		0		2.83	

Table III shows the response and delay times for each PMU. The limits specified in the amendment [3] are colored in red, and are valid for the 50 Hz reporting rate which was used in these tests. Results in Table III show that all units are within

the required response and delay times, which is consistent with Figs 3b, 3c, and 3d. The negative amplitude step has similar results and is not presented in this paper.

4) Phase Step Test: Line switching operations can cause step changes in the phase of the power system. Similar to the amplitude step, the phase step test focuses on the ability of the PMUs to follow these changes.

Fig 4a shows that the PMU A is quite different from the other two. Its performance is worse both in overshoot and delay time and the reason is not clear. PMUs B and C perform similar as in the Amplitude Step test. The FE and RFE are significantly different for this test as shown in Fig 4c and Fig 4d, respectively. This is due to the relation between phase, frequency and ROCOF which are defined in (3).

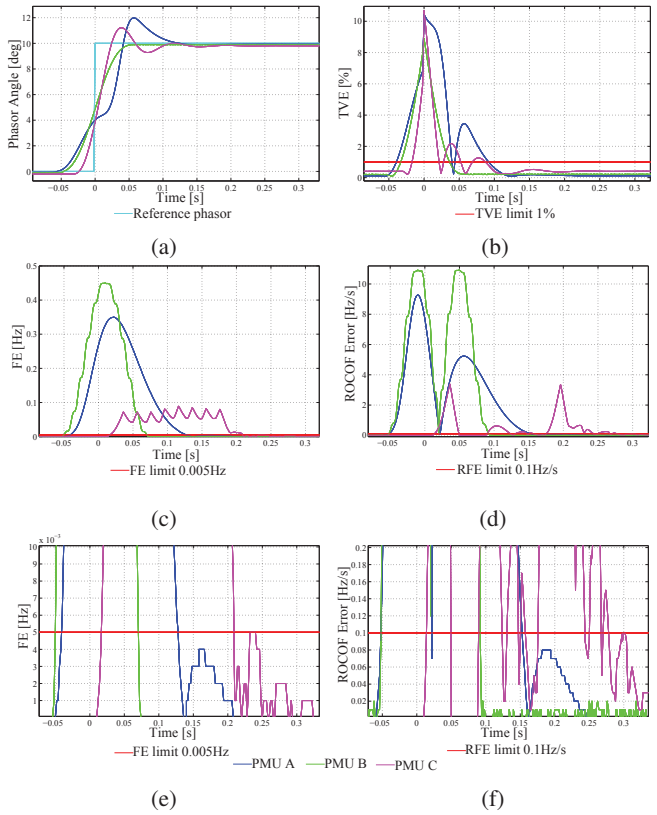

Fig. 4: Phase Step Test: a) PosSeq Voltage amplitude; b) PosSeq Voltage TVE; c) FE; d) RFE; e) FE (zoomed in) f) RFE (zoomed in)

Figs 4e and 4f are zoomed image of the Fe and RFE plots in order to clearly show where the limit line is. These plots can be used to verify the results in Table V. Overshoot and undershoot values are shown in Table IV.

5) Frequency ramp Test: The frequency ramp test was introduced by the 2011 standard [2]. It emulates a system separation scenario when the generation and load are imbalanced and the system frequency might increase or decrease depending on case. In order to cover both scenarios, for this test the injected signal has constant amplitude and phase while the frequency is changing linearly with a slope of $\pm 1 Hz/s$.

TABLE IV: Positive Phase Step, Overshoot and Undershoot compliance under C37.118.1a for M-class performance

Fs	50 Hz			
	Overshoot		Undershoot	
	Calculated [%]	Limit [%]	Calculated [%]	Limit [%]
PMU A	19.8	10	0.9	10
PMU B	0		1.18	
PMU C	12.2		7.17	

TABLE V: Positive Phase Step Response and Delay Times compliance under C37.118.1a for M-class performance

Fs	50 Hz							
	Response Time [ms]						Delay Time [ms]	
	TVE		FE		RFE			
PMU A	131	140	169	280	205	280	21.41	5
PMU B	69		120		144		0.63	
PMU C	104		223		264		4.35	

The range of the frequency used for this test is from 45 Hz up to 55 Hz. Fig 5a shows the reference and measured frequencies along the mentioned range. A detailed view is shown in Fig 5b where it is visible that all PMUs have a delay in the measurement. It could be the effect of the filtering of these devices. However, the reported frequency increases and decreases linearly which reveals no issues with the frequency estimation algorithms.

Fig 6a and Fig 6b show that PMU B does not measure correctly the amplitude of the phasor. It is probably caused by the frequency tracking algorithm. It manages to adjust the measurement window at the points where the amplitude is reported with accuracy. However, as the frequency ramps up, the tracking method of the PMU does not keep up and the amplitude of the phasor is measured incorrectly. PMU C shows a different behavior. As the frequency is linearly increasing, the unit measures amplitude with higher accuracy. On the other hand the TVE exceeds the 1% limit at 55 Hz which means that the angle is responsible. This is also what is happening with PMU A.

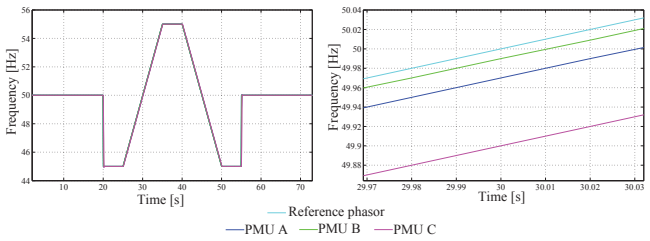

Fig. 5: Frequency Ramp Test: a) Signal frequency; b) Zoomed view at 50 Hz

Fig 6c shows that all PMUs are exceeding the FE limit, and this is due to the delay in the frequency measurement. Furthermore, the errors show that the PMUs performance is constant for entire ramp which supports the idea that the delay is due to slow filtering. All units report an accurate ROCOF

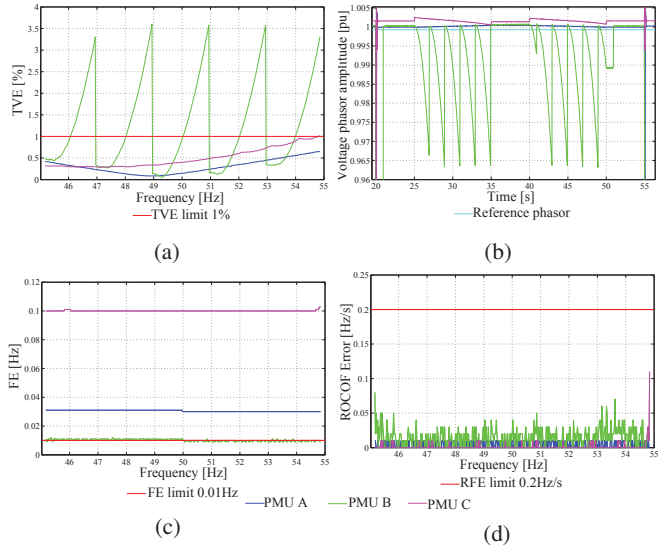

Fig. 6: Frequency Ramp: a) PosSeq Voltage TVE; b) PosSeq Voltage Amplitude; c) FE; d) RFE

as shown in Fig 6d.

The overall performance of the dynamic compliance tests under the M-class requirements of the 2014 amendment [3] are shown in the following tables:

TABLE VI: Pass/Fail for Amplitude Modulation, Phase Modulation, and Frequency Ramp Tests under C37.118.1a

Test M-class	Amod			Pmod			Framp		
Fs	50 Hz			50 Hz			50 Hz		
Error	TVE	FE	RFE	TVE	FE	RFE	TVE	FE	RFE
PMU A	F	P	P	F	F	P	P	F	P
PMU B	P	P	P	P	P	P	F	F	P
PMU C	P	P	P	P	F	F	F	F	P

TABLE VII: Pass/Fail for Positive Amplitude/Phase Step Tests under C37.118.1a

Test	Astep / Pstep					
Fs	50 Hz					
	Response Time			Delay Time	Overshoot	Undershoot
Error	TVE	FE	RFE			
PMU A	P / P	P / P	P / P	P / F	P / F	P / P
PMU B	P / P	P / P	P / P	P / P	P / P	P / P
PMU C	P / P	P / P	P / P	P / P	F / F	P / P

IV. Conclusion

This paper presents a method that can be used to test any kind of PMU using any test defined by the C37.118.1 standard. The dynamic compliance of PMUs from three different vendors was verified under the 2014 amendment [3] requirements.

The devices under test were built to satisfy the 2005 standard which did not define the dynamic compliance tests. Furthermore, the frequency ramp test was introduced in 2011 therefore these PMUs might lack the necessary algorithms to pass this test.

The analysis software is developed ”in-house” entirely in Matlab and it can be easily adapted to future changes of the performance requirements. Therefore, the tools presented in this paper make a good option when considering building a test setup for instrument validation, regarding portability, availability, and flexibility.

Acknowledgment

The authors would like to thank the Nordic Energy Research (Norden) which supports the Smart transmission grid operation and control (StronGrid) project and made this research possible.

References

[1] A. Bose, ”Smart transmission grid applications and their supporting infrastructure”, IEEE Trans on Smart Grid, vol. 1, pp. 1119, 2010.

[2] IEEE Standard for Synchrophasor Measurements for Power Systems - IEEE Std C37.118.1™-2011.

[3] Amendment 1: Modification of Selected Performance Requirements - IEEE Std C37.118.1a™-2014 (Amendment to IEEE Std C37.118.1™-2011).

[4] Narendra, K., Gurusinghe, D. R., & Rajapakse, A. D. Dynamic Performance Evaluation and Testing of Phasor Measurement Unit (PMU) as per IEEE C37. 118.1 Standard.

[5] K. Martin, T. Faris, J. Hauer, ”Standardized Testing of Phasor Measurement Units”, Fault and Disturbance Analysis Conference 2006, Georgia Tech, Atlanta, GA.

[6] IEEE Guide for Synchronization, Calibration, Testing, and System Protection and Control - IEEE C37.242™-2013.

[7] D. E. Bakken, A. Bose, C. H. Hauser, D. E. Whitehead, and G. C. Zweigle, ”Smart generation and transmission with coherent, real-time data”, Proceedings of the IEEE, vol. 99, no. 6, pp. 928951, 2011.

[8] IEEE C37.118-2005, IEEE Standard for Synchrophasors in Power Systems.

[9] IEEE Standard for Synchrophasor Data Transfer for Power Systems - IEEE Srd C37.118.2™-2011.

[10] Garcia-Valle, R., Yang, G. Y., Martin, K. E., Nielsen, A. H., & Ostergaard, J. (2010, October). DTU PMU laboratory developmentTesting and validation. In Innovative Smart Grid Technologies Conference Europe (ISGT Europe), 2010 IEEE PES (pp. 1-6). IEEE.

[11] Almas, Muhammad Shoaib, Jako Kilter, and Luigi Vanfretti. ”Experiences with steady-state PMU compliance testing using standard relay testing equipment.” Electric Power Quality and Supply Reliability Conference (PQ), 2014. IEEE, 2014.

[12] Martin, Kenneth E., John F. Hauer, and Tony J. Faris. ”PMU testing and installation considerations at the Bonneville power administration.” Power Engineering Society General Meeting, 2007. IEEE. IEEE, 2007.

[13] Doble, ”F6150 Power System Simulator” - https://www.doble.com/parts/files/File/F6150_Brochure_04-08.pdf

[14] StreamReader software developped by Bonneville Power Administration.

C
PHASOR MEASUREMENT UNIT TEST UNDER INTERFERENCE CONDITIONS

This paper has been submitted at the IEEE Transactions on Power System Delivery and is currently under review.

Phasor Measurement Unit Test under Interference Conditions

Radu Ghiga, *Student Member, IEEE*, Kenneth Martin, *Fellow, IEEE,* Qiuwei Wu, *Senior Member, IEEE,* and Arne Hejde Nielsen, *Senior Member, IEEE*

***Abstract*-- This paper investigates the performance of Phasor Measurement Units (PMUs) under interference conditions which can appear in a power system and are not tested by the C37.118.1 standard. Three PMUs from different vendors configured for the M-class requirements were used to test three possible interference condition scenarios. In the first scenario, noise is added to the PMU input signal. The test runs a sweep of Signal-to-Noise Ratios (SNR) and the accuracy versus the noise level is obtained. The second scenario injects multiple harmonics with the input to test the influence on accuracy. The last scenario focuses on instrument transformer saturation which leads to a modified waveform injected in the PMU. This test goes through different levels of Current Transformer (CT) saturation and analyzes the effect of saturation on the accuracy of PMUs. The test results show PMU measurements will be degraded when the input signal is distorted by high noise or a saturated current waveform, but is not particularly affected by multiple harmonics. This information can be used when selecting a PMU to ensure it will provide a reliable measurement for the intended use. It can also be used for developing more robust PMUs and applications resistant to degraded measurements.**

***Index Terms* — Interference conditions, Phasor Measurement Unit (PMU), PMU testing.**

I. Introduction

The performance of Phasor Measurement Units (PMU) has been a topic of high interest in recent years. The generalized synchrophasor definitions and compliance under steady-state and dynamic conditions are provided in the IEEE C37.118.1-2011 standard [1] and IEEE C37.118.1a-2014 amendment [2]. An IEEE Test Suite Specification guide for testing and calibrating PMUs with a greater level of uniformity is now available [3]. Substantial work has been carried out in implementing test platforms and verifying the compliance under [1] and [2] of commercial PMUs [4]-[7]. These studies determined that most of these devices are not compliant with the dynamic requirements. The classic synchrophasor measurement methods are Discrete Fourier Transform (DFT)-based. While they have a low computation burden, the accuracy of these methods show degraded performance under frequency offsets and dynamic conditions, such as phase modulation [8], [9].

Recent publications propose methods that improve the accuracy under different dynamic or interference conditions. An adaptive phasor and frequency tracking algorithm was proposed in [10] while [11] proposed a phase-locked-loop (PLL)-based technique in order to estimate dynamic phasors. Non-DFT dynamic signal models have been published in [12]-[15] claiming improvements under dynamic conditions. However, the performance of such models under noise or harmonic conditions has not been assessed [16]. The method proposed in [9] showed improved theoretical results under noise and harmonic conditions. New algorithms implemented in a prototype grid analyzer showed promising results for measurements carried out at distribution level [17]. However, most of the PMUs currently installed in today's power systems are of an older generation and are not fully compliant with the IEEE C37.118.1 standard, nor do they benefit from these more recent algorithm developments.

This paper presents testing of three commercial PMUs under three scenarios that occur in real power systems and are not covered by the current standard: high background noise, multiple harmonics, and current transformer (CT) saturation. The first test adds white noise to the AC signal. High noise can occur during switching and faults as well as during arcing, such as that created by a high resistance fault or failing equipment. In these situations, reasonably good PMU measurements would be expected (PMU measurements during faults are not expected to be accurate). In the second test, multiple harmonics are included with the AC signal, both at nominal and off-nominal system frequency. The standard only prescribes testing with a single harmonic at a time and only with the system frequency at nominal. This test can show if the present test in the standard covers harmonic interference that might be seen in real system operation. The third test is current measurement with saturated waveforms. CT saturation can occur with faulted or highly overloaded lines. DC flowing in the circuit can also lead to core saturation and measurement distortion [18]-[20]. Power converters used with the widely expanding renewable energy development can give rise to a DC component if the DC compensation sensor fails [21]. To obtain the best accuracy, PMUs are often connected to instrument CTs rather than protection CTs. This works well for most use, but during high overload conditions, these CTs may become saturated and provide misleading data. This test is intended to determine how significant the measurement impairments are and their characteristics.

The work was supported by the Nordic Energy Research (Norden) which supports the Smart transmission grid operation and control (StronGrid) project.

R. Ghiga, Q. Wu and A. H. Nielsen are with the Center for Electric Power and Energy (CEE), Department of Electrical Engineering, Technical University of Denmark (DTU), Kgs. Lyngby, 2800, Denmark (e-mail: rghiga@elektro.dtu.dk, qw@elektro.dtu.dk, ahn@elektro.dtu.dk).

K. Martin is a Principal Engineer at Electric Power Group, Pasadena, California, USA (e-mail: kenm8421@yahoo.com).

These tests examine several areas of potential PMU vulnerability that have not been fully addressed. The synchrophasor standard, C37.118.1, provides a number of requirements to assure PMUs will perform adequately in field use. While there are many tests that could be used, the number of tests and test conditions is limited in order to make certification practical. The tests chosen for the standard are expected to be representative of PMU performance in real operational conditions. However, without testing to compare PMU performance as determined under the standard with conditions that might be encountered in a real power system, the standard effectiveness is not fully known. These tests provide a comparison in the cases of added harmonics and white noise as well as highly distorted input signals.

These tests both validate the tests in the standard and quantify the point at which the impairment limits the measurement accuracy. This information will be helpful in specifying new requirements and performance limits in future PMU standards.

Since these tests are performed on production PMUs, they show the overall performance limitations. It is difficult to assess the impacts of all the error contributions in a product that has not been implemented, so having actual results to refer to is essential to validate signal models. Standards are based on models and experience with development, so having quantified test results to validate the assumptions is essential for the standard development cycle.

These tests are on current generation PMUs but illustrate typical limitations in PMU measurement. All three PMUs performed similarly in all tests despite using different hardware and algorithms. PMU designers can use this observation to focus on aspects of their estimation methods that might reduce vulnerability to these impairments without reducing other measurement capability. In some cases, impaired measurements may have characteristics that are unique and can be flagged. The applications that use PMU data can use such flags to reject the measurement and improve reliability. These tests can indicate such characteristics.

The paper is organized as follows. Section II describes these test signals and their generation. The test system is described in section III. Section IV presents the results and analysis. The conclusions are in Section V.

II. Analysis of Interference Conditions

A. Gaussian White Noise

The C37.118.1 standard defines two tests that check the PMU filtering capabilities. These are the Out-of-Band interference and harmonic rejection tests. It does not include tests with white noise, though its influence on signal acquisition and measurement is a classic problem that has been studied [22]. Previous research has proposed algorithms that may improve measurement precision under noisy signals for PMUs [9]. The noise and harmonic content for distribution networks was investigated in [16] by collecting power grid signals; analysis showed that the SNR at the distribution level was around 60 dB. This measurement is used as a guide for creating the tests and also for interpreting the results.

In this test, white noise is added to the fundamental frequency component of the voltage and current waveforms. The noise level is gradually increased and the error evaluated. The SNR value is calculated based on the white noise only, since other contributions are very small. Analyzing the results of such an SNR sweep will give good understanding of the precision that PMUs are capable under noisy signals.

The digitized signals are created using the signal model,

$$x(n) = A\cos(2\pi(f_0 + \Delta f)nT + \Phi) + w(n) \quad (1)$$

where A and Φ are the amplitude and initial phase angle of signal waveforms. The nominal system frequency is f_0 which is 50 Hz in this case. Δf is the deviation from the nominal frequency, and w(n) is zero mean white Gaussian noise with the power spectral density (PSD) of $\rho^2\ W/Hz$ [23].

The average power of signal x with w(n)=0 is calculated as [24],

$$P_x = \lim_{N\to\infty} \frac{1}{2N+1} \sum_{n=-N}^{N} |x(n)|^2 \quad (2)$$

where N is the number of sample points of signal x. The SNR is usually expressed in decibels [24], and the desired noise power is calculated based on signal power and desired signal-to-noise ratio as $P_{noise,\,dB}=P_{x,\,dB} - SNR_{dB}$.

The standard deviation of the white noise is,

$$\rho = \sqrt{10^{(P_{noise,dB}/10)}} \quad (3)$$

The result from (3) is used to calculate the term w(n) which is then added to (1).

The model described above reflects the effect of noise if the signal amplitude is kept constant. Hence both voltage and current amplitude is maintained at rated values for this test.

Testing at off-nominal frequencies can reveal issues with the processing algorithms of the PMU. For example, Fourier filters have very high rejection at the fundamental and the exact harmonic frequencies, but less rejection away from those points; consequently a fixed frequency Fourier filter may not give adequate rejection when the power system deviates from the nominal. This can be tested by changing the center frequency of the main signal. The standard specifies testing out-of-band rejection with an off-nominal frequency that is ±10% of the Nyquist frequency for the given reporting rate. For a reporting rate of 50 samples per second, the Nyquist frequency is 25 Hz and thus $\Delta f = \pm 2.5$ Hz. This deviation is used in these tests.

The test runs sequences of noise steps at each center frequency. In each sequence, the frequency is held constant and the noise level is increased by 5 dB at each step, starting at -80 dB and ending at -10 dB. The noise level is held constant for 5 seconds during each step. Table I lists the frequencies used in this test together with the noise levels, and rated signal values.

Fig. 1 shows example plots of the signal with noise. Fig. 1a shows the envelope of the voltage signal where the overall amplitude increases with noise. The waveform detail with different SNRs is shown in Fig. 1b and Fig. 1c.

TABLE I
White Noise Test

V [Vrms]	110		
I [Arms]	5		
f [Hz]	47.5	50	52.5
SNR [dB]	10 - 80 with 5 dB step increments		

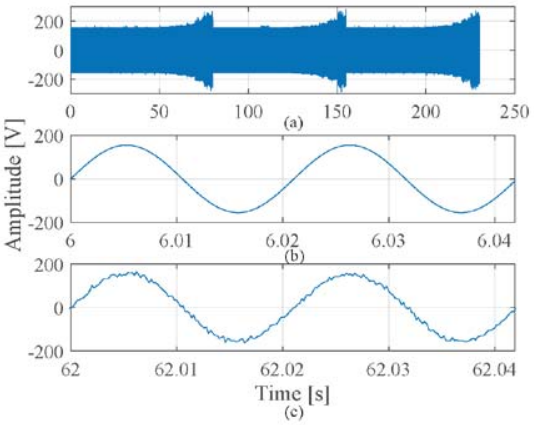

Fig. 1. Phase A Voltage Signal: (a) envelope of the signal showing the increased amplitude at the 3 test frequencies due to the injected noise; (b) Detailed view $f_0 = 47.5$ Hz, SNR = 80 dB; (c) Detailed view $f_0 = 47.5$ Hz, SNR = 25 dB;

B. Multiple Harmonics

The C37.118.1 standard requires testing harmonic interference rejection from the second harmonic up to the fiftieth. In this test, harmonics are added to the fundamental one harmonic at a time with a level is 1% (of the fundamental) for P class and 10% for M class. By contrast power systems often contain multiple harmonics in both currents and voltages that may exceed 10% of the fundamental. As an example, one of the phenomena that causes multiple harmonics is the moment when a transformer is energized (transformer inrush) [25], [26]. As another example, multiple harmonics may be present in grids with renewable energy, such as wind farms with Type 3 and Type 4 wind turbines [27]. The research in [28] shows that Type 3 wind turbines inject predominantly low order harmonics (5^{th}, 7^{th}, 11^{th}, and 13^{th}) at a relatively high harmonic level. It is mentioned in [27] that fast control action of the wind turbine power converter can create low order harmonics. It is therefore relevant to know how commercially available PMUs will perform when they will be used for measuring signals with multiple harmonic contents. This test investigates whether using multiple harmonics rather than a single harmonic exposes additional PMU harmonic rejection vulnerability.

This multiple harmonic test uses harmonics (both number and relative amplitude) that have been observed during transformer inrush. As there is an infinite number of harmonic frequency and amplitude combinations, this choice provides a realistic combination to use for test. The current and voltage contents are typically different.

For example, during transformer inrush, the 2^{nd} harmonic current can reach values up to 63% of the fundamental, depending on the moment when the transformer is energized and the remnant flux within the core [23], [29]. The voltage harmonic amplitude can vary during the first cycles of the inrush with the 5th and 6th harmonics reaching values of 11% and 35% of the fundamental [30]. The inrush phenomenon comes with high amplitude in the fundamental as well, which can reach values five times the rated current [26]. However, this test does not inject such large currents into the PMUs because this would exceed the PMU input capability and render the measurement unusable, which would not fulfill the purpose of the test. Hence, the amplitude of both voltages and currents is kept constant at the rated value of 110 V and 5 A.

This test includes single harmonics as specified in the standard and multiple harmonics between the 2^{nd} and 7^{th} as specified in Tables II and III. The values in these two tables are drawn from example situations presented in [29], [30].. The harmonics are tested in-phase, since there is no particular phase relationship reported. The test cases are run in sequence, each for 5 seconds. All cases are run both at nominal system frequency and off-nominal ($\Delta f = \pm 2.5$ Hz) as in the noise tests. Testing at off-nominal frequency checks rejection, as described in the previous section.

TABLE II
Current Harmonic Content [29]

Case number	Harmonic number						
	2^{nd}	3^{rd}	4^{th}	5^{th}	6^{th}	7^{th}	
1	31	13	2.5	2	1.8	1.2	**Amplitude in % of fundamental**
2	37	16	3	2.4	2.2	1.4	
3	44	19	3.6	2.8	2.6	1.6	
4	50	21	4.1	3.2	2.9	1.9	
5	56	24	4.6	3.7	3.3	2.1	
6	63	27	5.1	4.1	3.7	2.4	

TABLE III
Voltage Harmonic Content [30]

Case number	Harmonic number						
	2^{nd}	3^{rd}	4^{th}	5^{th}	6^{th}	7^{th}	
1	0	1.5	1.5	7.5	35	0	**Amplitude in % of fundamental**
2	0	3.8	7.6	7.7	3.8	0	
3	0	3.5	6.15	6.15	6.15	0	
4	0	3	4.6	8.5	4.6	0	
5	0	0	2.3	11	2.3	0	
6	0	3.8	7.4	11	35	0	

Fig. 2a shows Phase A voltage amplitude during the entire test (all 6 cases). The added amplitude due to harmonics can be seen. The harmonics in the signal are clearly visible in Fig. 2b, which is a section of plot (a) expanded to show the waveforms.

In order to check if the created waveforms are the same as the generated ones, the actual analog test signal was captured with an oscilloscope for comparison. This capture is shown in Fig. 2c.

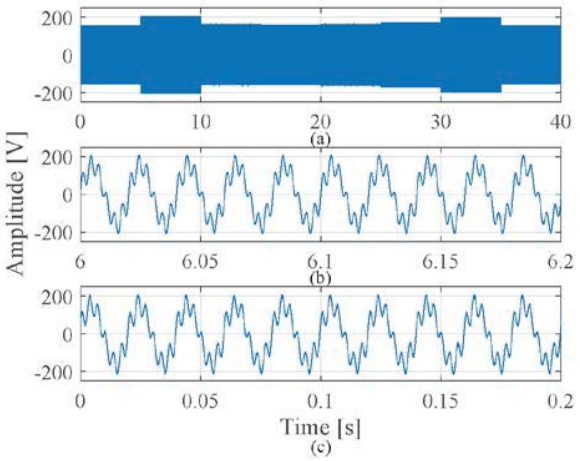

Fig. 2. Phase A Voltage Signal: (a) Voltage with the harmonic content from Table I; (b) Detailed view of the first case; (c) Oscilloscope measurement.

C. Current Transformer Saturation

A CT connects the PMU to the high currents in the transmission system. High currents that exceed the normal operation capability, such as during a fault, can cause the core to saturate and produce a highly distorted signal [31]. This can lead to mis-operation of relays and other equipment that uses these signals, such as preventing tripping of equipment at the correct time that results in equipment damage [32].

The PMU standard specifies measurement accuracy at 1% Total Vector Error (TVE) for most tests. To take the full advantage of this accuracy, the CT should be in that accuracy range or better. According to IEEE C37.110-2007 Guide for CTs for protective Relaying [33], the expected accuracy of protection CTs at rated current is only 3%. They will handle currents up to 20 times the rated current without losing more than 10% in accuracy, but this is not the focus of PMU measurements. More in the range of PMU operation, IEEE C57.13 standard for instrument transformers defines a metering category with accuracies between 0.3% and 1.2% for a current range of 10% - 100% [34]. However, this standard does not give requirements regarding over-current capability and consequent saturation of these cores.

Generally, users will select metering cores for better accuracy in the normal range of operation even though it may be more subject to saturation. This test aims to determine how a saturated current waveform affects the PMU measurement.

A mathematical model of a CT was implemented in Matlab based on the theory published by the IEEE Power System Relaying Committee (PSRC). It is not the purpose of this paper to derive the full CT model so only the background is shown here; the full description can be found in "CT Saturation and Theory Calculator" [35].

The equivalent circuit of the CT model is shown in Fig. 3, where i_p is the instantaneous primary current, i_2 represents the instantaneous real secondary current, i_e is the instantaneous excitation current, and v_e is the instantaneous excitation voltage. The number of CT turns is given by N, and Rs is the secondary winding resistance. The burden resistance is R_b, and inductance is L_b.

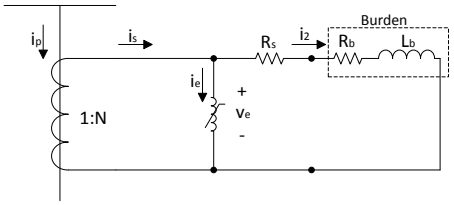

Fig. 3. CT model equivalent circuit

The excitation characteristic of a CT is illustrated by a plot of the secondary rms voltage versus the secondary rms current, on log-log axes, as shown in Fig. 4. This curve is usually factory supplied. The model is based on two parameters from this characteristic: the saturation voltage V_S, chosen according to [33], at the point where the excitation current is 10 amps, and the inverse of the slope for the region above the knee-point voltage referred to as S. The normal operating region for the CT is below the knee voltage. As long as the CT operates in this region, the output will be accurate and linear.

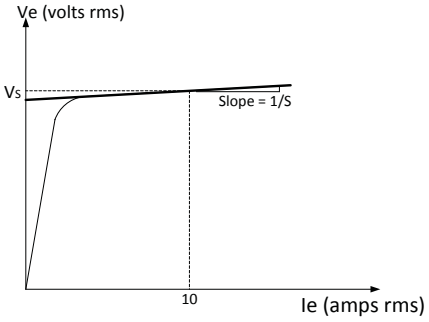

Fig. 4. Determination of the two required parameters from the CT excitation curve

The real secondary current i_2 is equal to the ideal current i_s for the curve below the knee-point. This does not occur above the knee-point, where the CT core is saturating. The method uses the two extracted parameters, Vs and S, to calculate the real secondary current i_2, considering the saturation effect. This is achieved by calculating the excitation (error) current i_e from Fig. 3. Because of the non-linearity of the system, instantaneous values of i_e are computed using simple step increments. After each value for the excitation current is known, the real current is calculated as,

$$i_2 = i_s - i_e \tag{4}$$

The full derivation of the method and equations can be found in [35].

The saturation level is quantified by the saturation factor Ks, which is defined as [33],

$$K_S = \frac{V_e}{V_S} = \frac{I_F * (Z_B + R_S)}{20 * I_2 * (Z_C + R_S)} \tag{5}$$

where I_F is the secondary current during a fault, I_2 is the rated secondary current, R_S is the winding resistance of the secondary side, Z_B is the burden impedance including

secondary devices and connection leads, and Z_C is the standard CT burden according to class.

To test the PMUs, waveforms simulating CT saturation are created using the method summarized in this section. The test runs in sequences of saturation levels, quantified by Ks. In each sequence, Ks is increased in steps of 0.16 starting at Ks=0.5 and ending at Ks=2. The waveforms start to saturate when Ks > 1.

The current level injected in the PMUs is increased along with Ks. This helps simulate a real event where the current supplied by a CT would exceed the rated value. The PMUs used have been tested according to the steady-state IEEE requirements in [36] and their accuracy is shown to be within standards limits for currents up to 200% the rated value.

In Fig. 5a and Fig. 5b, the red line overlaps the blue, meaning that the secondary current is identical to the ideal one. In Fig. 5b, the saturation factor Ks=1 meaning the CT is at its limit and will start to saturate. Fig. 5c shows the current waveform when Ks=2. The current represented by the red line is the one injected in the PMUs and the measurements are compared to the current represented by the blue line which is the ideal value.

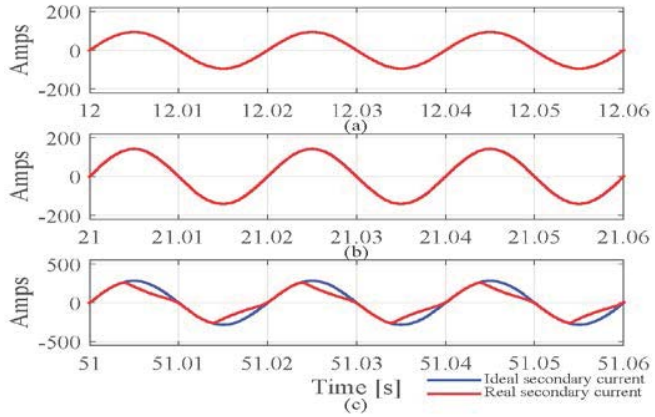

Fig. 5. Ideal vs real secondary current when: (a) K_S=0.65; (b) K_S=1; (c) K_S=2 (saturated core)

III. Test Setup

The lab test setup used is similar to setups used and published before [4]-[7], [37]-[41]. More advanced setups are described in [42]-[44].

The setup consists of a real time playback device that supplies analog voltage and current signals at a level and format suitable for PMU inputs (110 V-nominal voltage and 5-A nominal current) using recorded COMTRADE files. The output of the test set uses 16-bit D/A converters that are GPS synchronized, offering precise test start and signal time alignment. As such, the measurements can be aligned with the theoretical values at the evaluation stage.

Some of the PMUs under test come with their own GPS receivers built-in while others require a separate GPS receiver clock in order to obtain UTC synchronization. The receiver used in the test is rated with an accuracy of ±1 µs.

A number of possible error sources associated with the test setup consist of the playback device amplifier, GPS receiver and playback startup delay [5]. A calibration of the test set was carried out in order to verify the deviation in voltage amplitude from the theoretical value. The output of the test set was read with four high-accuracy voltmeters and the average of the four measurements was considered as the true value.

A correction factor was defined as the deviation of the average measured voltage from the theoretical value. The correction was calculated to be approximately 0.06 %.

The startup delay time was checked with an oscilloscope that was triggered on the 1 PPS signal obtained from the GPS receiver clock. All three phases were checked simultaneously, and a time lag of 142 µs was found. This translates into a phase error of 2.556 degrees and it was consistent through multiple tests.

It is obvious that these errors would cause high TVE and need to be compensated. This is achieved by introducing correction factors in the theoretical signals defined in (6) and achieving the compensated signal defined in (7),

$$Sig = X_m * \cos(2\pi ft + \theta) \tag{6}$$

$$Sig = [X_m * amp_{corr}] * \cos(2\pi ft - \theta_{corr} + \theta) \tag{7}$$

where $amp_{corr}$is the amplitude correction factor, and θ_{corr} is the phase angle correction factor.

In [1], it is recommended that the test uncertainty is maintained less than one-fourth of the accuracy requirement, and with the compensation, the test setup used here is within this requirement.

Fig. 6 shows a diagram of the complete test setup. The PC runs all the necessary software to build the test signals and analyze the results. The three PMUs under test are connected simultaneously to the signal generator and their measurements are recorded by the Phasor Data Concentrator (PDC). The blue arrows show the voltage inputs connected in parallel and the red arrows represent the current inputs connected in series.

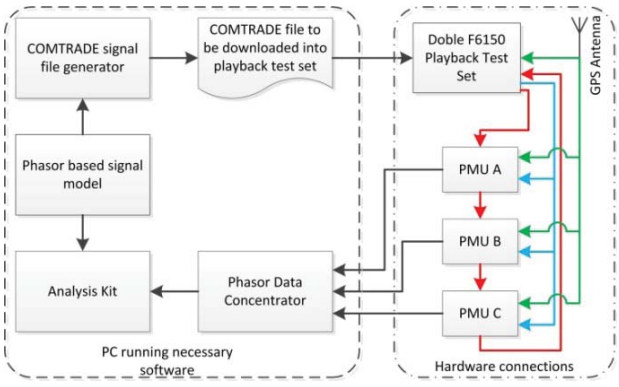

Fig. 6. Test setup diagram

IV. Test Results

This section presents the analysis of the PMU measurements under the three aforementioned scenarios. The testing parameters are shown in Table IV. The devices are set

to the M-class which includes better filtering for better performance, particularly under interference conditions.

Table IV
Testing Parameters

Test type	Signal frequency [Hz]	PMU Sampling Rate [samples/sec]	Observation interval	Processed samples for each interval
White Noise	47.5/50/52.5	50	All test segments are 5 seconds long	250 sample points
Multiple Harmonics	47.5/50/52.5			
Single Harmonic	47.5/50/52.5			
CT Saturation	50			

The performance is analyzed according to IEEE C37.118.1a by calculating the TVE, Frequency Error (FE), ROCOF Error (RFE). Error Calculation for Magnitude Error (ME), and Phase Error (PE) is defined as [3],

$$\mathrm{ME}(\%) = \frac{\sqrt{\hat{X}_r(n)^2 + \hat{X}_i(n)^2} - \sqrt{X_r(n)^2 + X_i(n)^2}}{\sqrt{X_r(n)^2 + X_i(n)^2}} \quad (8)$$

$$\mathrm{PE}(\mathrm{deg}) = \mathrm{atan}\left(\hat{X}_r(n), \hat{X}_i(n)\right) - \mathrm{atan}(X_r(n), X_i(n)) \quad (9)$$

Where $\hat{X}_r(n)$, and $\hat{X}_i(n)$ are sequences of phasor estimates from PMUs under test at time n, and $X_r(n)$, and $X_i(n)$ are sequences of theoretical phasor values of the input signal at the same time n.

All test segments are 5 seconds long. The maximum error for each segment is determined and used for the error plot.

A. *Gaussian White Noise Test*

The PMU performance under white noise conditions is presented in this subsection. The test is similar with the Out-of-Band test defined in IEEE C37.118.1, so the 1.3% TVE, 0.01 Hz FE, and 0.1% RFE limits are used to evaluate the measurements. The RFE limit in the standard is suspended for evaluations, but the old limit is used here as a reference for comparisons. The figures show how the accuracy of the measurement for phasors, frequency and rate of change of frequency is affected by different noise levels.

The TVE of the voltages and currents in Fig. 7 show that all PMUs are within the limits for high and medium signal-to-noise ratios. For SNRs around 30 dB and lower, the accuracy exceeds the 1.3% limit and continues to drop significantly afterwards.

In Fig. 8 and Fig. 9, it can be seen that the PMUs are more sensitive to noise when it comes to frequency estimation. In Fig. 8b, PMU A is more affected by noise than PMUs B and C, which shows there is a clear difference in the processing for the PMUs. Its frequency error is exceeding the 0.01 Hz limit at around 45 dB where the other devices have an accuracy of 5 mHz. A few possible reasons are presented in [45], such as the leakage effect for SNR higher than 35 dB and frequency deviation greater than 1 Hz.

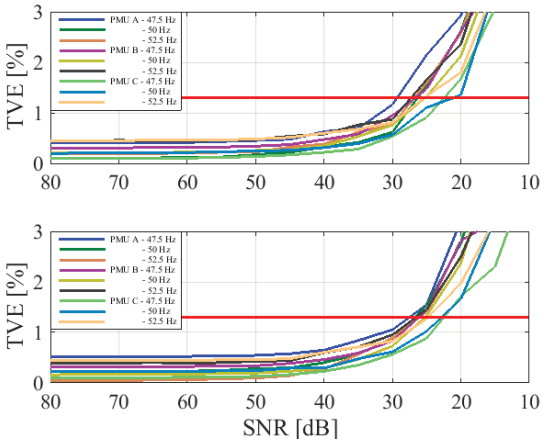

Fig. 7. Phase A; TVE limit = 1.3%; (a) Voltage; (b) Current

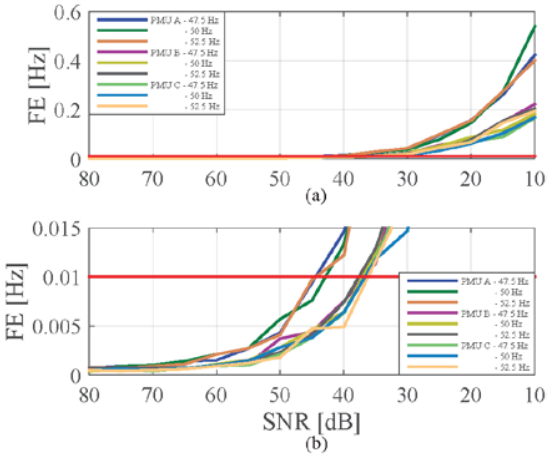

Fig. 8. Frequency Error: (a) Maximum error; (b) detail of (a) showing the error limit

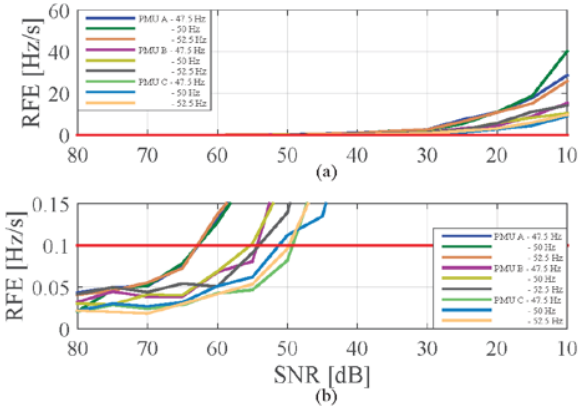

Fig. 9. ROCOF Error: (a) Maximum error; (b) detail of (a) showing the error limit

The ROCOF is even more affected by noise. PMU A is the first to exceed the limit at about 63 dB while the others still meet the requirement at 56 dB. Since the frequency from PMU A is more affected by noise than the others, it makes sense that its ROCOF measurement will be also.

Based on these results, it is clear that the frequency and ROCOF measurements are much more affected by noise, as

expected since these are the first and second derivatives of the phase angle. It can also be seen that the knee of the curve, where noise causes the error curves to deviate from the noise floor, is around 40 dB for phasors (TVE), 55 dB for frequency (FE), and 65 dB for ROCOF (RFE).

As long as the noise in the test signals remains above 65 dB SNR, the outcome of the tests specified by the standard will be unaffected. If signals with higher noise power are to be measured by PMUs, some compensation or adjustments should be made to the devices in order to reduce the error levels. Adjustments such as a longer observation window (number of cycles used by the PMU for estimation), an increased sampling rate, and a larger effective number of bits of the A/D sampling could improve the accuracy under noise conditions. Reference [46] describes details on how these adjustments affect the accuracy of the PMU, and advantages and possible disadvantages of such adjustments. A number of guidelines are also provided in [46] to help PMU designers make a balanced choice of these parameters.

B. Multiple Harmonics Test

The multiple harmonics test is an extension of what the standard requires. In this case, multiple harmonics are injected simultaneously and the accuracy of the PMUs is analyzed. The three phase voltages and currents have different harmonic components. Since the frequency of the power system is not always at its nominal value, the harmonic rejection capabilities of the PMUs are also tested at off-nominal frequencies. Fig. 10 and Fig. 11 show the TVE of the voltages and currents with multiple harmonics included, and signal frequencies of 50 Hz and 52.5 Hz, respectively. It is clear that, in both cases, the accuracy of the tested PMUs is well within the limits defined in the IEEE C37.118.1 standard.

The results of this test demonstrate that these PMUs provide sufficient filtering to suppress the multiple harmonics interference in these cases. The frequency measurement and ROCOF estimation are shown in Fig. 12 and Fig. 13. They are accurate for all PMUs in both nominal and off-nominal cases.

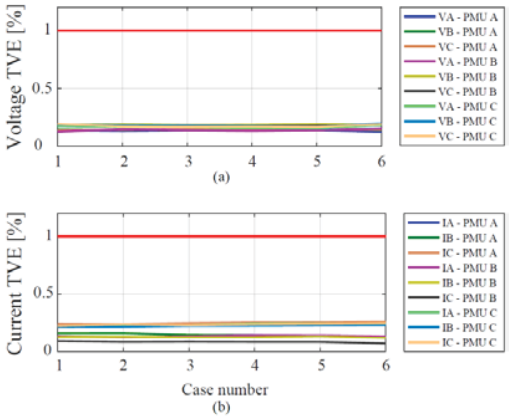

Fig. 10. Multiple harmonic rejection: (a) Voltage analysis; (b) Current analysis; Signals frequency f = 50 Hz

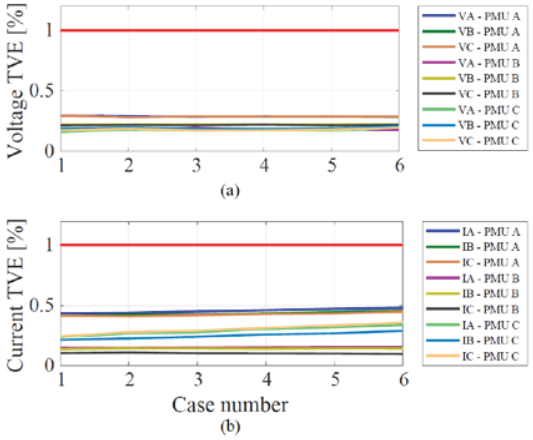

Fig. 11. Multiple harmonic rejection: (a) Voltage analysis; (b) Current analysis; Signals frequency f = 52.5 Hz

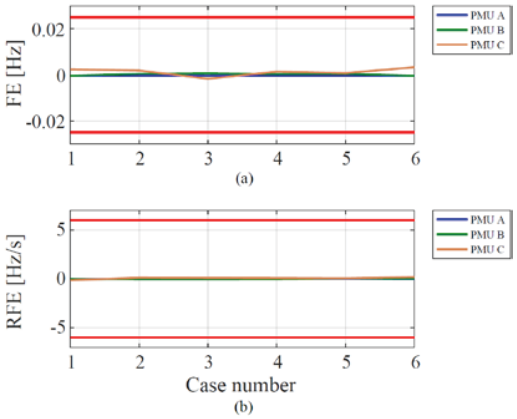

Fig. 12. Multiple harmonic rejection: (a) Frequency Error; (b) ROCOF Error; Signals frequency f =50 Hz

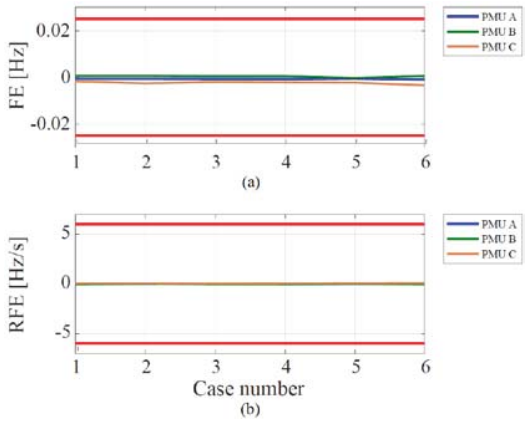

Fig. 13. Multiple harmonic rejection: (a) Frequency Error; (b) ROCOF Error; Signals frequency f =52.5 Hz

In addition, the devices are also tested for single harmonic interference at nominal and off-nominal frequencies. The injected signals contain one harmonic at a time, from 2nd to 50th. The amplitude of the harmonics is 10% of the fundamental. Fig. 14 to Fig. 17 show that the tested PMUs successfully filter the single harmonics at both nominal and off-nominal frequencies.

It can be concluded that these PMUs have sufficient filtering to suppress harmonic interference for both single and

multiple harmonic contents, even when the base frequency is off-nominal.

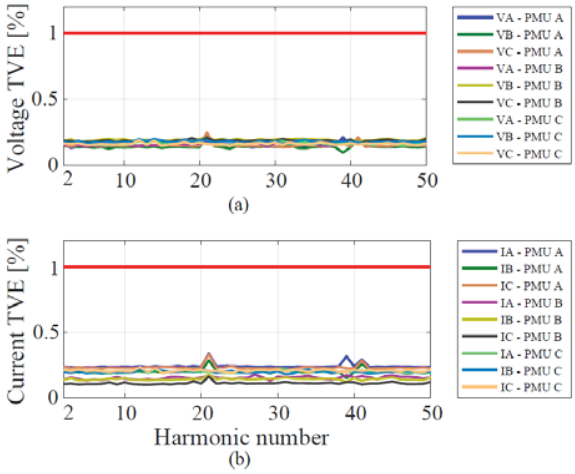

Fig. 14. Single harmonic rejection: signal frequency f = 50 Hz; (a) Voltage analysis; (b) Current analysis

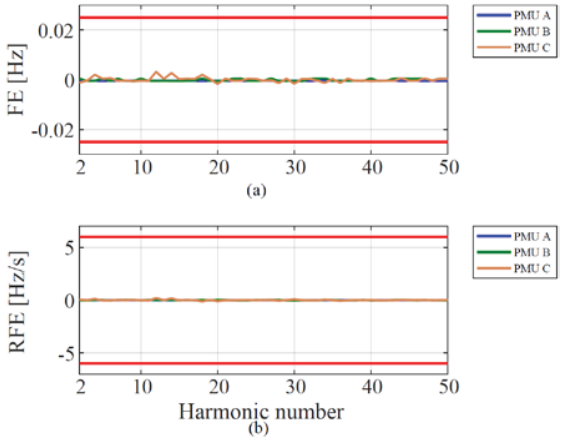

Fig. 15. Single harmonic rejection: signal frequency f = 50 Hz; (a) Frequency Error; (b) ROCOF Error

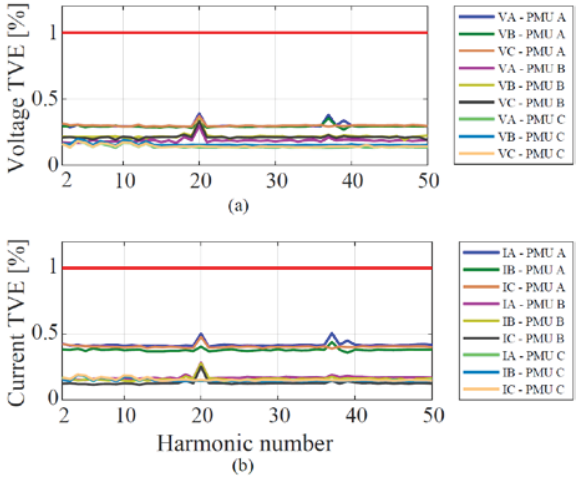

Fig. 16. Single harmonic rejection: signal frequency f = 52.5 Hz; (a) Voltage analysis; (b) Current analysis

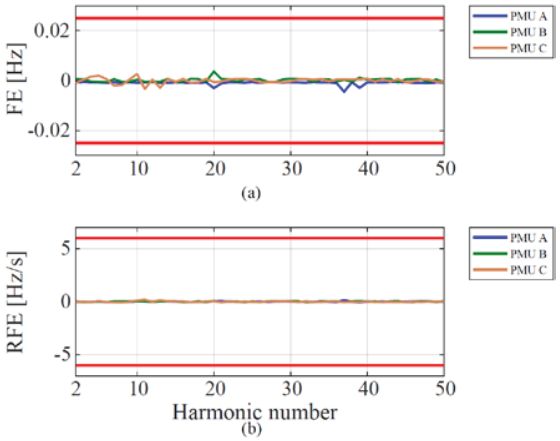

Fig. 17. Single harmonic rejection: signal frequency f = 52.5 Hz; (a) Frequency Error; (b) ROCOF Error

C. *Current Transformer Saturation Test*

This test is similar to the Amplitude Scan test defined in IEEE C37.118.1, so the 1% TVE limit is used for comparing the accuracy of the PMUs.

Fig. 18 shows the accuracy of the current measurement versus the saturation factor. It can be seen that all devices are within the limit as long as there is no saturation, $K_S \leq 1$. The performance decreases rapidly once saturation occurs.

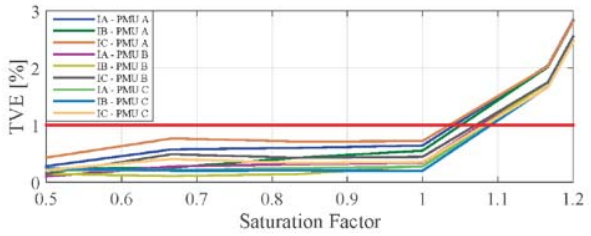

Fig. 18. CT saturation test: Current Total Vector Error

Fig. 19 and Fig. 20 give an insight to the amplitude and angle measurements. It is shown that the measured amplitude tends to flatten out as the saturation increases. In contrast, the measured angle shows an increase while it should stay constant. In Fig. 20，the angle of phase A is shown together with the reference value. All three phases of all PMUs are plotted in the figures, except for Fig. 20b, where only phase A of all PMUs is shown. Phases B and C follow the same trend as phase A, and this is visible in Fig 20a where the phase error for all angles increases.

The Frequency Error and ROCOF Error are not evaluated, because these PMUs use voltage measurements in order to estimate these quantities. For this test, the voltages were kept at the nominal value and the Frequency and ROCOF are not affected.

The results show that CT saturation degrades the accuracy of the PMU measurements. Correct choice and installation of CTs helps prevent saturation. However, it can still occur during faults, or if a DC current flows in the circuit and incorrect PMU measurements can reach the control algorithms. Following the specific trend where amplitude flattens and angle increases, the event could be detected from the PMU raw measurements and then indicated by a flag.

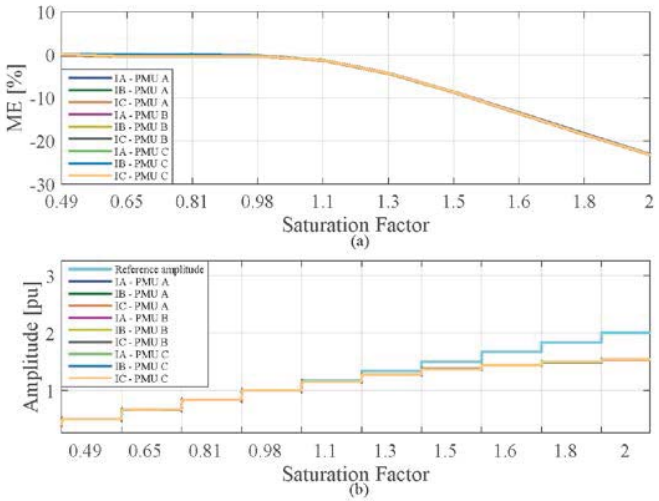

Fig. 19. CT saturation test: (a) Current Magnitude Error; (b) Current amplitude

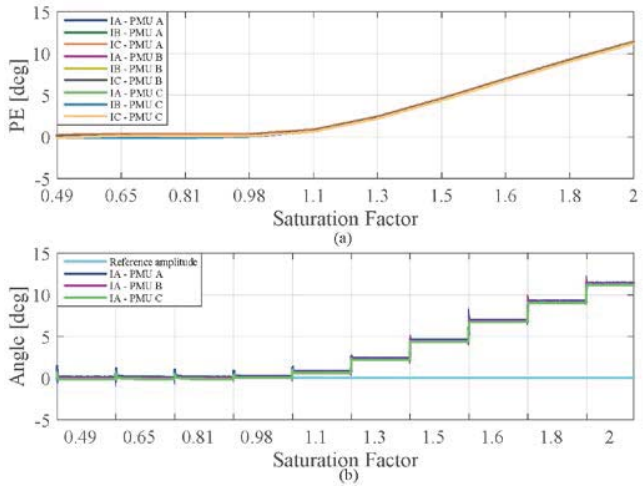

Fig. 20. CT saturation test: (a) Current Phase-A Error; (b) Current Phase-A angle

V. Conclusion

This paper has looked into the PMU performance under three plausible power system interference conditions. Three production PMUs were used in this test. They were all configured for M-class since it provides the greatest interference filtering and is expected to make the most precise measurements.

The testing uses white noise to test resistance to broad-band interference. It was shown that these PMUs successfully reject noise down to around 40dB SNR before the phasor measurements fail to meet the specifications. Frequency and ROCOF measurements fail below about 55 dB and 65 dB, respectively. Better filtering, or improved processing techniques will be required for acceptable results, particularly for frequency and ROCOF measurements, if PMUs are used in high noise environments.

Multiple harmonics tests show that these are rejected by the PMU filtering just the same as single harmonics both in nominal and off-nominal frequency cases. Phasors, frequency and ROCOF are accurately estimated and reported in all cases by the tested PMUs. This result indicates that the single harmonic testing at nominal frequency is adequate for verifying harmonic rejection.

PMU measurement failure starts at a low level of CT core saturation (Ks=1.2). This could lead to control or protection error if not detected. There seems to be a pattern in this case as amplitude flattens and angle increases but is not distinct enough to clearly identify such an event from the data itself. Since the phasor only includes the sinusoidal parameters, waveform distortion is not reported. It can be better detected from the raw measurement in the PMU and then indicated through an error flag that is transmitted with the data.

The emphasis was on PMU performance under impairments which could be seen in operating power systems, and the comparison with results that would be seen from C37.118.1 testing. The tests showed that noise degrades measurement at fairly high SNRs, especially for frequency and ROCOF estimations. While not surprising, this should encourage PMU designers to develop and implement methods more resistant to noise. The fact that single or multiple harmonics at nominal or off-nominal frequencies did not significantly degrade measurements indicates that current testing methods in the standard are adequate. Finally, distorted waveforms will certainly degrade the measurement, but possibly this is at a higher level than expected.

The results can also be used for PMU and phasor application development, particularly regarding signatures related to certain impairments. For example, an application designer could detect high noise through a tracking filter and use that to relax trigger points, making the application more robust. A small signature was noted with CT saturation distortion (flattening amplitude with decreasing phase angle). This is not distinct enough to flag the event, particularly as saturation will usually occur very fast. Finally, harmonic rejection proved to be good, so it is not likely to be an area that needs additional development.

VI. References

[1] IEEE Standard for Synchrophasor Measurements for Power Systems - IEEE Std C37.118.1™-2011.

[2] Amendment 1: Modification of Selected Performance Requirements - IEEE Std C37.118.1a™-2014 (Amendment to IEEE Std C37.118.1™-2011).

[3] "IEEE Synchrophasor Measurement Test Suite Specification," IEEE-SA Conformity Assessment Program, December 2014.

[4] R. Ghiga, Q. Wu, K. Martin, W. Ziad, L. Cheng and A. H. Nielsen, "Dynamic PMU Compliance Test under C37.118.1a™-2014," in *Proc. IEEE PES General Meeting*, Denver, CO, 2015, pp. 1-5.

[5] D.R. Gurusinghe, A.D. Rajapakse, and K. Narendra, "Testing and Enhancement of Dynamic Performance of a Phasor Measurement Unit," *IEEE Trans. Power Del.*, vol. 29, no. 4, August 2014.

[6] K. Narendra, D. R. Gurusinghe, and A.D. Rajapakse, "Dynamic Performance Evaluation and Testing of Phasor Measurement Unit (PMU) as per IEEE C37.118.1 Standard," *Presented at the Doble Client Committee Meetings Int. Protect. Testing Users Group, Chicago, IL, USA.*

[7] D.R. Gurusinghe, A.D. Rajapakse, and K. Narendra, "Evaluation of Steady-State and Dynamic Performance of a Synchronized Phasor Measurement Unit," in *Proc. IEEE Elect. Power Energy Conf., London, ON, Canada,* 2012, pp. 57-62.

[8] A. Phadke and B. Kasztenny, "Synchronized phasor and frequency measurement under transient conditions," *IEEE Trans. Power Del.*, vol. 24, no. 1, pp. 89–95, Jan. 2009.

[9] D. Macii, D. Petri, and A. Zorat, "Accuracy Analysis and Enhancement of DFT-Based Synchrophasor Estimators in Off-Nominal Conditions," *IEEE Trans. Instrum. Meas.*, vol. 61, no. 10, pp. 2653–2664, Oct. 2012.

[10] I. Kamwa, A. K. Pradhan, and G. Joos, "Adaptive phasor and frequency tracking schemes for wide-area protection and control," *IEEE Trans. Power Del.*, vol. 26, no. 2, pp. 744–753, Apr. 2011.

[11] M. Karimi-Ghartemani, B.T. Ooi, and A. Bakhshai, "Application of enhanced phase-looked loop system to the computation of synchrophasor," *IEEE Trans. Power Del.*, vol. 26, no. 1, pp. 22–32, Jan. 2011.

[12] J. A. de la O Serna, "Dynamic phasor estimates for power system oscillations," *IEEE Trans. Instrum. Meas.*, vol. 56, no. 5, pp. 1648–1657, Oct. 2007.

[13] J. A. de la O Serna, "Dynamic phasor estimates for power system oscillations and transient detection," in *Proc. IEEE PES General Meeting*, Montreal, QC, Canada, 2006, pp. 1-7.

[14] M. A. Platas-Garza and J. A. de la O Serna, "Dynamic phasor and frequency estimates through maximally flat differentiators," *IEEE Trans. Instrum. Meas.*, vol. 59, no. 7, pp. 1803–1811, Jul. 2010.

[15] L. Zhan and Y. Liu, "Improved WLS-TF algorithm for dynamic synchronized angle and frequency estimation," in *Proc. IEEE PES General Meeting*, National Harbor, MD, 2014, pp. 1–5.

[16] L. Zhan, Y. Liu, J. Culliss, J. Zhao, and Yilu Liu, "Dynamic Single-Phase Synchronized Phase and Frequency Estimation at the Distribution Level," *IEEE Trans. Smart Grid,* vol. 6, no. 4, pp. 2013-2022, July 2015.

[17] L. Zhan, J. Zhao, J. Culliss, Y Liu, Yilu Liu, S. G., "Universal Grid Analyzer Design and Development," in *Proc. IEEE PES General Meeting*, Denver, CO, USA, July 2015, pp. 1-5.

[18] J. G. Kappenman, V. D. Albertson, and N. Mohan, "Current Transformer and Relay Performance in the Presence of Geomagnetically-Induced Currents," *IEEE Trans. Power App. Syst.,* vol. PAS-100, no. 3, pp. 1078–1088, Mar. 1981.

[19] F. Bachinger, A. Hackl, P. Hamberger, Leikermoser, G. A. Leber, H. Passath, and M. Stoessl, "Direct current in transformers: Effects and compensation," in CIGRE Session, SC A2, Paris, Aug. 2012, pp. 1-5.

[20] K. Draxler and R. Styblíková, "Effect of Magnetization on Instrument Transformers Errors," *J. Electr. Eng.*, vol. 61, no. 7/s, pp. 50–53, 2010.

[21] G. Buticchi, E. Lorenzani, and G. Franceschini, "A DC Offset Current Compensation Strategy in Transformerless Grid-Connected Power Converters," *IEEE Trans. Power Del.*, vol. 26, no. 4, pp. 2743–2751, Oct. 2011.

[22] C. Offelli and D. Petri, "Weighting effect on the discrete time Fourier transform of noisy signals," *IEEE Trans. Instrum. Meas.*, vol. 40, no. 6, pp. 972–981, Dec. 1991.

[23] C. R. Mason, *The Art and Science of Protective Relaying*. 2nd ed., John Wiley, New York, 1986.

[24] J. G. Proakis and D. G. Manolakis, Digital Signal Processing, Principles, Algorithms, and Applications. 3rd ed., Prentice-Hall Inc., New Jersey, 1996.

[25] L. F. Blume, G. Camilli, S.B. Farnham, and H.A. Peterson, "Transformer Magnetizing Inrush Currents and Influence on System Operation," *AIEE Trans.*, vol. 63, no. 6, pp. 366-375, Jun. 1944.

[26] H. S. Bronzeado, P.B. Brogan, R. Yacamini, "Harmonic Analysis of Transient Currents During Sympathetic Interaction," *IEEE Trans. Power Syst.* , vol. 11, no. 4, pp. 2081-2056, Nov. 1996.

[27] B. Badrzadeh, M. Gupta, N. Singh, A. Petersson, L. Max, and M. Hogdahl, "Power system harmonic analysis in wind power plants—Part I: Study methodology and techniques," in *Proc. IEEE Ind. Appl. Soc. Annual Meeting*, Las Vegas, NV., Oct. 2012, pp.1-11.

[28] S. Liang, Q. Hu, and W. Lee, "A survey of harmonic emissions of a commercial operated wind farm," in *Proc. IEEE Industrial and Commercial Power Systems Technical Conf.*, Tallahassee, FL, USA, May 2010, pp. 1-8.

[29] Ahmed M. A. Alomar, Bakr E. M. Shamseldin, "Alternative Approaches for Distinguishing between Faults and Inrush Current in Power Transformers," *Scientific Research, Energy and Power Engineering*, pp. 143-160, Jul 2014.

[30] Ryan A. Turner, Kenneth S. Smith, "Transformer Inrush Currents. Harmonic Analysis in Interconnected Power Systems," *IEEE Ind. Appl. Mag.*, vol. 16, no. 5, pp. 14-19, Sept.-Oct. 2010.

[31] E. C. Segatto and D. V. Coury, "A power transformer protection with recurrent ANN saturation correction," in *Proc. IEEE PES General Meeting, vol.2,* 12-16 June 2005, pp. 1341-1346.

[32] I. M. El-Amin and N. H. Al-Abbas, "Saturation of Current Transformers and its Impact on Digital Overcurrent Relays," in *Proc. IEEE Transmission & Distribution Conference and Exposition: Latin America*, Aug. 2006, pp. 1-6.

[33] IEEE Guide for the Application of Current Transformers Used for Protective Relaying Purposes, IEEE Std C37.110™-2007.

[34] IEEE Standard Requirements for Instrument Transformers, IEEE Std C57.13™-2008.

[35] G. Swift, "CT Saturation Theory and Calculator," *IEEE Power Syst. Relaying and Control Committee*, pp 1-9, June 2001.

[36] R. Ghiga, Q. Wu, K. Martin, W. El-Khatib, L. Chen and A. H. Nielsen, "Steady-State PMU Compliance Test under C37.118.1a – 2014," in *Proc. IEE PES Innovative Smart Grid Technologies Conference Europe (ISGT Europe)*, Ljubljana, 2016, pp. 1-6.

[37] M. S. Almas, J. Kilter, and L. Vanfretti, "Experiences with steady-state PMU compliance testing using standard relay testing equipment," in *Proc. IEEE Electric Power Quality and Supply Reliability Conference (PQ),* 2014, pp.103-110.

[38] K. Martin, T. Faris, and J. Hauer, "Standardized Testing of Phasor Measurement Units," in *Proc. Fault and Disturbance Analysis Conference, Georgia Tech*, Atlanta, GA, 2006.

[39] R. Garcia-Valle, G. Yang, K. E. Martin, A. H. Nielsen, and J. Ostergaard, "DTU PMU laboratory development-Testing and validation," in *Proc. Innovative Smart Grid Technologies Conference Europe (ISGT Europe),* 2010, pp. 1-6.

[40] K.E. Martin, J.F. Hauer, and T.J. Faris, "PMU Testing and Installation Considerations at the Bonneville Power Administration," in *Proc. IEEE PES General Meeting, Tampa, FL,* 2007, pp. 1-6.

[41] K. Narendra, Z. Zhang, J. Lane, B. Lackey, and E. Khan, "Calibration and Testing of Tesla Phasor Measurement Unit (PMU) Using Doble F6150 Test Instrument," *iREP Symposium-Bulk Power System Dynamics and Control –VII, Revitalizing Operational Reliability,* August, 2007.

[42] Z. Huang, B. Kasztenny, V. Madani, K. Martin, S. Meliopoulos, D. Novosel, and J. Stenbakken, "Performance Evaluation of Phasor Measurement Systems," in *Proc. IEEE PES General Meeting,* Pittsburgh, PA, *2008,* pp.1-7.

[43] P. Komarnicki, C. Dzienis, Z. A. Styczynski, J. Blumschein, and V. Centeno, "Practical experience with PMU system testing and calibration requirements," in *Proc. IEEE PES General Meeting*, Pittsburgh, PA, 2008, pp. 1-5.

[44] G. Stenbakken, and T. Nelson, "Static Calibration and Dynamic Characterization of PMUs at NIST," in *Proc. IEEE PES General Meeting,* Tampa, FL, *2007,* pp 1-4.

[45] J. K. Hwang and Y. Liu, "Noise Analysis of Power System Frequency Estimated From Angle Difference of Discrete Fourier Transform Coefficient," *IEEE Trans. on Power Del.*, vol. 29, no. 4, pp. 1533-1541, Aug. 2014.

[46] D. Macii, D. Fontanelli, G. Barchi, and D. Petri, "Impact of Acquisition Wideband Noise on Synchrophasor Measurements: A Design Perspective," *IEEE Trans. Instrum. Meas.*, vol. 65, no. 10, pp. 2244-2253, Oct. 2016.

D
PHASOR MODEL OF FULL SCALE CONVERTER WIND TURBINE FOR SMALL-SIGNAL STABILITY ANALYSIS

This paper has been submitted at the IET International Conference on Renewable Power Generation, Wuhan, China

Phasor Model of Full Scale Converter Wind Turbine for Small-Signal Stability Analysis

Radu Ghiga, Qiuwei Wu and Arne Hejde Nielsen
Center for Electric Power and Energy
Department of Electrical Engineering
Technical University of Denmark (DTU)
Kongens Lyngby, 2800, Denmark
Emails: rhiga@elektro.dtu.dk, qw@elektro.dtu.dk and ahn@elektro.dtu.dk

***Abstract*—The small-signal stability analysis of power system electromechanical oscillations is a well-established field in control and stability assessment of power systems. The impact of large wind farms on small-signal stability of power systems has been a topic of high interest in recent years. This paper presents a phasor model of full scale converter wind turbines (FSCWTs) implemented in Matlab/Simulink for small-signal stability studies. The phasor method is typically used for dynamic studies of power systems consisting of large electric machines. It can also be applied to any linear system. This represents an advantage in small-signal stability studies which are based on modal analysis of the linearized model and are usually complemented with dynamic simulations. The proposed model can represent a single WT or an aggregated wind power plant (WPP). The implemented model for small-signal stability analysis was tested in the Kundur's two area system. The results show that the proposed WT model is accurately linearized and its impact on power system oscillation is similar to that of previous research findings.**

***Index Terms*-- modal analysis, phasor model, small-signal stability, wind turbine, wind power plant,**

I. Introduction

The installed capacity of wind power and the size of each installation have been increasing rapidly, with the European offshore sector installation just over 3 GW of wind power only in 2015 [1]. The role and impact of large penetration of wind power can be significant in the operation and security of the power system [2], [3]. A topic of interest is the effect of large Wind Power Plants (WPPs) on small-signal stability of power systems. The validity of the damping results depends on accurate representation of the WPP control systems, a fact known from control interactions of HVDC stations [4], [5] and investigated in [6] for a WPP voltage control system.

In a full scale converter wind turbine (FSCWT), the generator dynamics are decoupled from the grid dynamics. Hence, the WT generator cannot contribute to damping the system oscillations without additional control [7]. However, this type of configuration has the advantage of controlling both active and reactive power independently, and also allows independent impact assessment of these controls on power system oscillations.

The phasor simulation method in Matlab/Simulink is typically used to study low frequency electromechanical oscillations of power systems consisting of a large number of generators and loads. An advantage of this method is that sinusoidal voltages and currents are replaced with phasors expressed in the complex or polar form. Since the electromagnetic transients are not of interest, the dynamic simulation time is reduced [8]. Another advantage is that the phasor simulation can be used with any linear system, and small-signal stability studies are based on eigenvalue analysis of the linearized power system. Finally, the eigenvalue analysis is usually complemented with dynamic simulations of the non-linear system which can be several tens of seconds long. Hence, short simulation times are desired.

The aim of this paper is to present a FSCWT model that can be used in dynamic simulations, and can be linearized by the tools available in Simulink, without the need to build a separate state-space representation of the model. Therefore, a phasor FSCWT model with a permanent magnet synchronous generator (PMSG) is implemented in Matlab/Simulink. The model consists of detailed controls in order to catch the potential impact which might have on power system oscillations. The eigenvalues of the system are first analyzed with no wind power injected in the network, and then with increasing wind power penetration. To verify the accuracy of the linearized system, the linear and nonlinear responses of the system are compared.

This paper is organized as follows. In Section II, the WT concept is presented. Section III describes the controls implemented for this model. Section IV shows the results and conclusions are drawn in Section V.

II. Wind Turbine Concept

The concept of the FSCWT is shown in Fig. 1. The main parts are the wind turbine rotor, PMSG, FSC, filter and transformer. The FSC consists of a generator side and grid side that are connected by a DC-link circuit with a capacitor (C_{dc}). The generator three phase AC voltage is converted into DC voltage (V_{dc}) by the generator side converter. The DC voltage is then inverted back into AC by the grid side converter which uses a Phase-Locked Loop (PLL) to match the grid frequency and phase.

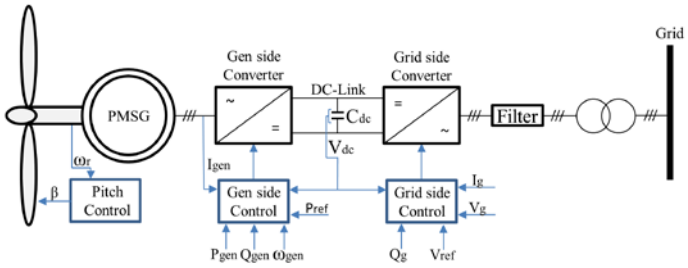

Fig. 1. Wind turbine concept

The control system of the FSCWT consists of three main controllers. The pitch controller regulates the angle of the blades (β) to prevent the rotor speed (ω_r) from exceeding its rated value. The generator side control adjusts the generator currents in order to control its active (P_{gen}) and reactive power (Q_{gen}) outputs. The grid side control maintains V_{dc} to its rated value, and controls the reactive power (Q_{grid}) output and the AC voltage at the terminal of the wind turbine.

III. Wind Turbine Phasor Model

The block diagram of the WT phasor model implemented in Simulink is shown in Fig. 2. The V_{abc}/V_{dq} block has a PLL implemented that computes the angle of the terminal voltage phasor and uses it to align the internal dq-reference. The WT is interfaced with the network through a controlled current source, and connects to the grid at the Point of Connection (POC). The remaining blocks are described in the following subsections.

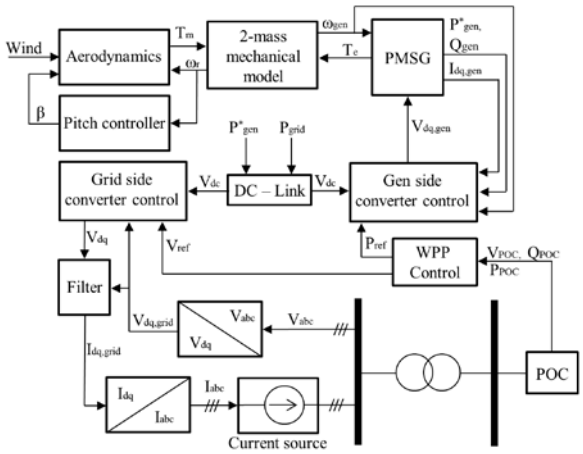

Fig. 2. Block diagram of the phasor model

A. Aerodynamic Model and Pitch Controller

The Aerodynamics block calculates the mechanical torque (T_m) as $T_m = P_m/\omega_r$. The mechanical power P_m converted from the wind speed is calculated inside this block as [9],

$$P_m = 0.5\rho A v^3 C_p(\lambda, \beta) \quad (1)$$

where ρ is the air density (kg/m^3), A is the rotor swept area (m^2), v is the wind speed (m/s), C_p is the power coefficient, and λ is the tip speed ratio (v_t/v), and v_t is the blade tip speed (m/s). The generic equation used to approximate C_p is given in [9].

Fig. 3 shows the pitch controller of the WT. The blade pitch angle (β) is calculated based on the error between the measured rotor speed and the reference value (ω_{ref} = 1.0 p.u.). The angle is kept at zero degree as long as the rotor speed does not exceed the reference value. An angle change rate limiter is implemented to model the blade rotation speed.

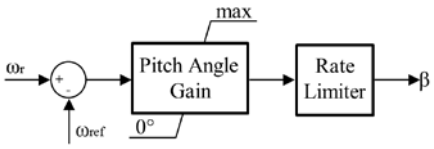

Fig. 3. Pitch controller

B. Mechanical Model

The mechanical model is used to simulate the wind turbine drive train which consists of the rotor hub with blades, rotor shaft, and generator rotor. In order to reflect the torsional shaft oscillations that can occur due to a sever network disturbance, a two-mass model should be implemented [10]. This model is also adequate when investigating the effect of wind gusts, or the change in the active power set-point [11].

Fig. 4 shows the mechanical model implemented in this paper, where H_t and H_g are the inertia constants of the rotor and generator, respectively [12]. The damping coefficient is D, and the shaft stiffness is K_{sf}.

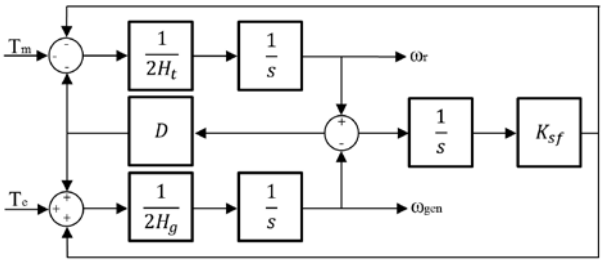

Fig. 4. Mechanical model (2-mass model)

C. Converter Control Models

The block diagram of the generator side converter control is shown in Fig. 5. The reactive power reference (Q_{ref}) is set to zero and the converter controls the d-axis current ($I_{d,gen}$) to achieve unity power factor at the generator terminals. The active power reference (P_{ref}) can be calculated based on a Maximum Power Point Tracking (MTTP) method [13], or it can be given by the WPP Control as shown in Fig. 2. The generator side controller adjusts the q-axis current ($I_{q,gen}$) in order to control the active power production (P_{gen}).

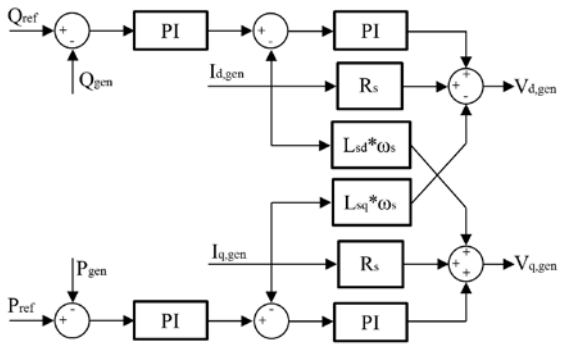

Fig. 5. Generator side controller

The grid side converter control shown in Fig. 6 keeps the DC-link voltage (Vdc) to its nominal value by controlling the d-axis grid current ($I_{d,grid}$). The AC voltage and reactive power at the WT terminal are controlled by adjusting the q-axis current ($I_{q,grid}$).

The reference voltage (V_{ref}) is calculated in the WPP Control block and sent to the WT in order to keep the AC voltage at the terminal to its rated value. The block diagram in Fig. 6 is based on [14].

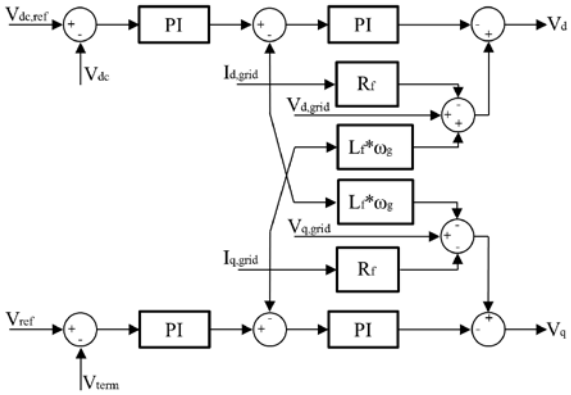

Fig. 6. Grid side controller

D. Permanent Magnet Synchronous Generator Phasor Model

The Matlab/Simulink library documentation [8] provides the differential equations of the generator electrical model in the d-q rotor reference frame, where all the quantities in the rotor reference frame are referred to the stator:

$$\frac{d}{dt}I_{d,gen} = \frac{V_{d,gen}}{L_{sd}} - \frac{R_s}{L_{sd}}I_{d,gen} + \frac{L_{sq}}{L_{sd}}I_{q,gen}\omega_s \quad (2)$$

$$\frac{d}{dt}I_{q,gen} = \frac{V_{q,gen}}{L_{sq}} - \frac{R_s}{L_{sq}}I_{q,gen} - \frac{L_{sd}}{L_{sq}}I_{d,gen}\omega_s - \frac{\psi_m\omega_s}{L_{sq}} \quad (3)$$

where $I_{dq,gen}$ are the stator current components, $V_{dq,gen}$ are the stator voltage components, ω_s is the stator electrical frequency, ψ_m is the flux of the permanent magnets, and $L_{sd,q}$ are the d-axis and q-axis inductances. The block diagram of the generator electric phasor model implemented in Simulink is shown in Fig. 7.

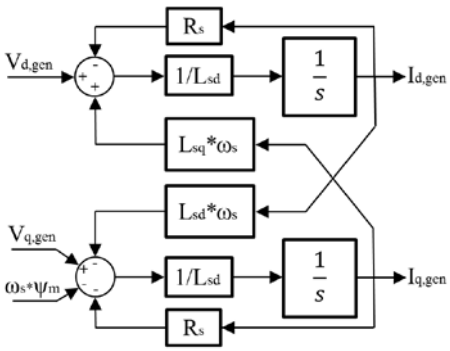

Fig. 7. Block diagram of the generator model

E. DC-Link Model

The power generated by the PMSG is supplied to the grid side converter through the DC-link. The dynamics of the capacitor voltage (V_{dc}) can be expressed as [15]:

$$\frac{dV_{dc}}{dt} = (P_{gen} - P_{grid})\frac{1}{V_{dc}C_{dc}} \quad (4)$$

The block diagram of the model is shown in Fig. 8.

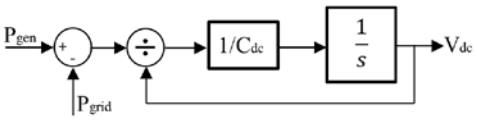

Fig. 8. DC-link model

F. Grid side RL filter phasor model

The wind turbine is connected to the transformer through a three phase RL filter. The single phase equivalent circuit is shown in Fig. 9, and the model is described by the following differential equations [16]:

$$V_{conv} - V_{grid} = L_f\frac{dI}{dt} + R_f I \quad (5)$$

where V_{conv} is the voltage at the converter side, and V_{grid} is the voltage at the grid side, and L_f and R_f are the filter inductance and resistance. The differential equations of the filter in the rotating d-q frame are as follows:

$$I_d = \frac{\omega}{L_f s}(V_d - V_{d,grid} - R_f I_d + L_f I_q) \quad (6)$$

$$I_q = \frac{\omega}{L_f s}(V_q - V_{q,grid} - R_f I_q - L_f I_d) \quad (7)$$

where $\omega = 2\pi F_{nom}$, and V_d, V_q are the dq-components of V_{conv}. The filter block diagram is shown in Fig. 10.

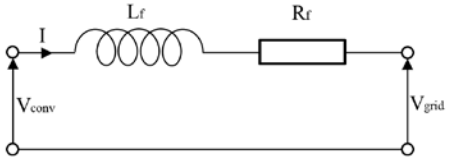

Fig. 9. Single phase RL-filter equivalent circuit

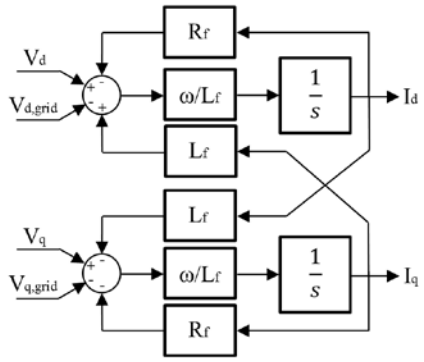

Fig. 10. RL filter block diagram in d-q rotating frame

G. WPP Control

The WPP control (WPC) in Fig. 2 measures the voltage (V_{POC}), active (P_{POC}) and reactive (Q_{POC}) powers at the POC. It sends voltage and active power references to the WPP. In this paper, the WPC consists of an active power controller shown in Fig. 11, and a voltage controller shown in Fig. 12.

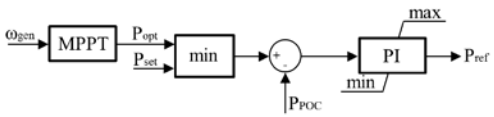

Fig. 11. Wind park active power controller

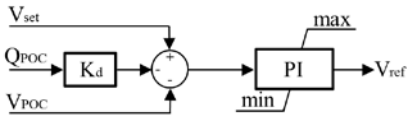

Fig. 12. Wind park voltage controller

The active power control is a simplified version of the one in [11]. The power reference (P_{ref}) is decided as the minimum between the optimal power (P_{opt}) and a value (P_{set}) chosen by the transmission system operator or WPP owner. In this paper, the WPP is an aggregated model and P_{opt} is calculated based on the MPPT method from [13].

A similar voltage control has been used in [7]. It calculates a voltage reference (V_{ref}) based on the measured reactive power (Q_{POC}) and measured voltage (V_{POC}), and sends it to the WPP. Consequently, the WPP adjusts its output accordingly so the voltage at the POC matches the reference voltage in the WPC. The value of the droop gain K_d is 0.04 as given in [7].

H. Wind Park Collector System

The aggregated model of the WPP is connected to the grid through a collector system modelled as a T-equivalent. For a WPP of 180 MW, the collector system parameters are given in Table I. Depending on the size of the WPP, the parameters are scaled using (8) and (9) so the voltage profile remains the same [7].

TABLE I. WPP Collector System Parameters

Collector parameters			**Park trasnformer**
R^* [Ω]	X^*_L [Ω]	B^*_C [μS]	X_T [%]
0.086	0.070	3219.7	12.2

$$z_{scale} = \frac{S^*_{base}}{S_{baseWP}}; \quad R_{col} = z_{scale} R^* \tag{8}$$

$$X_L = z_{scale} X^*_L; \quad B_{col} = \frac{B^*_C}{z_{scale}} \tag{9}$$

IV. Simulation Results

The analysis is performed in Matlab/Simulink where the power system model is implemented using the SimPowerSystems [17]. The phasor WT model presented in the previous section is included in the power system network as an aggregated WPP, and the small-signal stability is assessed by linearizing the model. The linearization is performed using the Simulink Control Design toolbox [18], directly on the initialized power system model. The Control Design toolbox uses exact linearization for every function in the model that has an analytical first derivative, and numerical perturbation is used for elements, such as look-up tables, that cannot be linearized analytically. This study is based on the Kundur's two area system shown in Fig. 13 to which the WPP is added. All generators are equipped with Power system Stabilizers (PSS) which are tuned as in [19].

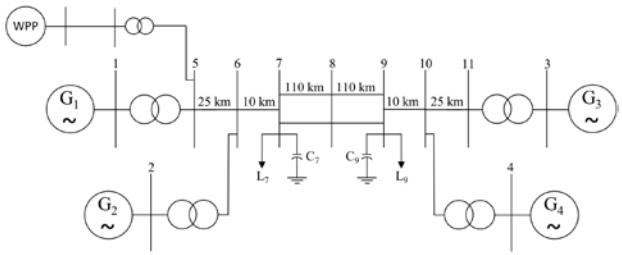

Fig. 13. Kundur's two area system case study

A. Case Study without Wind Power

The modal characteristics of the power system without wind power are analyzed first. The model is linearized and its eigenvalues are computed. One inter-area mode and two local area modes are present in the system and their characteristics are given in TABLE II. These values are very similar to the eigenvalues presented in [19] for the two area network, thus confirming these results are correct.

The modal analysis is complemented with time domain simulations of both the linear and non-linear systems in order to validate the linearization of the model. The oscillations are excited by a step increase of 1% in the excitation voltage reference of G_1. The rotor speeds of generators G_1 and G_3 are shown in Fig. 14. The inter-area mode is clearly visible as the generators swing against each other. The linear and nonlinear model responses overlap, validating the linearization.

TABLE II. Modal characteristics of the power system without wind penetration

Type of control	Eigenvalue/(Frequency in Hz, Damping Ratio)		
	Inter-area mode	***Area 1 Local Mode***	***Area 2 Local Mode***
PSS	-0.689 ± j4 (f=0.65, ζ=0.17)	-2.56 ± j8.42 (f=1.4, ζ=0.291)	-2.49 ± j8.9 (f=1.47, ζ=0.269)

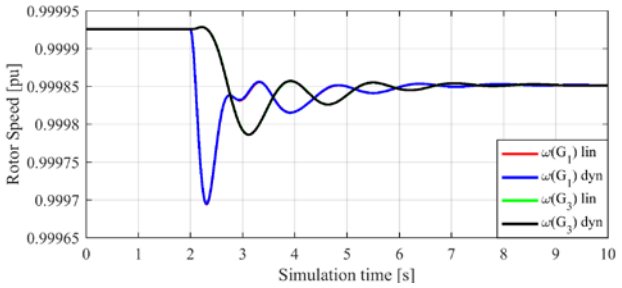

Fig. 14. Rotor response of generators G_1 and G_3 with no wind power

B. *Case Study with Wind Power*

For this case, the aggregated phasor WPP model is included in the two area system at bus 5 as shown in Fig. 13. The wind power injected in the system is increased from 30 MW to 560 MW in five steps. The WPP is a scaled up 5 MW WT with the parameters of the generator and drive train given in Table III.

Table III. Parameters for the wind turbine

Permanent Magnet Synchronous Generator	
Parameter	***Value***
Rated Power (P_{nom})	5 MW
Rated voltage (V_{nom})	0.69 kV
R_s	0.017 pu
L_{sd}	1.0 pu
L_{sq}	0.7 pu
Ψ_m	1.4 pu
Drive Train	
H_t	6.0 s
H_g	0.9 s
D	1.5
K_{sf}	296

It is known that the modal characteristics of the power system can be affected by a significant change in the dispatch of existing power units and the power flow [20]. In this study, only the influence of the proposed wind turbine model on the power system oscillations is of interest. Consequently, the system power flow is kept unchanged by lowering the power set-point of generator G_1 for each step increase in wind power. The dispatch of the other three generators remains constant, and so does the MVA rating of all generators.

The entire model is linearized and the modal characteristics of the system with wind power are shown in TABLE IV. The results confirm that the full-load converter wind turbine model has a small effect on the inter-are mode which is in agreement with previous findings [7]. Fig. 15 shows the rotor speeds of generators G_1 and G_3 for the linear and nonlinear models. The responses match and the inter-area oscillation is visible as the two generators swing against each other.

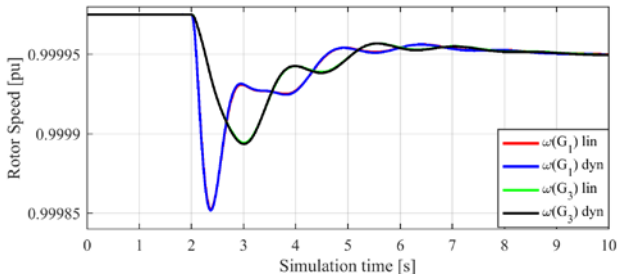

Fig. 15. Rotor responses of generators G_1 and G_3 with 560 MW wind power

TABLE IV. Modal characteristics of the power system with wind penetration

Wind Power [MW]	**Eigenvalue/(Frequency in Hz, Damping Ratio) with Wind Power**		
	Inter-area mode	***Area 1 Local Mode***	***Area 2 Local Mode***
30	-0.692 ± j3.99 (f=0.64, ζ=0.171)	-2.6 ± j8.35 (f=1.39, ζ=0.297)	-2.49 ± j8.9 (f=1.47, ζ=0.269)
50	-0.694 ± j3.99 (f=0.64, ζ=0.171)	-2.62 ± j8.3 (f=1.39, ζ=0.301)	-2.49 ± j8.9 (f=1.47, ζ=0.269)
100	-0.699 ± j3.97 (f=0.64, ζ=0.173)	-2.67 ± j8.18 (f=1.37, ζ=0.311)	-2.49 ± j8.9 (f=1.47, ζ=0.269)
200	-0.707 ± j3.94 (f=0.63, ζ=0.176)	-2.74 ± j7.92 (f=1.33, ζ=0.327)	-2.49 ± j8.89 (f=1.47, ζ=0.27)
560	-0.704 ± j3.79 (f=0.61, ζ=0.182)	-2.6 ± j7.02 (f=1.19, ζ=0.347)	-2.49 ± j8.89 (f=1.47, ζ=0.27)

The step change in the excitation voltage causes the G_1 terminal voltage to change. This affects the voltage at bus 5 where the wind turbine is connected. The WPP voltage control measures this change and acts on it. The responses of the voltage and reactive power change are shown in Fig. 16 and Fig. 17, respectively. The responses of the linear and nonlinear models overlap, confirming that the model has been linearized correctly.

Because the full-load converter decouples the wind turbine generator and drive-train dynamics from the grid dynamics, the active power output of the WT is not affected by the change in voltage. This is shown in Fig. 18 where the active power of both linear and nonlinear models match, and remain unchanged during the disturbance.

The degree of interaction of the WPP and generators in the inter-area oscillation is evaluated with the aid of the normalized participation factors shown in TABLE V. Generator G_3 has the highest participation in the inter-area mode, while the wind turbine has a negligible effect on this mode shape. A similar conclusion is drawn in [7].

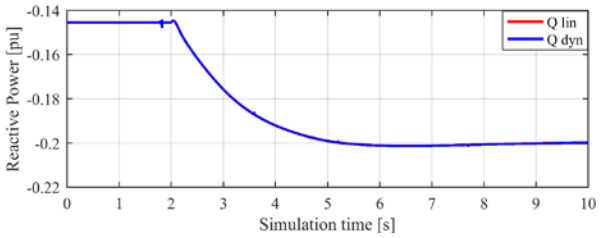

Fig. 16. Reactive power at WPP PCC

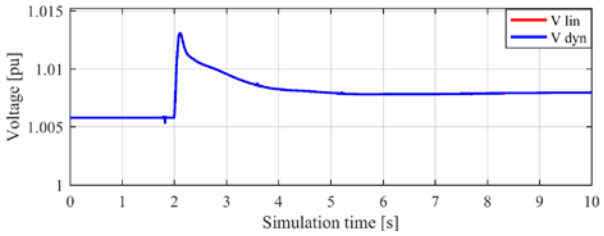

Fig. 17. Voltage at WPP PCC

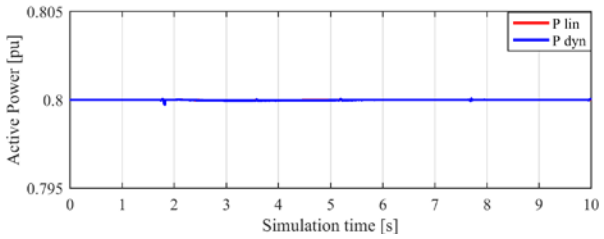

Fig. 18. Active power at WPP PCC

TABLE V. Normalized rotor participation factors

State variable	Participation factors for inter-area mode
δ (G_1)	0.32
δ (G_2)	0.15
δ (G_3)	1
δ (G_4)	0.87
δ_r (WPP)	$<10^{-2}$

V. Conclusion

In this paper, a phasor model of a FSCWT for small-signal stability assessment is implemented in Matlab/Simulink. The Simulink Control Design toolbox is used to linearize the entire initialized model and the linearization result is validated by comparing the step responses of the linear and nonlinear systems with dynamic simulations. The results show that the responses match for small disturbances (1% step in generator excitation voltage reference). Hence, the phasor model is linearized accurately.

The modal characteristics of the test system are analyzed with and without wind power, and the results match previous research findings. The participation factors show that the FSCWT does not have a significant impact on the inter-area mode, which confirms the results from previous research. Therefore, the proposed model can be used either as a single WT or as an aggregated model to perform small-signal stability studies of power systems with large wind penetration.

References

[1] Global wind energy Report 2015, April 2016. [Online]. Available: http://www.gwec.net/publications/global-wind-report-2/

[2] P. Ledesma, J. Usaola, and J. Rodriguez, "Transient stability of a fixed speed wind farm," *Renewable Energy*, vol. 28, no. 9, pp. 1341-1355, Jul 2003.

[3] V. Akhmatov, H. Knudsen, A. H. Nielsen, J. K. Pedersen, and N. Kjølstad Poulsen, "Modelling and transient stability of large wind farms," *International Journal of Electrical Power and Energy Systems*, vol. 25, no. 2, pp. 123–144, Feb 2003.

[4] J. Tang, "Reader's guide to subsynchronous resonance," *IEEE Trans. Power Syst.*, vol. 7, no. 1, pp. 150-157, Feb 1992.

[5] N. Rostamkolai, R. J. Piwko, E. V. Larsen, D. A. Fisher, M. A. Mobarak and A. E. Poitras, "Subsynchronous interactions with static VAR compensators-concepts and practical implications," *IEEE Trans. Power Syst.*, vol. 5, no. 4, pp. 1324-1332, Nov 1990.

[6] G. Tsourakis, B.M. Nomikos, C.D. Vournas, "Effect of wind parks with doubly fed asynchronous generators on small-signal stability," *Electric Power Systems Research*, vol. 79, no. 1, pp. 190-200, Jan 2009.

[7] T. Knuppel, J. N. Nielsen, K. H. Jensen, A. Dixon and J. Ostergaard, "Small-signal stability of wind power system with full-load converter interfaced wind turbines," *IET Renewable Power Generation*, vol. 6, no. 2, pp. 79-91, Mar 2012.

[8] MATLAB documentation center. [Online]. Available: https://www.mathworks.com/help/

[9] S. Heier, *Grid integration of wind energy conversion systems*, John Wiley & Sons, 1998.

[10] P. M. Anderson, *Subsynchronous resonance in power system*, IEEE Pres, New York, 1994.

[11] A. D. Hansen and I. D. Margaris. (2014). Type IV Wind Turbine Model DTU Wind energy. [Online]. Available: http://orbit.dtu.dk/en/publications/type-iv-wind-turbine-model(99b55843-deb3-49b9-b564-e664bc25fa99).html

[12] N. W. Miller, W. W. Pric, and J. J. Samches-Gasca. (2003, Oct.). Dynamic modeling of GE 1.5 and 3.6 Wind Turbine-Generators. GE-Power System Energy Consulting. [Online]. Available: https://pdfs.semanticscholar.org/4be9/52ff4ee3203db24ed461f8064abb00b8fa4e.pdf

[13] S. M. Muyeen, J. Tamura, and T. Murata, *Stability augmentation of a grid connected wind farm, Green Energy and Technology*, Springer-Verlag, 2009.

[14] V. Blasko and V. Kaura, "A new mathematical model and control of a three-phase AC-DC voltage source converter," *IEEE Trans. Power Electron.*, vol. 12, no. 1, pp. 116-123, Jan 1997.

[15] L.M. Fernandez, C.A. Garcia, and F. Jurado, "Operating capability as a PQ/PV node of a direct-drive wind turbine based on a permanent magnet synchronous generator," *Journal of Renewable Energy*, vol. 35, no 6, pp. 1308-1318, Jun 2010.

[16] P. Santiprapan, K-L. Areerak, and K-N. Areerak, "Mathematical Model and Control Stragety on DQ Frame for Shunt Active Power Filters," *Int. J. Elect., Computer, Energetic, Electronics and Communication Engineering*, vol. 5, no. 12, pp. 1664-1671, 2011.

[17] MATLAB documentation center, SimPowerSystems™ 6.6 – User's Guide, 2016.

[18] MATLAB documentation center, Simulink Control Design™ 4.4– User's Guide, 2016.

[19] P. Kundur, *Power System Stability and Control*, New York, NY, USA, McGraw-Hill, 1994.

[20] D. Wilson, J. Bialek and Z. Lubosny, "Banishing blackouts [power system oscillations stability]," *Power Engineer*, vol. 20, no. 2, pp. 38-41, April-May 2006.

E
INTER-AREA POWER OSCILLATION DAMPING CONTROLLER FOR FULL SCALE CONVERTER WIND TURBNIES USING PMU MEASUREMENTS

This paper is an unsubmitted manuscript

Inter-area Power Oscillation Damping Controller for Full-Scale Converter Wind Turbines Using PMU Measurements

Radu Ghiga, *Student Member, IEEE*, Qiuwei Wu, *Senior Member* IEEE, and Arne Hejde Nielsen, *Member, IEEE*

***Abstract*—In this paper, the effects on oscillation damping of large wind power plants (WPPs) based on full-scale converter wind turbines (WTs) is investigated. A wind park controller (WPC) that controls the active power and voltage output of the WPP is equipped, with either a phasor Power Oscillation Damper (POD) or a conventional power system stabilizer (PSS) type controller. The active power output of the WPP is modulated in order to help improve the damping of the inter-area oscillations. PMU measurements from remote locations are used as feedback signals for the PODs and the performance of the two controllers is compared with and without latency in the feedback signals. The Kundur's two-area, four-machine system, and the UK seven-generator, 18-node system are used as study cases for investigating the impact of the WPP on the inter-area oscillations.**

***Index Terms*—Full-scale converter wind turbines (FSCWTs), inter-area oscillation damping, phasor POD, power system stabilizer (PSS), small-signal stability, wind power.**

I. Introduction

POWER system oscillations are implicit in power systems consisting of synchronous generators [1]. Often in large interconnected power systems, oscillations occur between two areas of the system when they are connected through relatively weak AC transmission lines. These are referred to as inter-area oscillations, and have a frequency range of 0.1 to 0.7 Hz [2]. To ensure high damping of such oscillations, Power System Stabilizers (PSS) have been installed on the synchronous generators [2].

The power system has been changing recently due to the rapid development of renewable energies. The wind power sector has been increasing rapidly in the last fifteen years [3], and the impact of large wind power penetration on operation and security of the power system became a topic of interest [4], [5]. The impact of wind power plants (WPPs) on small signal stability has been investigated in a number of publications. The influence on power system oscillations of wind turbines (WTs) and WPPs based on fixed speed induction generators (FSIG) and doubly-fed induction generators (DFIG) was investigated in [6], [7] and was found that FSIG tend to improve inter-area oscillation damping. Several operating scenarios for DFIG presented in [8] found that DFIG integration mostly contributes positively to the damping of inter-area oscillations, with a few exceptions for certain scenarios. Full-scale converter based WTs have been included in the comparisons in [9] which concluded that the impact of DFIG and full-scale converter WTs is identical, while FSIG WTs contribute with slightly better system damping. The impact on small signal stability of the full-scale converter based WTs was also investigated in [10]. This study is based on a validated dynamic WT model provided by a vendor, which includes all the detailed controllers. It is found that the inter-area modes are largely unaffected by the WPPs based on the full converter configuration WTs. Another conclusion is that the participation in system oscillatory modes of the turbine's mechanical system is much smaller than that of the synchronous generators' mechanical system, which supports that there is a general decoupling between the grid dynamics and the WPP mechanical system [10].

Furthermore, the possibility of using the converter interfaced WTs to modulate their active or reactive power outputs to improve the damping of power system oscillations has been investigated in a number of publications. In [11]-[17], it has been proposed to equip the WPPs with a power oscillation damping controller (POD) that modulates the active power output (ΔP POD) in order to improve the damping. POD controllers that modulate the reactive power output (ΔQ POD) have been proposed in [11], [12], [18], [19], and [8], [11], [20], [21] investigated the use of both active and reactive power modulation to improve the damping of the power system oscillations.

Most of these controllers are based on the conventional PSS model consisting of a gain, a washout filter, and lead-lag compensator blocks and use local measurements as input signals. These POD controllers can become more efficient if the local measurements are replaced with remote feedback signals [22], [23]. Wide-area measurements systems (WAMS) have been increasingly adopted by utilities, and are offering access to such signals. Because WAMS are based on communications between measurement points in the network and a central data collection point, there is always a risk of latency or delay between the measurement moment and the time the data is available. Although with present technologies, the latency is usually limited to milliseconds, under unusual circumstances it can increase to hundreds of milliseconds or even more [24], [25]. This can adversely affect the POD controllers that use such signals [26], endangering the overall power system. Different solutions to solve the latency problem have been proposed

R. Ghiga, Q. Wu, and A. H. Nielsen are with the Center for Electric Power and Energy (CEE), Technical University of Denmark (DTU), Kongens Lyngby, 2800, Denmark (e-mails: rghiga@elektro.dtu.dk, qw@elektro.dtu.dk, ahn@elektro.dtu.dk).

in literature [27]-[29].

Unlike the conventional PSS model, the phasor POD, which is a concept implemented and commercialized by ABB [30]-[32], can easily compensate for the communication latency [33], [34]. The actual latency associated with each sample point can be calculated from the accurate time-stamping at both the phasor measurement units (PMU) and the control center [35]. This information is used by the phasor POD to compensate for the communication latency. This type of POD is already in use in a number of flexible AC transmission systems (FACTS) around the world, such as Thyristor Controlled Series Compensator (TCSC) and has shown promising results.

In this paper, a WPP based on full-scale converter WTs is equipped in turns with the phasor POD, and with the conventional PSS controllers in order to provide a comparison and highlight the benefits of each of them. PMU measurements are used as input signals for the two controllers, and the performance of the PODs is compared with and without latency in the measured signals.

Case studies on the Kundur's two-area, four-machine system, and the UK seven-machine, 18-node system show the performance of the WPP equipped with the controllers, in damping the inter-area oscillations.

The main contributions of this paper are summarized as follows:

- It is proposed to implement the phasor POD concept to be used with WPPs based on full-scale converter WTs.
- Two power system models are used as case studies to investigate and compare the impact of the WPP when using the Phasor POD and the conventional PSS type controllers.
- The controllers are compared with and without time latency in the input signals.
- Modal analysis is used together with dynamic simulations of the non-linear system in order to show the improvement on the damping of the inter-area modes.

II. Type 4 Wind Turbine Model

The wind turbine model used in this study has a Permanent Magnet Synchronous Generator (PMSG) and is interfaced through a full scale converter as shown in Fig. 1. The WT has variable speed operation to maximize the active power output, and is pitch controlled. It is represented with a reduced order, phasor type model suitable for dynamic and small signal analysis studies. For this study, an aggregated WT model is used and the oscillation damping capability of the WPP is investigated.

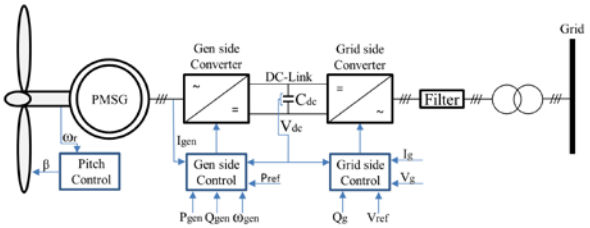

Fig. 1. Wind turbine concept used in the analysis

The block diagram of the overall connections is shown in Fig. 2. A brief description of the subsystems is given below.

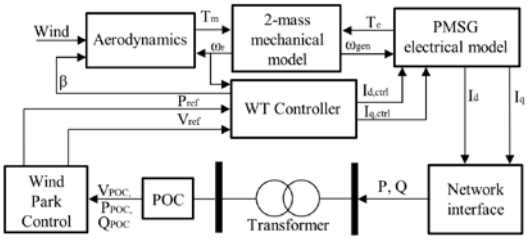

Fig. 2. Block diagram of the WT model

The **Aerodynamics** subsystem implements a variable wind speed aerodynamic model including power coefficient with pitch angle and tip-speed ratio as in [36].

The **mechanical model** is represented as a third order two mass model with the shaft stiffness and damping included [37].

The **electrical model** consists of a PMSG modeled in the dq-rotating reference frame, with all rotor quantities referred to the stator. The differential equations describing the dq-frame representation of the generator can be found in Matlab/Simulink library documentation [38]. This subsystem also models the dynamics of the DC-link capacitor voltage, assuming there is no power loss as in [39].

The **WT Controller** is divided into two parts. One controls the active and reactive power of the generator by acting on the generator side converter. In this case the d-axis is aligned with the flux of the permanent magnets, and the control is adjusting the d-axis current in order to keep the generator operating at unity power factor. The q-axis current is adjusted to control the active power production. The grid side converter control maintains the dc-link voltage at its rated value, and controls the voltage and reactive power at the WPP terminals. The WT controller contains a Phase-Locked Loop (PLL) that computes the angle of the terminal voltage phasor which is used to align the internal dq-reference.

The **Network interface** is represented by a controlled current source.

The **Wind Park Control (WPC)** is an outer control system which consists of two controllers, one for active power and one for voltage. The active power controller compares the reference power to the active power measured at the point of connection (POC) and uses a PI regulator to adjust the power set-point that is sent to the WPP. The controller is similar to the one presented in [40], where the reference value is the minimum between the value calculated based on a maximum power point tracking (MPPT) [41], and a value set by the WPP operator. The voltage controller is similar to the one proposed in [10]. It uses the voltage and reactive power measurements at the PCC to give a voltage set-point to the WPP.

The wind power park connects to the rest of the network through a collector grid modeled as a T-equivalent with half of the resistance and half of the inductance as a series impedance on each side, and the entire capacitance lumped as a shunt [10]. The collector grid parameters for a WPP of 180 MW are given in TABLE I. The parameters are scaled so that the voltage profile is unchanged when the size of the WPP is modified. The scaling factors are [10]:

$$z_{sc} = \frac{S^*_{base}}{S_{base,WPP}};\ R_{col} = z_{sc}R^*;\ X_{col} = z_{sc}X^*_L;\ B_{col} = \frac{B^*_C}{z_{sc}} \quad (1)$$

Where the superscript "*" refers to the values in TABLE I.

TABLE I
WPP COLLECTOR SYSTEM

Collector parameters		
R^* [Ω]	$X_L{}^*$ [Ω]	$B_C{}^*$ [μS]
0.086	0.070	3219.7

III. PHASOR POWER OSCILLATION DAMPER

During the power system oscillations the measured signals consist of two components; an average component which can be considered constant or slowly time varying, and the oscillatory components usually consisting of one or more modal frequencies. This approach focuses on extracting the oscillatory component, and representing it as a space phasor in a dq-coordinate system, which rotates with the same frequency as the power system oscillation frequency. This is done by expressing the measured signal as:

$$S(t) = S_{av}(t) + S_d(t)\cos\varphi(t) - S_q(t)\sin\varphi(t) \quad (2)$$

where S_{av} is the average component, S_d and S_q are the components of the dq-coordinate system, and $\varphi(t) = \omega t + \varphi_0$. Here, ω is the frequency of the dq-system, and φ_0 is the angle at which the phasor is locked to the dq-coordinate system.

The average and oscillatory components are estimated using the recursive least squares (RLS) algorithm proposed in [33]. The average and dq components form the parameter vector θ as follows:

$$\Theta = \begin{bmatrix} S_{av}(t) & S_d(t) & S_q(t) \end{bmatrix}^T \quad (3)$$

and the regression matrix $\emptyset$ is defined as:

$$\emptyset = [1 \quad cos\varphi(t) \quad -sin\varphi(t)]^T \quad (4)$$

The RLS algorithm updates the value of $\Theta(t)$ from its estimate $\Theta(t-1)$ calculated at the previous sampling instant. The steps describing the RLS algorithm are the following [42]:

1) Calculate the prediction error:

$$\varepsilon(t) = S(t) - \emptyset(t)\Theta(t-1) \quad (5)$$

2) Calculate the RLS gain vector $K_d(t)$:

$$K_d(t) = \frac{C(t-1)\emptyset^T(t)}{v + \emptyset(t)C(t-1)\emptyset^T(t)} \quad (6)$$

3) Update the covariance matrix C(t):

$$C(t) = \frac{[I - K_d(t)\emptyset(t)]\,C(t-1)}{v} \quad (7)$$

4) Update the parameter vector $\Theta(t)$:

$$\Theta(t) = \Theta(t-1) + K_d(t)\varepsilon(t). \quad (8)$$

In (6) and (7) v is the forgetting factor and its range is (0 1]. Setting $v = 1$ corresponds to "no forgetting" and estimating constant coefficients. In this case the estimated parameters S_{av}, S_d, and S_q are assumed to vary slowly with time, hence $v < 1$. The parameter vector $\Theta(t)$ is initialized with zeros, and the covariance matrix $C(t)$ is the identity matrix multiplied by a large number ($10^3 I$).

A. Latency compensation

The latency of the PMU measurements is a time delay (T_l) which from a phasor point of view translates into a phase lag in the received signal with respect to the original measurement in the power system. The phase lag is compensated by rotating the dq-frame to d'q'-frame with an angle $\theta = \omega T_l$, where ω is the angular frequency, as follows [33]:

$$\begin{bmatrix} S'_d \\ S'_q \end{bmatrix} = \begin{bmatrix} \cos\theta & -\sin\theta \\ \sin\theta & \cos\theta \end{bmatrix} \begin{bmatrix} S_d \\ S_q \end{bmatrix} \quad (9)$$

By further rotating the reference to d"q"-frame, an appropriate phase shift α is achieved [30]:

$$\begin{bmatrix} S^{"}_d \\ S^{"}_q \end{bmatrix} = \begin{bmatrix} \cos\alpha & -\sin\alpha \\ \sin\alpha & \cos\alpha \end{bmatrix} \begin{bmatrix} S'_d \\ S'_q \end{bmatrix} \quad (10)$$

The phase shift α is either calculated from the linear analysis of the power system, or it is the result of an adaptive algorithm as the one presented in [33]. The amplitude of the oscillation is represented in the dq-frame by the magnitude of the estimated phasor $|S_d(t) + jS_q(t)|$ which is a non-oscillatory and always positive value. The phasor magnitude is driven towards a zero reference with the aid of a PI controller which generates the phase shift $\alpha(t)$ as follows [33]:

$$\alpha(t) = -K_p|S_d(t) + jS_q(t)| - K_i\int|S_d(t) + jS_q(t)|dt \quad (11)$$

Where K_p and K_i are the proportional and integral gains of the PI controller.

The compensated and phase shifted phasor is transformed back into the time domain using the following [33]:

$$d(t) = [\cos\varphi(t) \quad -\sin\varphi(t)] \begin{bmatrix} S^{"}_d \\ S^{"}_q \end{bmatrix} \quad (12)$$

The signal $d(t)$ is scaled using the average estimated component $S_{av}(t)$ and then used as damping signal in the WPP.

Fig. 3 shows the block diagram of the phasor POD. Prior knowledge about the power system oscillatory modes is an advantage since it helps in the setting the frequency ω. The POD will act to damp the mode with this frequency. The power system operators usually have experience with the system and can advise with this choice.

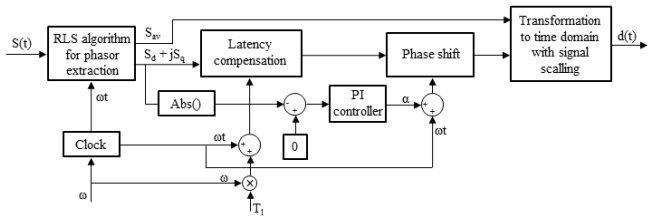

Fig. 3: phasor POD block diagram

IV. Study Case 1: Four Machine, Two-Area System

The first study case is based on the Kundur's four-machine, two-area system shown in Fig. 4 [2]. The aggregated WPP is connected to bus 5. The generators are represented by transient models and are equipped with the IEEE DC1A exciter. The network, generator, and exciter parameters are given in [2].

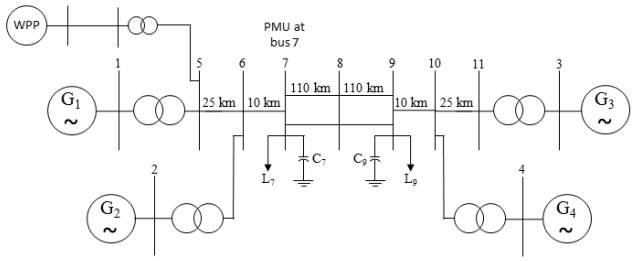

Fig. 4. Test system 1: four-machine, two-area system with WPP

The analysis is performed in Matlab/Simulink where the test system is modeled using the SimPowerSystems [43]. The linearization is performed using the Simulink Control Design [44], directly on the power system model defined and initialized.

A. Test system 1 modal characteristics

The modal characteristics of the test system are analyzed without wind power penetration to confirm the model is linearized correctly. In steady state approximately 343 MW flow through the 220 km intertie-line from Area 1 (G_1, G_2) to Area 2 (G_3, G_4). The eigenvalues of the local and inter-area modes are shown in TABLE II. Fig. 5 shows an overview of the complex plane with the test system eigenvalues.

TABLE II
Test System Modal Characteristics

Eigenvalue (λ) / (Frequency in Hz, Damping Ratio)		
Inter-area mode	*Area 1 Local Mode*	*Area 2 Local Mode*
λ_1 = -0.0175 ± j3.58 (f=0.57, ζ=0.005)	λ_2 = -0.591 ± j6.65 (f=1.06, ζ=0.089)	λ_3 = -0.555 ± j6.88 (f=1.1, ζ=0.08)

The modal analysis shows that the inter-area mode is poorly damped when the generators are modelled with dc exciters. This result is similar to the findings in [2], confirming the analysis is correct.

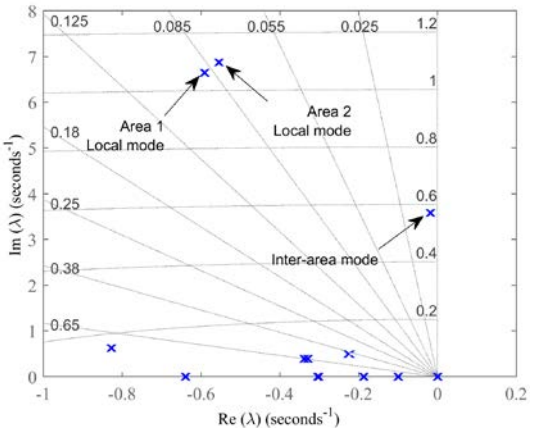

Fig. 5. Test system 1 eigenvalues (s-plane)

B. WPP impact on the inter-area oscillations

To contribute to the damping of the inter-area oscillations, the WPP is equipped with either the phasor POD, or the conventional PSS controllers. According to [17], the conventional PSS for wind turbines can be composed of a proportional controller, a limiter and a washout filter to limit the frequency range where the controller is active. The value of the washout filter time constant is chosen equal to 20 seconds, for the filter to be active at low frequencies (>0.1Hz). In addition, two lead-lag blocks are also implemented for the conventional PSS to help compensate for latency in the input signals. The damping signal (ΔP) is used to modulate the power reference in the WPC block as shown in Fig. 6. Consequently, WPP modulates its active power in order to damp the power system oscillations.

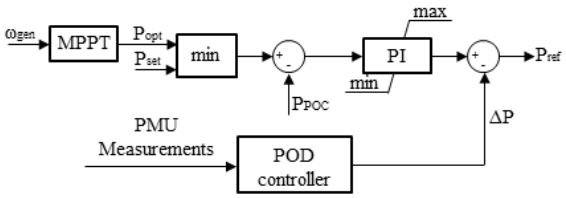

Fig. 6. WPC active power controller with POD

The PMU installed at bus 7 is configured to report the measurements at 60 samples per second. The current measured by the PMU is used as input signal for the PODs, and initially it is considered that there is no latency in the measured data.

The wind power injected in the system by the WPP is set to 400 MW. It is known that the modal characteristics of the power system can be affected if the power flow in the system is changed. In order to accommodate the injected wind power without changing the power flow, the power set-point of generator G_1 is modified. The eigenvalues of the test system with wind power, the phasor POD and the conventional PSS are described in Table III, and shown in Fig. 7.

TABLE III
Test System Modal Characteristics with WPP phasor POD and conventional PSS

Eigenvalue	WPP with phasor POD	WPP with conventional PSS
λ_1	0.984 ± j0.076 (f = 0.74, ζ=0.167)	0.981 ± j0.087 (f = 0.86, ζ=0.165)
λ_2	0.98 ± j0.101 (f = 0.99, ζ=0.146)	0.984 ± j0.102 (f = 0.99, ζ=0.106)
λ_3	0.984 ± j0.113 (f = 1.09, ζ=0.08)	0.984 ± j0.114 (f = 1.11, ζ=0.08)

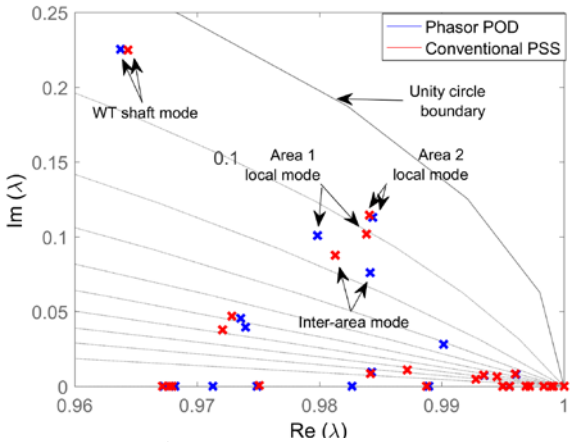

Fig. 7. Damping of inter-area mode with phasor POD (z-plane)

The system is now discrete due to the sampling rate of the PMU, thus the eigenvalues are displayed in the z-plane. It can be seen that the WPP has a positive impact on the inter-area mode, increasing its damping from 0.005 to 0.167 with the phasor POD, and up to 0.165 with the conventional PSS. Thus, the two controllers have similar performance for the damping of the inter-area mode.

Because the WPP is connected at bus 5 in area 1, it also has an impact on the local mode of this area. Both controllers improve the damping of the local mode, with the phasor POD showing a slightly better performance. The damping of the local mode in area 2 remains unchanged.

The modal analysis is a linear method and it should be complemented with time domain simulations of the non-linear system. The inter-area mode is excited by a step change of 1% in the excitation voltage of generator G_1. The intertie active power is shown in Fig. 8.It can be seen that the two controllers have similar performances.

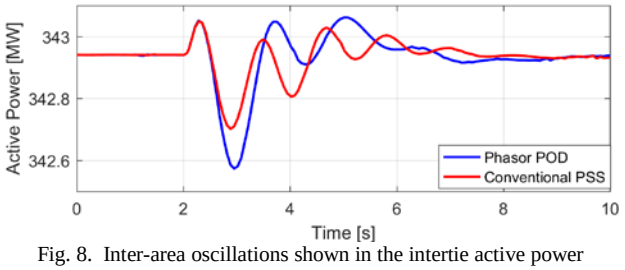

Fig. 8. Inter-area oscillations shown in the intertie active power

C. Comparison between the conventional PSS and phasor POD with PMU measurement latency

The performance of the WPP equipped first with the phasor POD, and then with the conventional PSS controllers is compared for the case when the POD input signal is lagging the signal measured at the PMU location. The study runs through a latency sweep with a range between 0 ms and 116 ms. The intertie active power is shown in Fig. 9. It can be seen that the phasor POD maintains its performance for the entire latency range. This shows the advantage of having a flexible way of compensating for different latencies which can be encountered in the communication and hardware infrastructure.

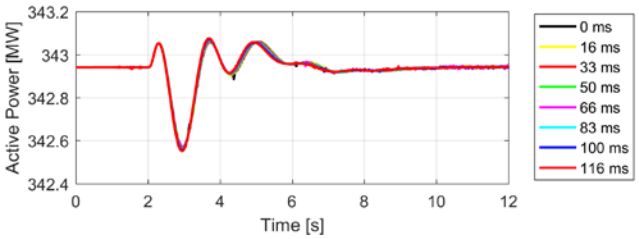

Fig. 9. Comparison between phasor and conventional PODs; no PMU latency

Next, the performance of the WPP with the conventional PSS is investigated for different input signal latencies. The intertie active power is shown in Fig. 10. The efficiency of the WPP equipped with the conventional PSS controller is decreasing as the latency is increasing. However, the power system oscillations are damped for latencies below 100 ms. After this point the WPP effect becomes detrimental since it contributes to the increase in amplitude of the oscillations, causing the system to become unstable. This shows that the lead-lag blocks offer good phase compensation for a range of latencies which is chosen at the design stage. If the latency exceeds the preset range, the performance of the conventional PSS will start decreasing.

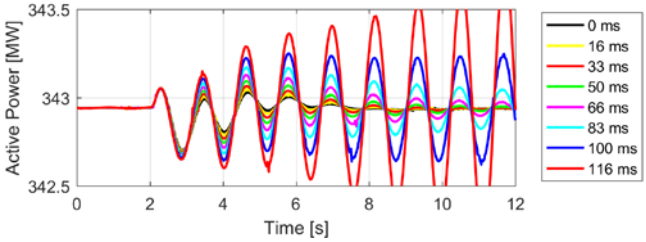

Fig. 10. Comparison between phasor and conventional PODs: (a) 16 ms PMU latency; (b) 32 ms PMU latency; (c) 48 ms PMU latency;

A clear benefit for using the WPP equipped with the phasor POD, and using remote PMU measurements as input signals is shown in this section. It is normal for some latency to be present when dealing with remote signals, and it is an advantage to be able to compensate for this delay. The phasor POD together with the accurate time stamping of the PMU measurements offers this capability.

V. Study Case 2: UK Seven-Generator System

The study is based on the seven-generator, 18-node power system shown in Fig. 11. The generators are aggregated machines, each representing a number of smaller and larger units. Furthermore, the system consists of six load, and the distribution of the loads and generation creates a power flow of from north to south of approximately 1900 MW on both lines l_{48} and l_{38}. The details of the power system parameters are given in [10]. The aggregated WPP with the corresponding collector grid is connected to the high voltage bus of generator G_2.

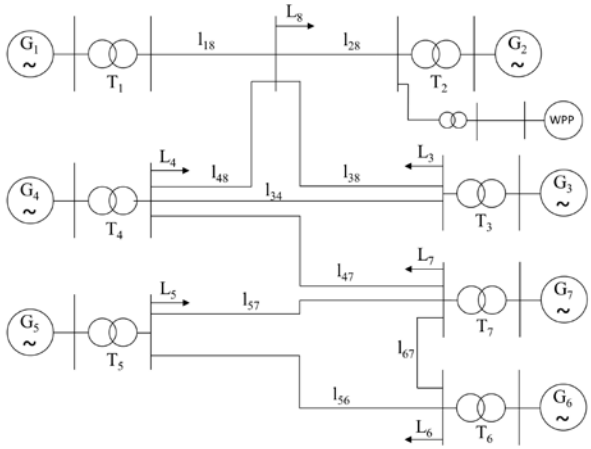

Fig. 11. Test System 2: 18-node, seven-generator system with WPP

A. *Test system 2 modal characteristic*

The modal characteristics of the seven-generator test system are analyzed without wind power. Fig. 12 shows the eigenvalues in the s-plane. Four inter-area modes are present in the system, and although lightly damped, the system is stable. The frequency and damping of the eigenvalues are given in Table IV.

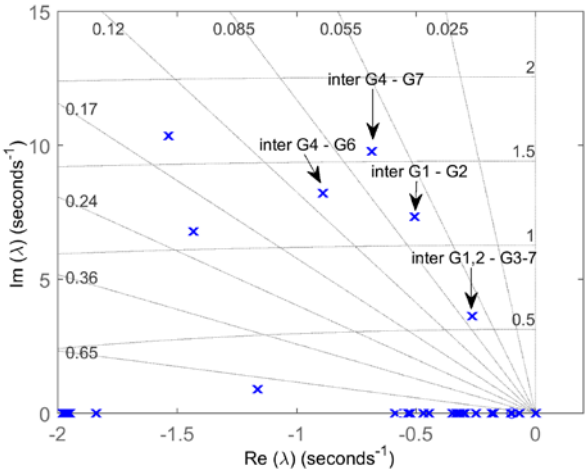

Fig. 12. Test system 2 eigenvalues (s-plane)

TABLE IV
CHARACTERISTICS OF THE INTER-AREA MODES WITHOUT WIND POWER

Eigenvalue	λ/(frequency in Hz, Damping Ratio)	Oscillatory mode description
λ_1	-0.265 ± j3.64 (f = 0.58, ζ=0.07)	Inter-area mode between $G_{1,2}$ - G_{3-7}
λ_2	-0.89 ± j8.22 (f = 1.31, ζ=0.108)	Inter-area mode between G_4 – G_6
λ_3	-0.685 ± j9.78 (f = 1.56, ζ=0.07)	Inter-area mode between G_4 – G_7
λ_4	-0.506 ± j7.34 (f = 1.17, ζ=0.07)	Inter-area mode between G_1 – G_2

The modal analysis is complemented with dynamic simulations showing response of the nonlinear system after a three-phase short circuit on line l_{48}. The fault is applied midway between the buses and it is cleared after 146 ms [10]. The active power flow on line l_{48} from north to south is shown in Fig. 13. The inter-area mode λ_1 between generators $G_{1,2}$ and G_{3-7} is excited by the short circuit and the oscillations can be seen in Fig. 13.

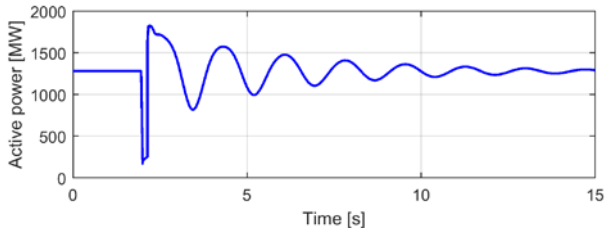

Fig. 13. Active power flow on line l_{48}

B. *WPP impact on damping the inter-area oscillations*

The capability of the WPP to improve the damping of the inter-area mode λ_1 is investigated in this subsection. The WPP is set to produce 1000 MW and the power set-point of generator G_2 is changed in order to keep the same power flow in the system.

A PMU is installed at the bus that connects lines l_{48} and l_{38}, and it is set to report the measurements at 50 samples per second. In this case the input signal for the POD is the active power flow in line l_{38} measured by the PMU.

For comparison, the WPP is equipped in turns with the phasor POD, and the conventional PSS. In contrast to the case shown in Section IV C, the conventional PSS used here consists also of lead-lag blocks to improve its performance under latency conditions.

The inter-area oscillations are excited by the three-phase short-circuit on line l_{48}. The fault is applied midway and it is cleared after 146 ms. Fig 13 shows the inter-area oscillations seen in the active power flow in line l_{48} in three cases; with no POD, with the phasor POD, and with the conventional PSS installed in the WPP. It can be seen that the WPP equipped with the phasor POD and conventional PSS, improves the damping of the oscillations. Moreover, the performance of these two controllers is very similar. A plot of the test system eigenvalues in the z-plane is shown in Fig. 15, and the details of the eigenvalues are given in Table V. It can be seen that the frequency and damping of the inter-area mode between generators $G_{1,2}$ and G_{3-7} are very similar, confirming that the performance of the phasor POD and conventional PSS is the same. It can also be noticed that the conventional PSS affects some of the other modes, while the phasor POD does not. This is because the phasor POD implemented in this study estimates the average and oscillatory components of a single mode and creates a damping signal for this mode.

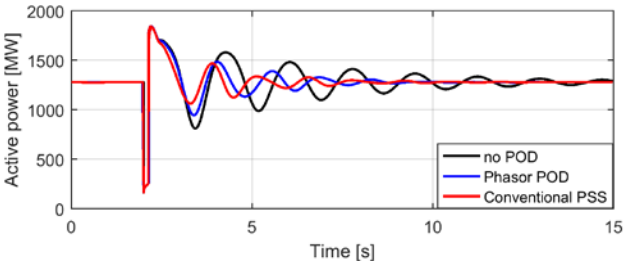

Fig. 14. Inter-area oscillations damping with no PMU latency

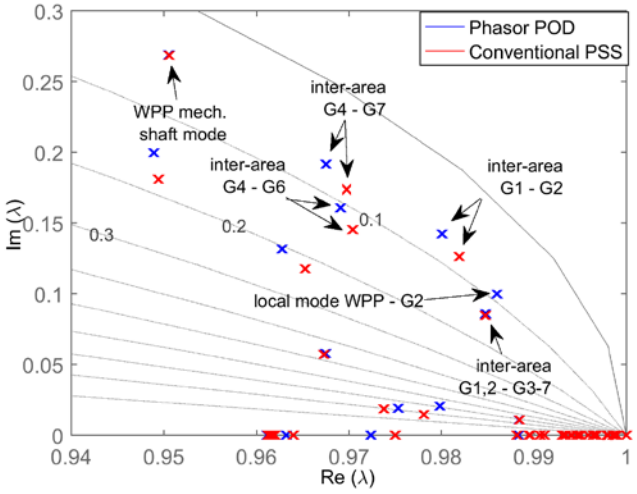

Fig. 15. Test system eigenvalues in z-plane; WPP with phasor POD and conventional PSS

TABLE V
TEST SYSTEM EIGENVALUES WITH WPP DAMPING IN Z-PLANE

Eigenvalue	WPP with phasor POD	WPP with conventional PSS
λ_1	0.985 ± j0.0859 (f = 0.7, ζ=0.131)	0.985 ± j0.0848 (f = 0.7, ζ=0.135)
λ_2	0.97 ± j0.161 (f = 1.32, ζ=0.108)	0.97 ± j0.145 (f = 1.19, ζ=0.127)
λ_3	0.968 ± j0.192 (f = 1.56, ζ=0.07)	0.97 ± j0.174 (f = 1.42, ζ=0.083)
λ_4	0.98 ± j 0.142 (f = 1.15, ζ=0.067)	0.982 ± j0.126 (f = 1.02, ζ=0.078)

C. Comparison between the conventional PSS and phasor POD with PMU measurement latency

The performance of the conventional PSS and phasor POD is investigated in a number of cases where the input signal is lagging the signal measured at the location of the PMU. The latency is varied between 0 ms and 140 ms in steps of 20 ms, thus creating a latency sweep that will quantify the performance of the controllers.

Fig. 16 shows the active power flow in line l_{48}. After the inter-area mode is excited, the WPP equipped with the conventional PSS controller is acting on damping the oscillations. It can be seen that as the latency increases the performance of the conventional PSS decreases. For latencies around 100 ms and above, the conventional PSS fails to provide sufficient damping and starts to affect the system in a negative way by sustaining the oscillations and even amplifying them, causing the system to become unstable.

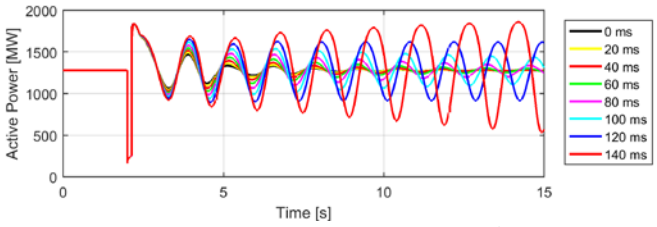

Fig. 16. Active power on line l_{48}; conventional PSS performance under latency conditions

Fig. 17 shows how the test system eigenvalue move, the direction is given by the arrow, when the latency is increasing. It can be seen that the damping of inter-area mode λ_1 is decreasing, and reaches the unity circle contour for a latency of 100ms. Above this value the eigenvalues of the inter-area mode are situated outside the unity circle showing the system becomes unstable.

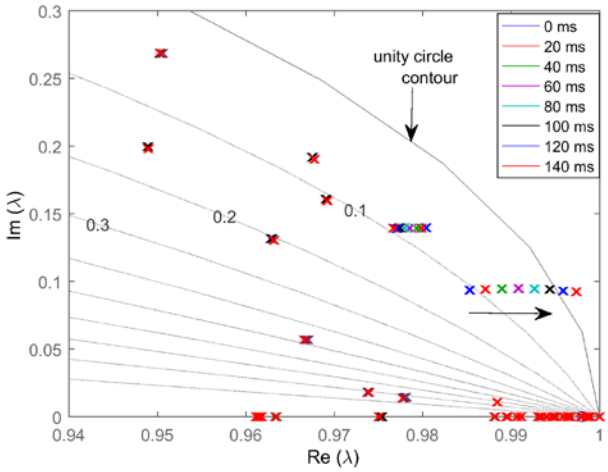

Fig. 17. Test system eigenvalues in z-plane; WPP with conventional PSS under latency conditions

The performance of the phasor POD is tested with the same latency sweep. Fig. 18 shows that the damping performance of the phasor POD is not affected by latencies in the input signal. Being able to easily compensate for the latency simply by changing the position of the dq-frame constitutes a major advantage the phasor POD has over the conventional PSS, especially since the information regarding the latency value is available thanks to the accurate time stamping of the measurements at the PMU and at the control center.

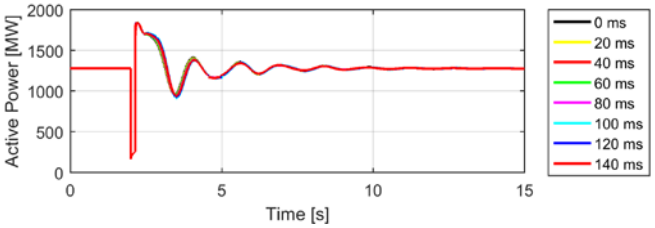

Fig. 18. Active power on line l_{48}; phasor POD performance under latency conditions

VI. CONCLUSION

This paper presents the impact of a WPP based on full-scale converter wind turbines on the damping of interconnected power system oscillations. The WPP is equipped with a POD controller that modulates the active power output in order to improve the system damping. Two types of POD controllers are investigated. One is a phasor POD which has been used before in FACTS devices like SVCs and TCSC. The advantage of this type of POD is that it can easily compensate for time delays in the input signal. This makes it a suitable choice when using WAMS, since some delay is always present when data communications are involved. The other POD is the conventional PSS type, which is well known and widely used with synchronous generators. The results show that when no time delay is present in the POD input signal, the controllers have similar performances. However, when the latency increases, the efficiency of the conventional PSS starts decreasing and eventually causes the WPP to increase the power system oscillations rather than damp them. The phasor POD, uses the time stamping

information from the PMUs and the data center to compensate for the delay. Therefore, it maintains its efficiency in damping the power system oscillations.

REFERENCES

[1] M. Klein, G. Rodgers, and P. Kundur, "A fundamental study of inter-area oscillations in power systems," *IEEE Trans.* Power Syst., vol. 6, no. 3, pp. 914-921, Aug 1991.

[2] P. Kundur, *Power System Stability and Control*, New York, NY, USA, McGraw-Hill, 1994.

[3] Global wind energy Report 2015, April 2016. [Online]. Available: http://www.gwec.net/publications/global-wind-report-2/

[4] P. Ledesma, J. Usaola, and J. Rodriguez, "Transient stability of a fixed speed wind farm," *Renewable Energy*, vol. 28, no. 9, pp. 1341-1355, Jul 2003.

[5] V. Akhmatov, H. Knudsen, A. H. Nielsen, J. K. Pedersen, and N. Kjølstad Poulsen, "Modelling and transient stability of large wind farms," *International Journal of Electrical Power and Energy Systems*, vol. 25, no. 2, pp. 123–144, Feb 2003.

[6] O. Anaya-Lara, F. Hughes, N. Jenkins, and G. Strbac, "Influence of windfarms on power system dynamic and transient stability," *Wind Engineering*, vol. 30, no. 2, pp. 107-127, Mar 2006.

[7] J.G. Slootweg, and W.L. Kling, "The impact of large scale wind power generation on power system oscillations," *Electric Power Systems Research*, vol. 67, no. 1, pp. 9-20, Oct 2003.

[8] N. R. Chaudhuri and B. Chaudhuri, "Impact of wind penetration and HVDC upgrades on dynamic performance of future grids," in *IEEE PES General Meeting*, San Diego, CA, 2011, pp. 1-8.

[9] C. Samarasinghe and D. Vowles, "Wind generation investigation project – effect of wind generation on small signal stability," The National Grid, TRANSPOWER New Zealand, Tech. Rep. Investigation 8, Mar. 2008.

[10] T. Knuppel, J. N. Nielsen, K. H. Jensen, A. Dixon and J. Ostergaard, "Small-signal stability of wind power system with full-load converter interfaced wind turbines," *IET Renewable Power Generation*, vol. 6, no. 2, pp. 79-91, Mar. 2012.

[11] J. L. Dominguez-Garcia, O. Gomis-Bellmunt, F. Bianchi, A. Sumper, and A. Sudria-Andreu, "Power System stabiliser capability of offshore wind power plants," in *Proc of the EWEA*, Copenhagen, 2012, pp. 29-32.

[12] L. Fan, H. Yin and Z. Miao, "On Active/Reactive Power Modulation of DFIG-Based Wind Generation for Interarea Oscillation Damping," *IEEE Trans. Energy Convers.*, vol. 26, no. 2, pp. 513-521, June 2011.

[13] F. M. Hughes, O. Anaya-Lara, N. Jenkins and G. Strbac, "A power system stabilizer for DFIG-based wind generation," *IEEE Trans. Power Syst.*, vol. 21, no. 2, pp. 763-772, May 2006.

[14] Z. Miao, L. Fan, D. Osborn and S. Yuvarajan, "Control of DFIG based wind generation to improve inter-area oscillation damping," in *IEEE PES General Meeting - Conversion and Delivery of Electrical Energy in the 21st Century*, Pittsburgh, PA, 2008, pp. 1-7.

[15] L. Sigrist and L. Rouco, "Design of damping controllers for doubly fed induction generators using eigenvalue sensitivities," in *IEEE/PES Power Systems Conference and Exposition*, Seattle, WA, 2009, pp. 1-7.

[16] G. Tsourakis and C. Vournas, "A controller for wind generators to increase damping of power oscillations," in *Proc. of IEEE International Symposium on Circuits and Systems*, Paris, 2010, pp. 2195-2198.

[17] G. Tsourakis, B. M. Nomikos and C. D. Vournas, "Contribution of Doubly Fed Wind Generators to Oscillation Damping," *IEEE Trans. Energy Convers.*, vol. 24, no. 3, pp. 783-791, Sept. 2009.

[18] A. Adamczyk, R. Teodorescu and P. Rodriguez, "Control of Full-Scale Converter based Wind Power Plants for damping of low frequency system oscillations," in *IEEE Trondheim PowerTech*, Trondheim, 2011, pp. 1-7.

[19] D. Gautam, V. Vittal, R. Ayyanar and T. Harbour, "Supplementary control for damping power oscillations due to increased penetration of doubly fed induction generators in large power systems," in *IEEE/PES Power Systems Conference and Exposition*, Phoenix, AZ, 2011, pp. 1-6.

[20] R. D. Fernandez, R. J. Mantz and P. E. Battaiotto, "Contribution of wind farms to the network stability," in *IEEE PES General Meeting*, Montreal, Que., 2006, pp.1-6.

[21] R.D. Fernández, R.J. Mantz, and P.E. Battaiotto, "Potential contribution of wind farms to damp oscillations in weak grids with high wind penetration," *Renewable and Sustainable Energy Reviews*, vol. 12, no. 6, pp. 1692-1711, Aug. 2008.

[22] J. H. Chow, J. J. Sanchez-Gasca, Haoxing Ren and Shaopeng Wang, "Power system damping controller design-using multiple input signals," *IEEE Control Syst. Mag.*, vol. 20, no. 4, pp. 82-90, Aug 2000.

[23] M. E. Aboul-Ela, A. A. Sallam, J. D. McCalley and A. A. Fouad, "Damping controller design for power system oscillations using global signals," *IEEE Trans. on Power Syst.*, vol. 11, no. 2, pp. 767-773, May 1996.

[24] G. T. Heydt, C. C. Liu, A. G. Phadke and V. Vittal, "Solution for the crisis in electric power supply," *IEEE Comput. Appl. Power*, vol. 14, no. 3, pp. 22-30, Jul 2001.

[25] J. Y. Cai, Zhenyu Huang, J. Hauer and K. Martin, "Current Status and Experience of WAMS Implementation in North America," *2005 IEEE/PES Transmission & Distribution Conference & Exposition: Asia and Pacific*, Dalian, 2005, pp. 1-7.

[26] J. W. Stahlhut, T. J. Browne, G. T. Heydt and V. Vittal, "Latency Viewed as a Stochastic Process and its Impact on Wide Area Power System Control Signals," *IEEE Trans. on Power Syst.*, vol. 23, no. 1, pp. 84-91, Feb. 2008.

[27] D. Dotta, A. S. e Silva and I. C. Decker, "Wide-Area Measurements-Based Two-Level Control Design Considering Signal Transmission Delay," in *IEEE Transactions on Power Systems*, vol. 24, no. 1, pp. 208-216, Feb. 2009.

[28] B. Chaudhuri, R. Majumder and B. C. Pal, "Wide-area measurement-based stabilizing control of power system considering signal transmission delay," *IEEE Trans. on Power Syst.*, vol. 19, no. 4, pp. 1971-1979, Nov. 2004.

[29] R. Majumder, B. Chaudhuri, B. C. Pal and Qing-Chang Zhong, "A unified Smith predictor approach for power system damping control design using remote signals," in *IEEE Transactions on Control Systems Technology*, vol. 13, no. 6, pp. 1063-1068, Nov. 2005.

[30] L. Angquist, "Method and a Device for Damping Power Oscillations in Transmission Lines," U.S. Patent 6 559 561, May 6, 2003.

[31] H. F. Latorre and L. Angquist, "Analysis of TCSC providing damping in the interconnection Colombia-Ecuador 230 kV," in *IEEE PES General Meeting*, 2003, Vol. 4, pp. 2366.

[32] L. Angquist and C. Gama, "Damping algorithm based on phasor estimation," in *Proc. of IEEE PES Winter Meeting*, Columbus, OH, 2001, vol.3, pp. 1160-1165.

[33] N. R. Chaudhuri, S. Ray, R. Majumder and B. Chaudhuri, "A New Approach to Continuous Latency Compensation With Adaptive Phasor Power Oscillation Damping Controller (POD)," *IEEE Trans. on Power Syst.*, vol. 25, no. 2, pp. 939-946, May 2010.

[34] N. R. Chaudhuri, B. Chaudhuri, S. Ray, and R. Majumder, "Wide-area phasor power oscillation damping controller: a new approach to handling time-varying signal latency," *IET Gener. Transm. Distrib.*, vol. 4, no. 5, pp. 620-630, May 2010.

[35] P. Korba, R. Segundo, A. Paice, B. Berggren, and R. Majumder, "Time delay compensation in power system control," E. U. Patent EP08 156 785, May 23, 2008.

[36] S. Heier, Grid integration of wind energy conversion systems, John Wiley & Sons, 1998.

[37] N. W. Miller, W. W. Pric, and J. J. Samches-Gasca. (2003, Oct.). Dynamic modeling of GE 1.5 and 3.6 Wind Turbine-Generators. GE-Power System Energy Consulting. [Online]. Available: https://pdfs.semanticscholar.org/4be9/52ff4ee3203db24ed461f8064abb00b8fa4e.pdf

[38] MATLAB documentation center. [Online]. Available: https://www.mathworks.com/help/

[39] L.M. Fernandez, C.A. Garcia, and F. Jurado, "Operating capability as a PQ/PV node of a direct-drive wind turbine based on a permanent magnet synchronous generator," *Journal of Renewable Energy*, vol. 35, no 6, pp. 1308-1318, Jun 2010.

[40] A. D. Hansen and I. D. Margaris. (2014). Type IV Wind Turbine Model DTU Wind energy. [Online]. Available: http://orbit.dtu.dk/en/publications/type-iv-wind-turbine-model(99b55843-deb3-49b9-b564-e664bc25fa99).html

[41] S. M. Muyeen, J. Tamura, and T. Murata, Stability augmentation of a grid connected wind farm, Green Energy and Technology, Springer-Verlag, 2009.

[42] K. J. Astrom and B. Witternmark, *Adaptive Control*, 2nd ed. Reading, MA: Addison-Wesley, 1995.

[43] MATLAB documentation center, SimPowerSystems™ 6.6 – User's Guide, 2016.

[44] MATLAB documentation center, Simulink Control Design™ 4.4– User's Guide, 2016.

www.elektro.dtu.dk/cee

Department of Electrical Engineering
Centre for Electric Power and Energy (CEE)
Technical University of Denmark
Elektrovej 325
DK-2800 Kgs. Lyngby
Denmark
Tel: (+45) 45 25 35 00
Fax: (+45) 45 88 61 11
E-mail: cee@elektro.dtu.dk

[Skriv: ISBN XX-XXXXX-XX-X (eller slet)]